Elsevier Editorial System(tm) for Lithos
Manuscript Draft

Manuscript Number: LITHOS6792R2

Title: The magmatic evolution and genesis of the Quaternary basanite-trachyphonolite suite of Itasy (Madagascar) as inferred by geochemistry, Sr-Nd-Pb isotopes and trace element distribution in coexisting phases

Article Type: Regular Article

Keywords: basanites, trachyphonolites, mineral trace elements, titanite removal, crustal contamination, Itasy, Madagascar

Corresponding Author: Dr. Leone Melluso,

Corresponding Author's Institution: Università di Napoli Federico II

First Author: Leone Melluso

Order of Authors: Leone Melluso; Tucker D Robert; Ciro Cucciniello; Anton P le Roex; Vincenzo Morra; Rocky L Rakotoson, Dr.

Abstract: The Itasy is a Pleistocene-Holocene volcanic field in central Madagascar, located to the west of the Ankaratra volcanic complex. It comprises scoria cones and lava domes (>120), with associated pyroclastic fall and mafic lava flows, covering an area of ab. 400 km2. The last volcanic episodes probably dated ca. 6000-7100 y BP; warm springs and geysers are active. The juvenile samples comprise a peculiar, almost bimodal, rock suite ranging from potassic leucite-kaersutite-bearing basanites, tephrites and phonotephrites, to benmoreites and titanite-haüyne-bearing trachyphonolites (MgO from 9-10 wt.% to 0.1 wt.%). These rocks show continuous and overlapping variations in the bulk-rock and phase composition (olivine, clinopyroxene, amphibole, feldspar, leucite, haüyne, nepheline, oxides, apatite, titanite, glass and other accessories). The basanites have homogeneous isotopic composition (87Sr/86Sr=0.70366-0.70378, 143Nd/144Nd=0.51274-0.51277, 206Pb/204Pb=18.7-18.9, 207Pb/204Pb=15.53-15.56; 208Pb/204Pb=38.89-39.01), and a marked enrichment in the most incompatible elements (LILE and HFSE reach 100-215 times primitive mantle). These features are consistent with low degrees of partial melting of a volatile-, LILE- and HFSE-rich, amphibole-bearing peridotitic mantle induced by uplift during an E-W-directed extensional regime, as is found in central Madagascar. The marked changes in the geochemical composition, and small variations of the Sr-Nd-Pb isotopes in the trachyphonolites (87Sr/86Sr=0.70425-0.70446, 143Nd/144Nd=0.51266-0.51269, 206Pb/204Pb=18.18-18.39, 207Pb/204Pb=15.49-15.51; 208Pb/204Pb=38.38-39.57) with respect to basanites and tephrites point to a limited amount of crustal contamination by the relatively low-206Pb/204Pb, low-143Nd/144Nd, high-87Sr/86Sr Precambrian basement rocks (of Middle Archean to Late Proterozoic age), and highlight the geochemical effects of titanite and anorthoclase removal on the trace element fractionation trends, a feature also shown in the trace element composition of the phenocrysts in the trachyphonolites.

Revision Notes

Click here to download Revision Notes: revisionnotes2.doc

Dear Editors of Lithos,
in this revised version, we specifically rewrote the last part of the Introduction and Geological setting, from line 97 to line 106, in order to closely meet the requirements of the Reviewer and to not make this introduction too wordy.
We also made minor corrections to the English text throughout, and added an article of ours, now in press with doi. No changes were made to tables, figures and supplementary material.

Abstract

The Itasy is a Pleistocene-Holocene volcanic field in central Madagascar, located to the west of the Ankaratra volcanic complex. It comprises scoria cones and lava domes (>120), with associated pyroclastic fall and mafic lava flows, covering an area of ab. 400 km^2. The last volcanic episodes probably dated ca. 6000-7100 y BP; warm springs and geysers are active. The juvenile samples comprise a peculiar, almost bimodal, rock suite ranging from potassic leucite-kaersutite-bearing basanites, tephrites and phonotephrites, to benmoreites and titanite-haüyne-bearing trachyphonolites (MgO from 9-10 wt.% to 0.1 wt.%). These rocks show continuous and overlapping variations in the bulk-rock and phase composition (olivine, clinopyroxene, amphibole, feldspar, leucite, haüyne, nepheline, oxides, apatite, titanite, glass and other accessories). The basanites have homogeneous isotopic composition ($^{87}Sr/^{86}Sr$=0.70366-0.70378, $^{143}Nd/^{144}Nd$=0.51274-0.51277, $^{206}Pb/^{204}Pb$=18.7-18.9, $^{207}Pb/^{204}Pb$=15.53-15.56; $^{208}Pb/^{204}Pb$=38.89-39.01), and a marked enrichment in the most incompatible elements (LILE and HFSE reach 100-215 times primitive mantle). These features are consistent with low degrees of partial melting of a volatile-, LILE- and HFSE-rich, amphibole-bearing peridotitic mantle under conditions of uplift during an E-W-directed extensional regime, as found in central Madagascar. The marked changes in the geochemical composition, and small variations of the Sr-Nd-Pb isotopes shown by the trachyphonolites ($^{87}Sr/^{86}Sr$=0.70425-0.70446, $^{143}Nd/^{144}Nd$=0.51266-0.51269, $^{206}Pb/^{204}Pb$=18.18-18.39, $^{207}Pb/^{204}Pb$=15.49-15.51; $^{208}Pb/^{204}Pb$=38.38-39.57) with respect to basanites and tephrites point to a limited amount of crustal contamination of the relatively low-$^{206}Pb/^{204}Pb$, low-$^{143}Nd/^{144}Nd$, high-$^{87}Sr/^{86}Sr$ Precambrian basement rocks (of Middle Archean to Late Proterozoic age), and highlight the geochemical effects of titanite and anorthoclase removal on the trace element fractionation trends, as also shown in the trace element composition of the phenocrysts in the trachyphonolites.

- The Itasy volcanic field has basanites, tephrites, phonotephrites, benmoreites and trachyphonolites
- These rocks are the result of fractional crystallization and crustal contamination
- Titanite and anothoclase removal is essential petrogenetic process in the trachyphonolites
- The mantle source of the basanites is similar to that of the other Cenozoic rocks of central Madagascar

The magmatic evolution and genesis of the Quaternary basanite-trachyphonolite suite of Itasy (Madagascar) as inferred by geochemistry, Sr-Nd-Pb isotopes and trace element distribution in coexisting phases

L. Melluso*[1], R.D. Tucker**, C. Cucciniello*, A.P. le Roex***, V. Morra*, A. Zanetti****, R.L. Rakotoson*****

*DISTAR, Università di Napoli Federico II, Napoli, Italy
**BRGM, Orleans, France
***University of Cape Town, Rondebosch, Republic of South Africa
****IGG-CNR, Pavia, Italy
*****Analamaitsy, Antananarivo, Madagascar

[1]corresponding author: melluso@unina.it

Abstract

The Itasy is a Pleistocene-Holocene volcanic field in central Madagascar, located to the west of the Ankaratra volcanic complex. It comprises scoria cones and lava domes (>120), with associated pyroclastic fall and mafic lava flows, covering an area of ab. 400 km^2. The last volcanic episodes probably dated ca. 6000-7100 y BP; warm springs and geysers are active. The juvenile samples comprise a peculiar, almost bimodal, rock suite ranging from potassic leucite-kaersutite-bearing basanites, tephrites and phonotephrites, to benmoreites and titanite-haüyne-bearing trachyphonolites (MgO from 9-10 wt.% to 0.1 wt.%). These rocks show continuous and overlapping variations in the bulk-rock and phase composition (olivine, clinopyroxene, amphibole, feldspar, leucite, haüyne, nepheline, oxides, apatite, titanite, glass and other accessories). The basanites have homogeneous isotopic composition ($^{87}Sr/^{86}Sr$=0.70366-0.70378, $^{143}Nd/^{144}Nd$=0.51274-0.51277, $^{206}Pb/^{204}Pb$=18.7-18.9, $^{207}Pb/^{204}Pb$=15.53-15.56; $^{208}Pb/^{204}Pb$=38.89-39.01), and a marked enrichment in the most incompatible elements (LILE and HFSE reach 100-215 times primitive mantle). These features are consistent with low degrees of partial melting of a volatile-, LILE- and HFSE-rich, amphibole-bearing peridotitic mantle induced by uplift during an E-W-directed extensional regime, as is found in central Madagascar. The marked changes in the geochemical composition, and small variations of the Sr-Nd-Pb isotopes in the trachyphonolites ($^{87}Sr/^{86}Sr$=0.70425-0.70446, $^{143}Nd/^{144}Nd$=0.51266-0.51269, $^{206}Pb/^{204}Pb$=18.18-18.39, $^{207}Pb/^{204}Pb$=15.49-15.51; $^{208}Pb/^{204}Pb$=38.38-39.57) with respect to basanites and tephrites point to a limited amount of crustal contamination by the relatively low-

$^{206}Pb/^{204}Pb$, low-$^{143}Nd/^{144}Nd$, high-$^{87}Sr/^{86}Sr$ Precambrian basement rocks (of Middle Archean to Late Proterozoic age), and highlight the geochemical effects of titanite and anorthoclase removal on the trace element fractionation trends, a feature also shown in the trace element composition of the phenocrysts in trachyphonolites.

Keywords: basanites, trachyphonolites, mineral trace elements, titanite removal, crustal contamination, Itasy, Madagascar

1. Introduction and Geological setting

Madagascar is the site of abundant Cenozoic-to-Recent volcanism (Woolley, 2001; Tucker et al., 2008; Cucciniello et al., 2011, 2016, 2017), which crops out from the northernmost regions of the island (Cap d'Ambre/Bobaomby, Massif d'Ambre) to the southwest (Ankililoaka, Tulear region; Fig. 1a). This volcanism is the response to extensional processes and uplift active since the Cenozoic of the Madagascan lithosphere, with changing orientation of the stress pattern in different sectors of the island (Nicollet, 1984; Piqué et al., 1999; Cucciniello et al., 2016, 2018). The changing ages and lithological characteristics of the exposed crustal domains are reflected in the different isotopic composition of the mantle-derived Cenozoic rocks, suggesting a strong lithospheric control in the genesis of the latter (Tucker et al., 2014; Melluso et al., 2016; Cucciniello et al., 2018).

The central field of alkaline igneous rocks consist of four different volcanic-dominated massifs, from east to west: Takarindiona, Alaotra, Ankaratra and Itasy (Fig. 1a). The eastern massifs of Takarindiona and Alaotra are relatively small, structurally controlled Miocene-Pliocene fissural eruptions and spatter cones (Melluso et al., 2011a), emplaced along or near the western margin of the oldest rocks in Madagascar (~3.2 Ga gneisses of the Antongil/Masora domain). The Ankaratra and Itasy are significantly larger in size and more diverse in morphology, as they include lava domes, massive flow eruptions, spatter cones, and various phreatomagmatic rings and cones (cf. Brenon and Bussiere, 1959; Woolley, 2001; Cuciniello et al., 2017). The Ankaratra covers an area of ~3600 km^2 and reaches 2395 mt. elevation. Like the eastern fields, the age of activity in the Ankaratra spans from Miocene to Recent (Tucker et al., 2008; Rufer et al., 2014; Cucciniello et al., 2017).

The Itasy volcanic field is a much smaller (roughly 400 km^2) and younger version of the Ankaratra; it crops out at roughly 1200 mt. a.s.l., in a north-south-trending graben located in the Precambrian basement (e.g., Andrianaivo and Ramasianoro, 2010, 2011), whose western limits are best indicated by a long NNE-SSW normal fault (Fig. 1b). The volcanic field is the coalescence of more than 120 scoria cones (e.g., Kassigie, also known for a presumed eruption in 2001, likely a landslide in its SW

sector), with lava flows (e.g., along the western master fault), lava domes (e.g., Ngilofotsy, west of Analavory; Fig. 1b; Supplementary Fig. 1), and pyroclastic rocks in the facies of pyroclastic fall deposits, small-scale pyroclastic flows and maar craters (cf. Supplementary Fig. 1; Razafiniparany et al., 1974). According to Bussiere (1957, and references therein), the sequence of volcanic events is established by cross-cutting relationships. It includes: *(a)* oldest eruptions of trachyte and trachyphonolite, *(b)* deposition of lacustrine sediments bearing fossils of Pleistocene or younger age (i.e. plant fragments, and bones of hippos, lemurs, and *Aepyornis*), (*c*) lava flows and pyroclastic eruptions of basanite and tephrite, and *(d)* recent strombolian and phreatomagmatic eruptions of basanitoids. Given the small volume, the scattered nature of magmatism and the structural complexity of this part of Madagascar, the eruptive history of the Itasy area is only generally known. What is clear, however, is that the age of the volcanism must be young, certainly less than 1 Ma. This is consistent with the geologic youthfulness of the volcanic landforms, their relationship to Pleistocene or younger fossils, the historical record of seismic and geothermal activity (Brown et al., 2015), and an $^{40}Ar/^{39}Ar$ plateau age of 97±6 ka for a trachyphonolite sampled near Analavory (R.D. Tucker, unpub. data). During and after formation of the lacustrine basins, the region is believed to have experienced regional E-W extension and differential uplift that fractured the natural dams, drained the tectonic lakes, and produced its rugged topography. The bounding faults of the Itasy graben (Fig. 1b) are but one manifestation of this near-surface extensional stress field. These features, including the volcanism of Itasy and Ankaratra, are a response to still unresolved forces, recently imaged in a regional seismological survey (Pratt et al., 2017; Fig. 1c) that acted throughout the Malagasy lithosphere in Miocene and younger time.

The Itasy and the Ankaratra are built upon a Precambrian basement complex of Neoarchean granitic gneiss (2.7-2.5 Ga, Betsiboka Suite) and Neoproterozoic quartzite and schist (<1.0 Ga, Ambatolampy Group), and both are bounded by faults near the apex of the Taná virgation, where the gneissic fabrics turn sharply from N-S to E-W strike directions (Roig et al., 2012; Tucker et al., 2014).

Petrogenetic studies on the Ankaratra volcanic rocks were recently published (Melluso et al., 2016; Cucciniello et al., 2017). This paper is focused on the petrogenesis of the Itasy, probably the least known Late Cenozoic *volcanic* field in Madagascar. Lacroix (1923) and Bussiere (1957) first identified the featuring petrographic characteristics of the main lithologies, including the presence of haüyne in the felsic samples, allowing them to make comparison to rocks of the Massif Central in France. We report the range of chemical and isotopic composition of the Itasy bulk rocks and mineral phases, and highlight magmatic processes of within-plate magma series which acted during the ascent in the crust. We also focus on the petrogenetic relationships and differences with other

105 Cenozoic volcanic districts of Madagascar, particularly those of the central Madagascar, which were
106 emplaced through the same Precambrian domains.
107
108 **2. Classification and petrography**
109
110 Sixty-nine samples were collected throughout the volcanic field (Fig. 1b). They are representative of
111 scoria and lava flows cropping out in the graben, and of the several volcanic domes of evolved
112 composition (trachytic *s.l.*), which occur in the same areas as scoria cones and lavas. The analytical
113 techniques are fully described in the appendix. According to petrography, T.A.S., R_1R_2 classification
114 diagrams (Fig. 2), and CIPW norms (Supplementary Table S1), the fresh samples are basanites,
115 tephrites, rare phonotephrites and benmoreites (*trachyandesites*), and trachyphonolites, with a
116 bimodal character (Fig. 2, Table 1 and Supplementary Table S1). The *mafic* rocks have potassic
117 affinity, given that their Na_2O/K_2O ratios are close to the unity; the CIPW norms have no normative
118 leucite. The trachyphonolites do not reach fully peralkaline conditions [P.I., peralkaline index, molar
119 (Na+K)/Al <0.98], with the exception of the groundmass of evolved samples (see below). The
120 samples with L.O.I. values > 2 wt.% (mostly scoria) have signs of chemical alteration, and thus were
121 excluded from the discussion and from the classification diagrams. A synopsis of the observed
122 mineral assemblages for various lithotypes is reported in the Supplementary Table S2.
123 **Basanites**, **tephrites** and **phonotephrites** are variably porphyritic (in both lava and scoria facies),
124 with zoned, Ti-rich purple-green clinopyroxene, olivine (with small Cr-spinel inclusions), amphibole
125 and oxide phenocrysts and megacrysts in a fine grained, feldspar-rich mesostasis, to almost aphyric
126 facies, with purple-green clinopyroxene, oxide and olivine microlites in fine-grained or glassy
127 groundmass, often without amphibole. The latter phase is found in both scorias and lavas
128 (Supplementary Fig. S1). Amphibole is almost always poikilitic over clinopyroxene (Supplementary
129 Fig. S1), and may show reaction relationships with the latter; it is often replaced by secondary
130 rhönite. There is complete lack of feldspar phenocrysts. Apatite microphenocrysts and microlites are
131 ubiquitous, particularly in the phonotephrite RT-06I-398, and leucite is often present in the
132 groundmass, together with haüyne, phonolitic glass and alkali feldspar (Supplementary Fig. S1;
133 Supplementary Table S2).
134 **Benmoreites**; sample RT06I-387 (the "*ordanchite*" of Lacroix and Bussiere) has rare phenocrysts of
135 plagioclase, clinopyroxene, amphibole and opaque oxides, set in a trachytic/aphanitic mesostasis
136 (Supplementary Fig. S1).
137 **Trachyphonolites** range from porphyritic to nearly aphyric, and are characterized by phenocrysts of
138 anorthoclase and/or sanidine, plus rarer titanite, green clinopyroxene, amphibole and opaque oxides,

set in a trachytic mesostasis that also has apatite, nepheline, haüyne, sodalite, clinopyroxene, other accessories and interstitial glass (Supplementary Fig. S1; Supplementary Table S2).

3. Mineral compositions

Olivine in basanites and tephrites is usually zoned, with composition ranging from Fo_{81} to Fo_{55} [Fo is 100 Mg/(Mg+Fe) in atoms], with MnO up to 0.52 wt.% and CaO up to 0.73 wt.% in the most Fe-rich compositions (Supplementary Table S3). Some crystals appear too Mg-rich to be in equilibrium with the host rock composition [e.g., the rounded Fo_{81} (xeno)crystal in the RT-06I-398 phonotephrite; Supplementary Table S3].

Oxides. **Cr-spinel** is rare and chemically zoned in the Mg-rich olivine cores of basanite RT-06I-354B [Cr_2O_3 =8.7-28.7 wt.%; Cr#=47-57; Cr# is 100Cr/(Cr+Al) in atoms]. **Ilmenite** is also very rare; it was found in the basanite RT-06I-354b as an exsolved phase (Supplementary Fig. S1) and is rich in geikielite component (MgO=7.8-13.3 wt.%), consistent with its crystallization from a mafic melt. **Titaniferous magnetite** is the main oxide; it shows increase in MnO and magnetite component (*s.s.*) and decrease in TiO_2, Al_2O_3 and MgO from mafic to evolved rocks (Supplementary Table S4 and Supplementary Fig. S2).

Clinopyroxene ranges from diopside [Mg#=82, TiO_2=1.3 wt.%; Mg# is 100Mg/(Mg+Fe)] to titanaugite (Mg#=68; TiO_2=5.75 wt.%, ca. 19 mol.% $CaTiAl_2O_6$) in basanites and tephrites, and from titanaugite (Mg#=67; TiO_2=5.1 wt.%) to aegirinaugite (Mg#=22; Na_2O=5 wt.%, ca. 38 mol.% aegirine) in the trachyphonolites (Fig. 3). The composition of clinopyroxene is therefore indicative of the degree of evolution of the host lithotypes, as shown in the Ti-Al and Mg-Ti diagrams (Supplementary Fig. S3). The evolved rocks have the lowest Mg#, Ti and Al and the highest Mn (and Na) concentrations; the calculated Al^{VI} is absent or strongly subordinated with respect to Al^{IV} (Supplementary Fig. S3; Supplementary Table S5). The compositional ranges are well within those already observed in the Ankaratra and in the other Cenozoic volcanic areas of Madagascar (e.g., Melluso et al., 2011a; Cucciniello et al., 2017 and references therein).

Amphibole is potassian kaersutite in basanites and tephrites (TiO_2=4.1-5.1 wt.%; Mg#=58-72), and potassian kaersutite/Fe-kaersutite to pargasite (TiO_2=1.2-4.6 wt.%; Mg#=23-56) in benmoreite and trachyphonolites (Fig. 3). Amphibole has the highest Mg# in the most Mg-rich lava sample (RT-06I-354B), and has *systematically* lower Mg# than the coexisting clinopyroxene, confirming its later appearance in the crystallization order (Supplementary Table S6; Supplementary Fig. S1), and thus bearing no chemical evidence for its crystallization at mantle depths. As with clinopyroxene, there is no correlation between proxies of the crystallization pressure (e.g., the calculated Al^{VI}) and the composition of amphibole in its host lithology (Supplementary Fig. S4). **Biotite** (Mg#=70-76;

TiO_2=6.5-6.8 wt.%) is very rare. **Rhönite** [$Ca_2(Mg,Fe^{2+},Fe^{3+},Ti)_6(Si,Al)_6O_{20}$] is often found as a (subsolidus) rim of amphibole.

Feldspar. Tiny microlites of labradorite (An_{56-59}) to oligoclase (An_{27}) are found in the groundmass of basanites and tephrites, with additional interstitial anorthoclase (Fig. 4a), whereas a continuous trend from andesine (An_{42}) to anorthoclase and sanidine (up to Or_{57}) is found in the trachyphonolites (Fig. 4a). Sr is higher than Ba in plagioclase; they reach 1.9 and 4 wt.%, as oxides, respectively, in alkali feldspar grains of trachyphonolites (Supplementary Table S7). The overall chemistry is more restricted than that observed for the feldspars at the Ankaratra volcanic complex (Fig. 4a).

The interstitial **glass** is trachyphonolitic to phonolitic in composition (Supplementary Table S7).

Feldspathoids. **Leucite** has been found in the groundmass of the basanites; **haüyne** is found in phonotephrites, benmoreites and, particularly, in the groundmass of the trachyphonolites. Haüyne has a significant compositional range, with an almost continuous increase of Na and Cl and decrease of Ca, K and S towards the late crystallized **sodalite** microlites, also found as rims of zoned crystals (Fig. 4b, 4c; Supplementary Fig. S1; Supplementary Table S8). The composition of the volatile-bearing feldspathoids broadly matches the chemical variation of the Mt. Vulture analogues (which are likely the most complete series of sodalite-group *magmatic* feldspathoids), with the exclusion of the most potassic varieties (cf. Fig. 4b, and Melluso et al., 2011b and references therein). A Si-rich **nepheline** ($Q_{8-24}Ks_{5-13}Ne_{68-78}$ in wt.%), with low K_2O (up to 4 wt.%) and variable CaO (up to 2.8 wt.%) completes the groundmass assemblage of holocrystalline samples, including basanites and tephrites (Supplementary Fig. S5; Supplementary Table S8). The Itasy nepheline differs most markedly from that of the Madagascan olivine melilitites, the latter having low silica and very high K (10-12.6 wt.% K_2O; Melluso et al., 2011a; Supplementary Fig. 5), though it still occurs as a groundmass phase, and matches the nephelines of Ankaratra and Ankililoaka (Cucciniello et al., 2017, 2018).

Titanite occurs as rare phenocrysts in benmoreite and trachyphonolites (Supplementary Fig. 1) and modally decreases in the most evolved rocks; it usually co-crystallizes with clinopyroxene. The FeO_t varies from 1.6 and 7.4 wt.%, the $\sum REE_2O_3$ range from 1.4 to 5.7 wt.%, and ZrO_2 reaches concentrations as high as 7.8 wt.%, but it is usually far lower (0-4 wt.%). **Apatite** is ubiquitous as a groundmass phase, and can be found also as microphenocrysts in the phonotephrites. The concentration of F varies from 1.4 to 4.9 wt.% Cl can be high (up to 1.8 wt.%; average 1.19 wt.%), and SO_3 is locally significant (up to 1 wt.% in crystals of a tephrite and 2.3 wt.% in crystals of phonotephrite RT-06I-398; Supplementary Table S9). Rare crystals of **britholite** [$(Ca,LREE,Th)_5(SiO_4,PO_4)_3(OH,F)$] ($SiO_2$=21.7 wt.%; $\sum REE_2O_3$=52 wt.%, F=1.9 wt.%, no Cl and SO_3) are found in the groundmass of trachyphonolites. **Zircon** has been found in the interstices of a trachyphonolite. **Fluorite** is also noted, as well as **hiortdahlite** [ideally

$(Ca,Na)_3(Zr,Ti)Si_2O_7(F,O,OH)_2$] in the groundmass of the trachyphonolite RT-061-379 (Supplementary Table 9). Hiortdahlite has been noted in the Ampasindava phonolites (northern Madagascar; Cucciniello et al., 2016) and, together with the Na-rich clinopyroxene, indicates the transition of the groundmass liquids to peralkaline compositions. Other accessories and secondary zeolites (mostly analcime around nepheline) are present in the interstices.

4. Bulk-rock geochemistry

The concentration of MgO, Cr and Ni in the most primitive basanites (9-9.2 wt.%, 277-288 ppm and 154-164 ppm, respectively), the Mg# (56-59) and the relatively low forsterite content of the olivine phenocrysts indicate that the most primitive Itasy rocks can be considered as evolved liquid compositions which suffered previous removal of Mg-rich olivine, Cr-spinel and Mg-rich clinopyroxene from more primitive basanites. At the same time, basanites and tephrites have high concentration of TiO_2 (3-4.7 wt.%) and P_2O_5 (0.6-1.9 wt.%) (Table 1; Supplementary Table S1). The variations of CaO, TiO_2, Al_2O_3, Fe_2O_{3t} and alkalies of the mafic rocks, and the mineral composition in basanites and tephrites depict trends at least qualitatively compatible with removal of pyroxene, amphibole, olivine and oxides, and minor or negligible removal of feldspar and apatite (Supplementary Fig. S5). The transition from phonotephrite to benmoreite and trachyphonolites is characterized by no significant variation of Al_2O_3, a change of slope of many minor and trace element trends, a drop in the concentration of P_2O_5, and a decrease of Y with MgO. The concentration of Ba and Sr also drops in the most evolved trachyphonolites (Supplementary Fig. S6). The variations of Rb and Ba of the basanites and other features suggest some heterogeneity in the composition of the mafic parental magmas. The Zr/Hf ratios increase from 45 in the basanites to 60 in the evolved trachyphonolites, whereas the Nb/Ta ratio is 14-15 in the basanites and 21-28 in the most evolved trachyphonolites (Table 1; Supplementary Fig. S7). The La/Nb, Ba/Nb, Ce/Pb and Nb/U ratios of the least evolved basanites (La/Nb=0.83-0.88, Ba/Nb=8-12, Ce/Pb=30-41 and Nb/U=42-52) match the values expected from mantle-derived magmas free of effects related to crustal contamination in the source or *en route* to the surface, and the low Zr/Nb of the basanites (4.2-4.8) indicate a highly enriched source region (Melluso et al., 2016 and references therein). The REE patterns of the mafic rocks (Supplementary Fig. S8a) are smooth and highly fractionated (La/Yb_n=24-27), have no peaks or troughs at Eu, and increase in the total REE concentration (279-800 ppm) from basanites to the phonotephrites. Starting from the phonotephrites RT-06I-398 and RT-06I-397, the REE patterns of benmoreites and trachyphonolites become increasingly concave, with a marked decrease of intermediate-REE to values even lower than those of the basanites (sample RT-061-357B; Supplementary Fig. S8a, c, d, e), largely constant La_n and Lu_n, and small

troughs at Eu (Eu/Eu*=0.79). These characteristics are highlighted when REE are compared to the concentration of the least evolved basanite RT-061-354B (Supplementary Fig. S8e). The mantle normalized patterns of the Itasy basanites (Fig. 5a, 5b) are almost flat from Rb to Th, have a peak at Nb and Ta, a trough at K and Pb, and a smooth decreasing slope towards the HREE, with no trough at Zr and Hf, confirming the similarity of the trace element enrichment in the mantle sources throughout the Cenozoic province (cf. Melluso et al., 2016). The very marked geochemical differences with the primitive (MgO=9-12 wt.%) *haüyne-leucite*-basanites of Mt.Vulture (Italy), which were generated in a subduction-modified upper mantle source (e.g., Beccaluva et al., 2002), and the similarities with the potassic basanites of the Virunga area (Congo-Rwanda, western branch of the East African Rift), another within-plate volcanic area as is Itasy (e.g., Rogers et al., 1992), are highlighted in Fig. 5.

5. The concentration of trace elements in titanite, clinopyroxene, kaersutite and anorthoclase of Itasy trachyphonolites

The mantle normalized patterns of the evolved rocks (Fig. 5c) show relative decrease of P, Ti, Ba, Sr, Ta, Y and middle-REE, and relative increase of Rb, Th, U, Nb, Zr and Hf from the least to the most evolved trachyphonolites. In order to understand the changes of the chemical composition of the trachyphonolites, we also investigated the geochemistry of titanite, kaersutite, clinopyroxene and anorthoclase phenocrysts of the trachyphonolite RT-06I-355 (Table 2; Fig. 6; Supplementary Fig. S8). The **titanites** have very high concentration of REE (ΣREE=28,000-31,500 ppm), Y (1730-2250 ppm), Ta (650-1130 ppm), Th (134-187 ppm), V (216-328 ppm) and Hf (140-202 ppm), high Zr (4500-5800 ppm), Nb (6200-15230 ppm), U (15-27 ppm) and La/Yb_n ratios (19-28), no troughs at Eu in the chondrite-normalized REE diagrams (Supplementary Fig. S8b), and low Ba (42-49 ppm), Pb (<1.1 ppm) and Sr (54-382 ppm). The Nb/Ta ratio of the titanites is low (8-13) and the Th/U is high (8.5-10.3), with respect to typical chondritic ratios (15 and 3.6-4, respectively). The titanites also have slight chemical zoning, with an increasingly concave REE pattern (Table 2; Supplementary Fig. S8b). The patterns of the Itasy titanites are generally similar, but displaced to higher REE concentrations, to those reported by Marks et al. (2008) and Melluso et al. (2010) on titanites of alkaline intrusive rocks of variable degree of evolution (clinopyroxenites, ijolites, monzosyenites, to agpaitic nepheline syenites; Supplementary Fig. 8g), which also have widely variable Nb/Ta ratios (8-66). The Itasy titanite/bulk-rock elemental ratios are of the same magnitude of the partition coefficients of Olin and Wolff (2012) only for La, Ce and Lu (Supplementary Fig. 8f). **Kaersutite** is a corroded phase, and has a different trace element pattern, with a concentration of

ΣREE which is one or two orders of magnitude lower than the concentration of REE of the coexisting titanites (911 ppm; La_n= 419 times chondrite; Table 2). It still has relatively high Li (144 ppm), Y (81 ppm), Zr (732 ppm), Nb (200 ppm), moderate Ba (1100 ppm) and very low Rb, Pb, Th and U, when compared to the host-rock bulk composition (Table 1; Fig. 6b). The **clinopyroxene** has low concentration of REE (ΣREE=350-690 ppm; La/Yb_n=8-15), and very low concentration of other elements (Table 2), excluding Zn (600-662 ppm). **Anorthoclase** has high and variable Ba (1500-28220 ppm), Sr (534-4300 ppm), Rb (7-98 ppm), Pb (4.6-9 ppm) and Eu (0.5-1.6 ppm). These elements peak in the mantle-normalized diagrams (Fig. 6b). Other chemical details can be found in the Table 2.

6. Isotopic composition of the Itasy rocks

The isotopic composition of Itasy rocks is reported in the Table 3. The basanites (MgO= 7-10 wt.%) have a restricted range of $^{87}Sr/^{86}Sr$ (0.70366-0.70378), $^{143}Nd/^{144}Nd$ (0.51274-0.51277) and Pb isotopes ($^{206}Pb/^{204}Pb$=18.7-18.9; $^{207}Pb/^{204}Pb$=15.53-15.56; $^{208}Pb/^{204}Pb$=38.89-39.01), which indicate a largely uniform mantle source, characterized by low time-integrated Rb/Sr and Sm/Nd ratios. This source is isotopically similar, but not identical, to that of the mafic alkaline rocks of the Ankaratra (nephelinites, basanites and alkali basalts; cf. Melluso et al., 2016; Cucciniello et al., 2017; Fig. 7) and to that of the olivine melilitites to the east and northeast of Ankaratra (Melluso et al., 2011a), which do not have evidence of crustal contamination. The phonotephrites have $^{87}Sr/^{86}Sr$=0.70394-0.70398, $^{143}Nd/^{144}Nd$= 0.51273-0.51274, $^{206}Pb/^{204}Pb$=18.74-18.84, $^{207}Pb/^{204}Pb$=15.53-15.54 and $^{208}Pb/^{204}Pb$=38.97-39.02, all values broadly similar (or indistinguishable in some isotope ratios) to those of the basanites, whereas the benmoreite and the trachyphonolites have higher $^{87}Sr/^{86}Sr$ (0.70430-0.70446) and lower $^{143}Nd/^{144}Nd$ (0.51266-0.512682), $^{206}Pb/^{204}Pb$ (18.18-18.39), $^{207}Pb/^{204}Pb$ (15.49-15.51) and $^{208}Pb/^{204}Pb$ (38.38-38.57) than the mafic rocks. Therefore, the isotopic composition of the Itasy rocks changes with MgO. A broadly similar isotopic variation between associated mafic and evolved rocks has been noted in both Cretaceous and Cenozoic volcanic rocks of Madagascar (cf. Cucciniello et al., 2010, 2013, 2017) and indicates that, if basanites and trachyphonolites (which crop out in the same area and have the same stratigraphic age) are part of a comagmatic suite, the evolved rocks suffered interaction with the old, low-Pb/Pb basement rocks during magmatic evolution in low-pressure magma reservoirs. This part is developed in the discussion.

7. Discussion

7.1. The unusual transition between basanites/tephrites and trachyphonolites

The Itasy volcanic rocks have some interesting petrogenetic features shared with those of other volcanic areas worldwide: 1) the leucite-bearing basanites recall analogues found in other areas (e.g., the Roman Province, the western branch of the East African Rift); 2) the presence of haüyne (±sodalite)-bearing alkaline volcanic rocks is found in alkaline rocks of various tectonic settings (e.g., Massif Central: Vatin-Perignon, 1968; Eifel: Wörner and Schmincke, 1984; Tenerife: Bryan, 2006; Mt. Etinde: Nkombou et al., 1995; Mt. Vulture: Beccaluva et al., 2002; Melluso et al., 1996, 2011b, among other places), and indicate abundant sulfur in the oxidized state (and chlorine as well); 3) trachyphonolites similar to those of Itasy are common evolved lithotype of other major volcanic areas (e.g., Suswa, Kenya; Phlegrean Fields-Ischia, Italy). These trachyphonolites are the product of low-pressure fractional crystallization processes, possibly in an open system. From a more general view, basanites and tephrites (and maybe also some nephelinite types) are associated with phonolites *s.s.*, rather than trachyphonolites, as is found in northernmost Madagascar and elsewhere (e.g., le Roex et al., 1990; Ablay et al., 1998; Melluso et al., 2007; Berger et al., 2014). In contrast, trachytes (trachyphonolites) are typically associated with (potassic or sodic) alkali and transitional basalts (e.g., Marion Island, le Roex et al., 2012; St. Helena, Kawabata et al., 2010 and references therein; Ischia-Phlegrean Fields, Fedele et al., 2008; Melluso et al., 2012, 2014; Libya, Lustrino et al., 2012; Mauritius: Sheth et al., 2003; Ashwal et al., 2016; Ethiopian Rift, Ronga et al., 2010; Kenya Rift: White et al., 2012).

The magmatic evolution of the Itasy basanites and tephrites (the most Mg-rich of them equilibrated with olivine at temperatures just lower than 1200°C, according to Roeder and Emslie, 1970), is without any evidence of removal of plagioclase or leucite, because these phases are found exclusively as tiny groundmass microlites (e.g., Supplementary Fig. 1). Sodic plagioclase appears as a phenocryst phase in benmoreites; anorthoclase and Na-sanidine (plus rare mafic phases) are the dominant phenocrysts and groundmass phases in the trachyphonolites. It is thus evident that removal of Na-feldspars was essential for the evolution of (sodic) trachyphonolitic liquids towards the phonolite minimum. This is also indicated by the position of the evolved samples in the Petrogeny Residua's System, which plot between the trachytic and the phonolitic minima (slightly less than 900°C, at 1 kbar P_{H2O}), hence within the silica undersaturated field (Fig. 8a, b). The tendency of the bulk-rock trachyphonolitic compositions to plot close to the composition of their (Na-rich) alkali feldspars (Fig. 4a) can be considered as the *normal* evolution towards the pertinent minimum melt compositions. The lack of *phenocrysts* of sodic feldspathoids is another indication that the bulk-rock compositions approach, but do not reach, the phonolitic minimum. For comparison, the phonolites

(*s.s.*) of northernmost Madagascar (Melluso et al., 2007; Cucciniello et al., 2016) have nepheline phenocrysts, and plot on the alkali feldspar-nepheline cotectics (Fig. 8b).

The volatiles that left trace in the Itasy magmatic system are H_2O (hosted in amphibole, apatite, the rare biotite, and glass), SO_3 (hosted in the haüyne-sodalite solid solutions and in apatite), Cl (hosted in sodalite, apatite and glass) and F (hosted in apatite, amphibole, glass, fluorite and other accessories). No evidence for a significant role of CO_2 in the petrogenesis of the Itasy basanites and trachyphonolites has been found, as expected by the insignificant maximum quantity of this compound that can be theoretically dissolved in basanitic melts at low pressure, when compared to H_2O (e.g., Shishkina et al., 2014), a quantity even lower in trachytes and phonolites (e.g., Webster et al., 2014). The Itasy basanites and tephrites have significant amounts of kaersutite, indicating that the magmatic crystallization took place in a H_2O-rich environment at relatively early differentiation stages. Kaersutite is unknown in basanites and alkali basalts (and nephelinites too) of the nearby Ankaratra complex, that have mostly anydrous mineral assemblages, and occurs as a phenocryst phase only in a few benmoreites (Cucciniello et al., 2017). Kaersutite *s.s.* crystallizes in mafic, hydrous, feldspar-bearing (or -normative), high-Ti alkaline magmas, and has a range of crystallization depths from the uppermost mantle (e.g., Irving and Green, 2008; Pilet et al., 2010) to shallow conduits or shallow intrusions (e.g., Melluso et al., 2005, 2007); hence this phase is more a chemical than a barometric indicator (cf. Supplementary Fig. S4). Sulfur was at least partially partitioned in the S-bearing apatite before reaching saturation as haüyne, in the groundmass of the phonotephrites and in the evolved rocks; sulfur decreases in the latest crystallized groundmass, as testified by the presence of sodalite (cf. also Supplementary Fig. S1).

7.2. Petrogenetic modelling: the essential role of titanite and anorthoclase removal in the geochemical evolution of the trachyphonolites, and open-system processes

The petrogenetic study of the Itasy volcanic rocks is focused on the genetic relationships between this bimodal suite of mafic and evolved rocks, with their changing isotopic ratios and the marked decrease in the degree of silica undersaturation of the evolved rocks. Despite the compositional gap between mafic and evolved rocks shown in the diagrams, involving a marked change of density, temperatures and time of storage in shallow reservoirs, we observe the following: 1) the mineral phases have a continuous compositional change from mafic, through intermediate, to felsic rocks, as a typical consequence of fractional crystallization processes (see above); 2) the bulk-rock compositions have the expected changes considering the variety and amount of the phenocryst phases, thus excluding effects of magma mixing; 3) many basanites and tephrites are rich in phenocrysts/megacrysts of kaersutite (a phase significantly lower in silica than clinopyroxene but

with similar density), whose significant removal could help increase the concentration of SiO_2 of residual melts.

The variation diagrams (Supplementary Fig. S6) and the petrography of the mafic rocks indicate that clinopyroxene, amphibole, olivine and magnetite (for Fe and Ti) are probably the best candidates to form the subtracted mineral assemblages in the transition from basanites to phonotephrites. Among several models using the major element compositions of bulk-rocks and their phenocryst phases, the transition from basanites (e.g. RT-06I-354B) to tephrites (RT-061-395) and benmoreite (RT-06I-387) can be accounted for by 37% and 56% removal of ultramafic assemblages, respectively. The transition from the benmoreite RT-06I-387 to the trachyphonolite RT-06I-375B needs 61% removal of monzonitic assemblages. The total transition from the basanite RT-06I-354B to a trachyphonolite (e.g., sample RT-06I-375B) was modelled with 71.4% removal of ultramafic assemblages (cf. Supplementary Table S10). The results we choose have low ΣR^2 (values of $\Sigma R^2 << $ or <0.5 can be considered for modelling, but they are not proof of geological reliability), but the high kaersutite/clinopyroxene ratio involved in some transitions between mafic rocks is always to be matched with the actual subtracted assemblages, which are, of course, largely unknown.

Thermodynamic models of magmatic evolution (e.g., MELTS) are not able to account for the presence of kaersutite, sodalite-group minerals, titanite and a number of other petrographic features of alkaline rock suites, including the crystallization sequence, the phase composition and their actual amount. LeMasurier et al. (2011) hypothesized a significant role for kaersutite removal in order to account for the petrogenesis of evolved silica oversaturated rocks starting from basanite parental magmas; in our case, we show that this effect must be limited to the transition from tephrites to benmoreites, because the final transition to the most evolved Itasy trachyphonolites cannot involve significant removal of amphibole (kaersutite is already a minor phenocryst phase in the least evolved trachyphonolites).

A number of observations and models indicate that the Itasy benmoreites and trachyphonolites could be comagmatic with the basanites, through (also) the effects of kaersutite removal. The trace element variations using thorium as the most incompatible element were modelled using the Rayleigh equation (Supplementary Fig. S7). The following features are of interest: a) assuming that Th behaves in a closed system (an approximation that cannot be guaranteed during AFC processes, see below) and that is the most incompatible element, the total amount of crystallization needed to reach the phonotephritic liquids is roughly 60%, and is 75-80% to reach evolved trachyphonolites, starting from the least evolved basanites; b) the transition from basic to intermediate rocks is characterized by several major changes in the slope of the trace elements vs. the Th concentration and, therefore, in their bulk partition coefficients (D); this change in slope takes place at different evolution points (Supplementary Fig. S6 and S7); c) tantalum (Ta) behaves as a highly compatible element in the

417 trachyphonolites, thus strongly decouples from the geochemically similar element Nb; roughly
418 similar fractionation is noted between Hf and Zr, whereas U and Th behave sympathetically (the
419 Th/U ratio ranges between 3.6 and 4.4, both values in basanites); d) lead (Pb) increases more than
420 that expected from a perfectly incompatible behaviour (modelling requires $D_{Pb}<0$; Supplementary
421 Fig. S7), strongly suggesting the introduction of external Pb during crustal contamination processes;
422 e) the chemical composition of the trachyphonolites is scattered, indicating that the magmatic
423 evolution took place in independent magma feeder systems, hence with variable distribution,
424 crystallization and removal of phases.
425 The petrography, the increasingly concave REE patterns of the trachyphonolites, the trace element
426 concentration of the titanite phenocrysts, and numerical modelling using both published partition
427 coefficients and the mineral composition determined by LA-ICP-MS (Supplementary Fig. S8)
428 indicate a major effect of titanite on the fractionation of middle-REE, Y, Ta and other elements,
429 even though full quantification of the extent of removal of an accessory phase cannot be obtained
430 through major oxide mass balance calculations or trace element behaviour. The trend to the most
431 evolved trachyphonolites can be obtained through 0.7-1% removal of titanite (cf. Supplementary
432 Fig. S8c, d). Removal of small amounts of titanite is commonplace in evolved alkaline rocks (cf. the
433 extremely similar patterns reported in Ulrych et al., 2006; Lustrino et al., 2012; Melluso et al., 2014,
434 2017 and references therein), and the effects observed in this work are broadly those expected
435 utilizing known titanite/melt partitioning data (e.g., Olin and Wolff, 2012; Supplementary Fig. S8c,
436 Supplementary Table S11). Apatite can have a roughly similar behaviour regarding middle-REE
437 fractionation, although to a lower extent (the partition coefficients of apatite can be lower of a factor
438 of 3-4; cf. Supplementary Table S11 and Supplementary Fig. S8c), but has negligible effect on the
439 concentration of Ta, Hf, Zr and Nb. Removal of other phases such as clinopyroxene or amphibole, in
440 the amount observed in the least evolved trachyphonolites (Supplementary Fig. S1), cannot have
441 appreciable role in preferentially removing middle- from heavy-REE in evolved melts (cf.
442 partitioning data of Tiepolo et al. 2007; Fedele et al., 2009; Melluso et al., 2017; this work), and so
443 is for other accessory phases *absent* at Itasy (e.g., melanite garnet, or significant zircon).
444 The evolved samples of Itasy show compelling evidence for open-system evolution, as seen from the
445 isotopic variations and elemental evidence above. We performed an AFC model (DePaolo, 1981)
446 utilizing all the isotopic systematics, pertinent trace elements and compositions of the Madagascan
447 basement in the area. The results highlight the effects of prolonged fractional crystallization (roughly
448 70%) and limited, though widely variable, crustal contamination (the values of the
449 assimilation/cumulus rate, -r-, are <0.3) of known felsic rocks of the Precambrian basement (details
450 in Fig. 9). The model takes into account the marked changes in the bulk partition coefficients of
451 many elements at varying levels of magmatic evolution (Supplementary Fig. S8). The

phonotephrites (samples RT-06I-397 and RT-06I-398) still need limited amount of crustal contamination in order to account for their slightly differing isotopic ratios compared to those of basanites and tephrites. The abrupt change of partition coefficients in the evolved rocks and a limited change of the parameter "r" (Fig. 9) led to the bimodal isotopic compositions. It is also evident that the effects of crustal contamination did not act uniformly throughout the Itasy suite, and that other processes could have been operative in the Itasy feeder system, including silica increase that may be expected from interaction with the felsic lithologies of the Madagascan basement, and the presence of alkali basaltic parental magmas (more SiO_2-rich than a basanite), of which there is no evidence, *to date*.

7.3. The mantle sources of Itasy in the context of the Cenozoic magmatism of Madagascar

The Itasy basanites have Sr-Nd-Pb-isotopic ratios indicating a source geochemically and isotopically different from that of convecting asthenosphere, which experienced a distinct evolution with time. This is fully consistent with what is known in the Cenozoic mafic rocks of the central Madagascar (Ankaratra, Takarindiona and Alaotra), which were emplaced through Archean crust (Melluso et al., 2011a, 2016; Cucciniello et al., 2017). Primitive basanitic magmas with the petrographic and geochemical characteristics similar to those of the Itasy imply low degrees of partial melting (ca. 3%) of a hydrous, amphibole-bearing lherzolite, and hence at depths and temperatures where *pargasitic* amphibole can be a stable phase of a peridotite (say, <90-100 km; e.g., Kovacs et al., 2017), as previously suggested by earlier work in central and northern Madagascar (Melluso and Morra, 2000; Melluso et al., 2016 and references therein; Rocco et al., 2017), and elsewhere (cf. le Roex et al., 2001; Green and Falloon, 2015). A relatively shallow depth of the (lithospheric) source region of the Itasy basanites is also indicated by a rootless low-velocity zone (supposedly melt-, volatile- or light phases-bearing) just beneath the Moho, extending at depths of 50-80 km (Fig. 1c; Pratt et al., 2017). The E-W-trending extensional processes active in central Madagascar seem to have favoured moderate uplift of this geochemically enriched, volatile-bearing lithospheric mantle, bringing it above the solidus and forming the Itasy low-volume basanitic lava field. The source of the Itasy basanites must be characterized by a significant enrichment of highly incompatible elements (cf. the low Ba/Nb and Zr/Nb ratios, and the shape of the mantle normalized patterns), with particular reference to the HFSE, in agreement with a fully within-plate origin, without subduction-related components or low-pressure crustal contamination. The source of the Itasy basanites cannot be depleted asthenospheric -or primitive- mantle, assuming any reasonable degrees of partial melting and considering the isotopic composition (cf. also Melluso et al., 2016 and Cucciniello et al., 2018, for a regional review). Finally, in terms of trace element and isotopic composition, the sources of the

Cenozoic volcanic rocks of Madagascar share very little with those giving rise the Cretaceous *tholeiitic* magmatism, implying different melting regimes of differently located mantle sources (cf. Melluso et al., 2001, 2005, 2011a, 2016; Cucciniello et al., 2010, 2013, 2017).

8. Conclusions

The Itasy volcanic field, the most recently active in Madagascar, is characterized by an association of high-TiO_2, potassic, basanites/tephrites/phonotephrites, and benmoreites/ trachyphonolites, in the facies of pyroclastic rocks and lava flows, with the highly featuring presence of Ti-rich amphibole (and leucite) in mafic/intermediate rocks and haüyne-sodalite in evolved rocks. Recognizing the possibility of independent basanitic parental magmas and different liquid lines of descent, leucite basanite magmas evolved through removal of olivine, clinopyroxene, kaersutite and magnetite to reach the volumetrically minor benmoreitic and trachyphonolitic compositions. These latter rocks are likely the result of low-pressure fractional crystallization of anorthoclase/sanidine-bearing (*syenitic*) assemblages and minor crustal contamination of the high-$^{87}Sr/^{86}Sr$, low- $^{143}Nd/^{144}Nd$, -$^{206}Pb/^{204}Pb$, -$^{207}Pb/^{204}Pb$ and -$^{208}Pb/^{204}Pb$, old granitic-migmatitic basement of the area, with the evidence of minor titanite removal (perhaps <2%), as part of syenitic/monzosyenitic cumulates. Titanite is demonstrated to be a very efficient scavenge of intermediate-REE, Y, Ta and V, and slightly less so for Nb, Zr and Hf in the Itasy trachytic (*s.l.*) magmas (cf. Table 2); its removal, even in small amounts, significantly increases ratios between otherwise geochemically similar elements (e.g., Zr/Hf, Nb/Ta) when compared to those of the associated mafic rocks. Another minor but interesting result of this study is the evidence that the concentration of rare earths or other strategic elements in the most highly evolved alkaline magmas cannot be considered a rule working worldwide, due to the presence of accessory phases on the liquidus, which effectively scavenge these elements in less evolved melts. *Also* due to the removal of titanite and other accessory phases, the geochemical characteristics of trachytic (*s.l.*) rocks *worldwide* cannot give unambiguous indication about those of associated (or parental) mafic magmas, or even to indicate mantle signatures of any kind, including ratios of elements thought to be highly incompatible. The geochemical and isotopic characteristics of the leucite-basanites broadly match those of the nearby Ankaratra volcano and of the rest of the Cenozoic volcanic districts of Madagascar (Melluso et al., 2016), and testify to a mantle source having marked enrichment in LILE, HFSE and volatile elements (H_2O, Cl, F, SO_3), as noted in other within-plate strongly alkaline rocks worldwide and, intriguingly, also in some subduction-related alkaline rocks. The broadly E-W extensional processes common in central Madagascar triggered low-degree partial melting of enriched, volatile-rich, lithospheric mantle, and generated the low-volume Itasy basanites, without the need to invoke the

action of mantle plumes. Enriched geochemical components of within-plate origin are commonplace in the Madagascan lithospheric mantle (Melluso et al., 2016; Rocco et al., 2017). Finally, the unusual petrogenetic association between basanites and trachyphonolites, and the likely significant removal of kaersutitic amphibole in some basanites and tephrites, are of importance in identifying the volatile species of within-plate alkaline rocks in the mantle sources and during the magmatic evolution.

A high-resolution geochronological framework is now needed to establish an accurate age span for the Itasy, if a significant temporal lapse exists between mafic and evolved rocks, and the relationships between timing of volcanism and extensional tectonics of central Madagascar.

Acknowledgements

This paper is dedicated to the memory of Fabio Carmine Mazzeo.

Alessio Langella, Sergio Bravi, Petrus Le Roux, Roberto de' Gennaro, Vohangy Ratrimo, Dieudonné Razafimahatratra, Vincenza Guarino, Luigi Franciosi and Lorenzo Fedele are gratefully thanked for helping us in sampling, data acquisition and comments on an early draft of the manuscript. The constructive reviews of Jean-Paul Liégeois and Michael Marks and advice of the Editor-in-chief Xian-Hua Li were very helpful to improve contents and presentation of an early version of the manuscript.

This paper was supported by grants provided by PRIN2015 (grant 20158A9CBM) and LR5 (Regione Campania) to L. Melluso, and Fondi Ricerca di Ateneo (DR_3450_2016) to C. Cucciniello.

References

Ablay, G.J., Carroll, M.R., Palmer, M.R., Martí, J., Sparks, R.S.J., 1998. Basanite–phonolite lineages of the Teide–Pico Viejo volcanic complex, Tenerife, Canary Islands. Journal of Petrology 39, 905-936.

Andrianaivo, L., Ramasianoro, V.J., 2010. Relation between regional lineament systems and geological structures: implications for understanding structural controls of geothermal system in the volcanic area of Itasy, Madagascar. Proceedings World Geothermal Congress, Bali, 1-9.

Andrianaivo, L., Ramasianoro, V.J., 2011. Relations between drainage pattern and fracture trend in the Itasy geothermal prospect, central Madagascar. Madamines 2, 22-39.

Ashwal, L.D., Torsvik, T.H., Horvath, P., Harris, C., Webb, S., Werner, S., Corfu, F., 2016. A mantle-derived origin for Mauritian trachytes. Journal of Petrology 57, 1645–1675.

557 Battistini, R., 1962. Le massif volcanique de l'Itasy (Madagascar). Annales Geographie 384, 167-
558 178.
559 Beccaluva, L., Coltorti, M., Di Girolamo, P., Melluso, L., Milani, L., Morra, V., Siena, F., 2002.
560 Petrogenesis and evolution of Mt. Vulture alkaline volcanism (Southern Italy). Mineralogy and
561 Petrology 74, 277-297.
562 Berger, J., Ennih, N., Mercier, J.-C.C., Liegeois, J.-P., 2014. Extreme trace element fractionation in
563 Cenozoic nephelinites and phonolites from the Moroccan Anti-Atlas (Eastern Saghro). Lithos 210-
564 211, 69-88.
565 Boynton, W.B., 1984. Cosmochemistry of rare earth elements: meteorite studies. In Henderson P.
566 (ed.) Rare Earth Element Geochemistry. Elsevier, Amsterdam, 63-114.
567 Brenon, P., Bussiere, P., 1959. Le volcanism à Madagascar. Bulletin Volcanologique 21, 77-93.
568 Brown, S.K., Sparks, R.S.J., Mee, K., Vye-Brown, C., Ilyinskaya, E., Jenkins, S.F., Loughlin, S.C.,
569 2015. Country and regional profiles of volcanic hazard and risk. In: Loughlin S.C., Sparks, R.S.J.,
570 Brown, S.K., Jenkins, S.F., Vye-Brown, C. (eds.): Global Volcanic Hazards and Risk. Cambridge
571 University Press.
572 Bryan, S.E., 2006. Petrology and geochemistry of the Quaternary caldera-forming, phonolitic
573 Granadilla eruption, Tenerife (Canary Islands). Journal of Petrology 47, 1557-1589.
574 Bussiere, P., 1957. Part XII. Le massif volcanique de l'Itasy. In: Besairie, H., Boulanger, J., Brenon,
575 P., Bussiere, P., Emberger, A., de St. Ours, J.: Le Volcanisme à Madagascar. Travaux du Bureau
576 Géologique no. 83, Service Géologique de Madagascar, Tananarive, 240 pp.
577 Cucciniello, C., 2016. Tetra-Plot: A Microsoft Excel spreadsheet to perform tetrahedral diagrams.
578 Periodico di Mineralogia 85, 115-119.
579 Cucciniello C., Langone A., Melluso L, Morra V., Mahoney J.J., Meisel T., Tiepolo M., 2010. U-Pb
580 ages, Pb-Os isotopes and platinum group element (PGE) composition of the west-central
581 Madagascar flood basalt province. The Journal of Geology 118, 523-541.
582 http://dx.doi.org/10.1086/655012
583 Cucciniello C., le Roex A.P., Jourdan F., Morra V., Grifa C., Franciosi L., Melluso L., 2018. The
584 mafic alkaline volcanism of SW Madagascar (Ankililoaka, Tulear region): $^{40}Ar/^{39}Ar$ ages,
585 geochemistry and tectonic setting. Journal of the Geological Society, London, in press,
586 http://dx.doi.org/10.1144/jgs2017-139
587 Cucciniello, C., Melluso, L., Jourdan, F., Mahoney, J.J., Meisel, T., Morra, V., 2013. ^{40}Ar-^{39}Ar ages
588 and isotope geochemistry of Cretaceous basalts in northern Madagascar: refining eruption ages,
589 extent of crustal contamination and parental magmas in a flood basalt province. Geological
590 Magazine 150, 1-17. http://dx.doi.org/10.1017/S0016756812000088

591 Cucciniello, C., Melluso, L., le Roex, A.P., Jourdan, F., Morra, V., de' Gennaro, R., Grifa, C., 2017.
592 From nephelinite, basanite and basalt to peralkaline trachyphonolite and comendite in the
593 Ankaratra volcanic complex, Madagascar: $^{40}Ar/^{39}Ar$ ages, phase compositions and bulk-rock
594 geochemical and isotopic evolution. Lithos 274-275, 263-271.
595 http://dx.doi.org/10.1016/j.lithos.2016.12.026
596 Cucciniello, C., Melluso, L., Morra, V., Storey, M., Rocco, I., Franciosi, L., Grifa, C., Petrone,
597 C.M., Vincent, M., 2011. New ^{40}Ar-^{39}Ar ages and petrogenesis of the Massif d'Ambre volcano,
598 northern Madagascar. In: Beccaluva, L., Bianchini, G., Wilson, M. (eds.) Volcanism and
599 Evolution of the African Lithosphere. Geological Society of America Special Papers 478, 257-
600 282. http://dx.doi.org/10.1130/2011.2478(14)
601 Cucciniello, C., Tucker, R.D., Jourdan, F., Melluso, L., Morra, V., 2016. The age and petrogenesis
602 of the alkaline magmatism of Ampasindava Peninsula and Nosy Be archipelago, northern
603 Madagascar. Mineralogy and Petrology 110, 309-331. http://dx.doi.org/10.1007/s00710-015-
604 0387-1
605 DePaolo, D.J., 1981. Trace element and isotopic effects of coupled fractional crystallization and
606 crustal contamination processes. Earth and Planetary Science Letters 53, 189-202.
607 Fedele, L., Lustrino, M., Melluso, L., Morra, V., Zanetti, A., Vannucci, R., 2015. Trace element
608 distribution in plagioclase, alkali feldspar, Ti-magnetite, biotite and apatite in evolved potassic
609 liquids from Campi Flegrei (Southern Italy). American Mineralogist 100, 233-249. doi:
610 10.2138/am-2015-4995
611 Fedele, L., Scarpati, C., Lanphere, M.A., Melluso, L., Morra, V., Perrotta, A., Ricci, G., 2008. The
612 Breccia Museo formation, Campi Flegrei, southern Italy: geochronology, chemostratigraphy and
613 relationships with the Campanian Ignimbrite eruption. Bulletin of Volcanology 70, 1189-1219.
614 http://dx.doi.org/10.1007/s00445-008-0197-y
615 Fedele, L., Zanetti, A., Lustrino, M., Melluso, L., Morra, V., Vannucci, R., 2009. Insights on
616 clinopyroxene/liquid trace element partitioning in natural trachyte-phonolite systems: a EMP/LA-
617 ICP-MS case study from Campi Flegrei (Italy). Contributions to Mineralogy and Petrology 158,
618 337-356. http://dx.doi.org/10.1007/s00410-009-0386-5
619 Galer, S.J.G., Abouchami, W., 1998. Practical application of lead triple spiking for correction of
620 instrumental mass discrimination. Mineralogical Magazine 62A, 491-492.
621 Green, D.H., Falloon, T.J., 2015. Mantle-derived magmas: intraplate, hot-spots and mid-ocean
622 ridges. Scientific Bulletin 60, 1873-1900.
623 Gupta, A.K., 2015. Origin of potassium-rich silica-deficient igneous rocks. Springer, 536 pp. ISBN:
624 978-81-322-2082-1

625 Irving, A.J., Green, D.H., 2008. Phase relationships of hydrous alkalic magmas at high pressures:
626 production of nepheline hawaiitic to mugearitic liquids by amphibole-dominated fractional
627 crystallization within the lithospheric mantle. Journal of Petrology 49, 741-756.
628 Kawabata, H., Hanyu, T., Chang, Q., Kimura, J.-I., Nichols, A.R.L., Tatsumi, Y., 2011. The
629 petrology and geochemistry of St. Helena alkali basalts: evaluation of the oceanic crust-recycling
630 model for HIMU OIB. Journal of Petrology 52, 791-838.
631 http://dx.doi.org/10.1093/petrology/egr003
632 Kovacs, I., Lenkey, L., Green, D.H., Fancsik, T., Falus, G., Kiss, J., Orosz, L., Angyal, J., Vikor Z.,
633 2017. The role of pargasitic amphibole in the formation of major geophysical discontinuities in
634 the shallow upper mantle. Acta Geodynamica et Geophysica 52, 183–204.
635 Kröner, A., Hegner, E., Collins, A.S., Windley, B.F., Brewer, T.S., Razakamanana, T., Pidgeon,
636 R.T., 2000. Age and magmatic history of the Antananarivo Block, Central Madagascar, as
637 derived from zircon geochronology and Nd isotopic systematics. American Journal of Science
638 300, 251-288.
639 Lacroix, A., 1923. Mineralogie du Madagascar. vol. 3. Augustin Challamel, Paris.
640 LeMasurier, W.E., Choi, S.H., Kawachi, Y., Mukasa, S.B., Rogers, N.W., 2011. Evolution of
641 pantellerite-trachyte-phonolite volcanoes by fractional crystallization of basanite magma in a
642 continental rift setting, Marie Byrd Land, Antarctica. Contributions to Mineralogy and Petrology
643 162, 1175–1199.
644 le Roex, A.P., Chevallier, L., Verwoerd, W.J., Barends, R., 2012. Petrology and geochemistry of
645 Marion and Prince Edward islands, southern Ocean: magma chamber processes and source region
646 characteristics. Journal of Volcanology and Geothermal Research 223-224, 11-28.
647 le Roex, A.P., Cliff, R.A., Adair, B.J.I., 1990. Tristan da Cunha, South Atlantic: geochemistry and
648 petrogenesis of a basanite-phonolite lava series. Journal of Petrology 31, 779-812.
649 le Roex, A.P., Späth, A., Zartman, R.E., 2001. Lithospheric thickness beneath the southern Kenya Rift:
650 implications from basalt geochemistry. Contributions to Mineralogy and Petrology 142, 89-106.
651 Lessing, P., Grout, C.McD., 1971. Haüynite from Edwards, New York. American Mineralogist 56,
652 1096-1100.
653 Lustrino, M., Cucciniello, C., Melluso, L., Tassinari, C.C.G., de' Gennaro, R., Serracino, M., 2012.
654 Petrogenesis of Cenozoic volcanic rocks in the NW sector of the Gharyan volcanic field, Libya.
655 Lithos 155, 218-235. http://dx.doi.org/10.1016/j.lithos.2012.09.003
656 Lyubetskaya, T., Korenaga, J., 2007. Chemical composition of Earth's primitive mantle and its
657 variance: 1. methods and results. Journal of Geophysical Research 112, B03211.
658 http://dx.doi.org/10.1019/2005JB004223
659 Marks, M.A.W., Coulson, I.M., Schilling, J., Jacob, D.E., Schmitt, A.K., Markl, G., 2008. The

660 effect of titanite and other HFSE-rich mineral (Ti-bearing andradite, zircon, eudialyte)
661 fractionation on the geochemical evolution of silicate melts. Chemical Geology 257, 153–172.
662 Melluso, L., Cucciniello, C., le Roex, A.P., Morra, V., 2016. The geochemistry of primitive volcanic
663 rocks of the Ankaratra volcanic complex, and source enrichment processes in the genesis of the
664 Cenozoic magmatism in Madagascar. Geochimica et Cosmochimica Acta 185:435-452.
665 http://dx.doi.org/10.1016/j.gca.2016.04.005
666 Melluso, L., de' Gennaro, R., Fedele, L., Franciosi, L., Morra, V., 2012. Evidence of crystallization
667 in residual, Cl-F-rich, agpaitic, trachyphonolitic magmas and primitive Mg-rich basalt-
668 trachyphonolite interaction in the lava domes of the Phlegrean Fields (Italy). Geological
669 Magazine 149, 532-550.
670 Melluso, L., Guarino, V., Lustrino, M., Morra, V., de' Gennaro, R., 2017. The REE- and HFSE-
671 bearing phases in the Itatiaia alkaline complex (Brazil), and geochemical evolution of feldspar-
672 rich felsic melts. Mineralogical Magazine 81, 217-250. doi: 10.1180/minmag.2016.080.122
673 Melluso, L., le Roex, A.P., Morra, V., 2011a. Petrogenesis and Nd-Pb-Sr- isotope geochemistry of
674 the olivine melilitites and olivine nephelinites ("ankaratrites") in Madagascar. Lithos 127, 505-
675 521. http://dx.doi.org/10.1016/j.lithos.2011.08.003
676 Melluso, L., Morra, V., 2000. Petrogenesis of late Cenozoic mafic alkaline rocks of the Nosy Be
677 archipelago (northern Madagascar): relationships with the Comorean magmatism. Journal of
678 Volcanology and Geothermal Research 56, 129-142
679 Melluso, L., Morra, V., Brotzu, P., Mahoney, J.J., 2001. The Cretaceous igneous province of central-
680 western Madagascar: evidence for heterogeneous mantle sources, crystal fractionation and crustal
681 contamination. Journal of Petrology 42, 1249-1278.
682 Melluso, L., Morra, V., Brotzu, P., Tommasini, S., Renna, M.R., Duncan, R.A., Franciosi, L.,
683 d'Amelio, F., 2005. Geochronology and petrogenesis of the Cretaceous Antampombato-
684 Ambatovy complex and associated dyke swarm, Madagascar. Journal of Petrology 46, 1963-
685 1996.
686 Melluso, L., Morra, V., de' Gennaro, R., 2011b. Coexisting Ba-feldspar and melilite in a melafoidite
687 lava of Mt. Vulture, Italy: role of volatiles and alkaline earths in bridging a petrological
688 incompatibility. The Canadian Mineralogist 49, 983-1000.
689 http://dx.doi.org/10.3749/canmin.49.4.983
690 Melluso, L., Morra, V., Di Girolamo, P., 1996. The Mt. Vulture volcanic complex (Italy): evidence
691 for distinct parental magmas and for residual melts with melilite. Mineralogy and Petrology 56,
692 226-250.
693 Melluso, L., Morra, V., Guarino, V., de' Gennaro, R., Franciosi, L., Grifa, C., 2014. The
694 crystallization of shoshonitic to peralkaline trachyphonolitic magmas in a H_2O-Cl-F- rich

695 environment at Ischia (Italy), with implications for the feeder system of the Campania Plain
696 volcanoes. Lithos 210-211, 242-259. http://dx.doi.org/10.1016/j.lithos.2014.10.002
697 Melluso, L., Morra, V., Riziky, H., Veloson, J., Lustrino, M., Del Gatto, L., Modeste, V., 2007.
698 Petrogenesis of a basanite-tephrite-phonolite volcanic suite in the Bobaomby (Cap d'Ambre)
699 peninsula, northern Madagascar. Journal of African Earth Sciences 49, 29-42.
700 Melluso, L., Srivastava, R.K., Guarino, V., Zanetti, A., Sinha, A.K., 2010. Mineral compositions
701 and magmatic evolution of the Sung Valley ultramafic-alkaline-carbonatitic complex (NE India).
702 The Canadian Mineralogist 48, 205-229; http://dx.doi.org/10.3749/canmin.48.1.205
703 Miller, C., Zanetti, A., Thöni, M., Konzett, J., Klötzli, U., 2012. Mafic and silica-rich glasses in
704 mantle xenoliths from Wau-en-Namus, Libya: Textural and geochemical evidence for
705 peridotite–melt reactions. Lithos 128-131, 11-26.
706 Nkoumbou, C., Déruelle, B., Velde, D., 1995. Petrology of Mount Etinde nephelinite series. Journal
707 of Petrology 36, 373-395.
708 Nicollet, C., 1984. Le volcanism dans le Sud-Ouest de Madagascar. Journal of African Earth
709 Sciences 2, 383-388.
710 Olin, P.H., Wolff, J.A., 2012. Partitioning of rare earth and high field strength elements between
711 titanite and phonolitic liquid. Lithos 128, 46-54.
712 Pilet, S., Ulmer, P., Villiger, S., 2010. Liquid line of descent of a basanitic liquid at 1.5 GPa:
713 constraints on the formation of metasomatic veins. Contributions to Mineralogy and Petrology
714 159, 621–643.
715 Pratt, M.J., Wysession, M.E., Aleqabi, G., Wiens, D.A., Nyblade, A.A., Shore, P., Rambolamanana,
716 G., Andriampenomanana, F., Rakotondraibe, T., Tucker, R.D., Barruol, G., Rindraharisaona, E.,
717 2017. Shear velocity structure of the crust and upper mantle of Madagascar derived from surface
718 wave tomography. Earth and Planetary Science Letters 458, 405-417.
719 Razafiniparany, A., Joo, J., Rakotomavo, G., Rakotoarivony, X., 1974. Carte géologique
720 Soavinandriana (M47). Service Géologique, Antananarivo, Madagascar. 1/100,000.
721 Rocco, I., Zanetti, A., Melluso, L., Morra, V., 2017. Ancient depleted and enriched mantle
722 lithosphere domains in northern Madagascar: geochemical and isotopic evidence from spinel-to-
723 plagioclase-bearing ultramafic xenoliths. Chemical Geology 466, 70-85.
724 http://dx.doi.org/10.1016/j.chemgeo.2017.05.016
725 Roeder, P.L., Emslie, R.F., 1970. Olivine-liquid equilibrium. Contributions to Mineralogy and
726 Petrology 29, 275-289.
727 Rogers, N.W., De Mulder, M., Hawkesworth, C.J., 1992. An enriched mantle source for potassic
728 basanites: evidence from Karisimbi volcano, Virunga volcanic province, Rwanda. Contributions
729 to Mineralogy and Petrology 111, 543–556.

730 Ronga, F., Lustrino, M., Marzoli, A., Melluso, L., 2010. Petrogenesis of a basalt-comendite-
731 pantellerite rock suite: the Boseti volcanic complex, Main Ethiopian Rift. Mineralogy and
732 Petrology 98, 227-243. http://dx.doi.org/10.1007/s00710-009-0064-3.
733 Roig, J.Y., Tucker, R.D., Delor, C., Peters, S.G., Théveniaut, H., 2012. Carte géologique de la
734 République de Madagascar à 1/1,000,000. Ministère des Mines, PGRM, Antananarivo,
735 République de Madagascar, 1 color sheet.
736 Rufer, D., Preusser, F., Schreurs, G., Gnos, E., Berger, A., 2014. Late Quaternary history of the
737 Vakinankaratra volcanic field (central Madagascar): insights from luminescence dating of
738 phreatomagmatic eruption deposits. Bulletin of Volcanology 76, 817-837
739 Sheth, H.C., Mahoney, J.J., Baxter, A.N., 2003. Geochemistry of lavas from Mauritius, Indian
740 Ocean: mantle sources and petrogenesis. International Geology Review 45, 780-797.
741 Shishkina, T.A., Botcharnikov, R.E., Holtz, F., Almeev, R.R., Jazwa, A.M., Jakubiak, A.A., 2014.
742 Compositional and pressure effects on the solubility of H_2O and CO_2 in mafic melts. Chemical
743 Geology, 112-129.
744 Tanaka, T., Togashi, S., Kamioka, H., Amakawa, H., Kagami, H., Hamamoto, T., Yuhara, M.,
745 Orihashi, Y., Yoneda, S., Shimizu, H., Kunimaru, T., Takahashi, K., Yanagi, T., Nakano, T.,
746 Fujimaki, H., Shinjo, R., Asahara, Y., Tanimizu, M., Dragusanu C., 2000. JNdi-1: a neodymium
747 isotopic reference in consistency with LaJolla neodymium. Chemical Geology 167, 279-281.
748 Tiepolo, M., Bottazzi, P., Palenzona, M., 2003. A LASER probe coupled with ICP-double-focusing
749 sector-field mass spectrometer for in situ analysis of geological samples and U-Pb dating of
750 zircon. The Canadian Mineralogist 41, 259-272.
751 Tiepolo, M., Oberti, R., Zanetti, A., Vannucci, R., Foley, S.F., 2007. Trace-element partitioning
752 between amphibole and silicate melt. Reviews in Mineralogy and Geochemistry, 67, 417-452.
753 Tucker, R.D., Ashwal, L.D., Handke, M.J., Hamilton, M.A., LeGrange, M., and Rambeloson, R.A.
754 1999a. U–Pb geochronology and isotope geochemistry of the Archean and Proterozoic rocks of
755 north-central Madagascar. The Journal of Geology 107: 135–153. doi:10.1086/314337
756 Tucker, R.D., Conrad, J., Key, R.M., Pitfield, P.E.J., Randriamananjara, T., Taylor, C.D.,
757 Goodenough, K.M., Thomas, R.J., 2008. $^{40}Ar/^{39}Ar$ geochronology of Mesozoic and younger
758 igneous rocks, Madagascar, in: Revision of the geologic and mineral cartography of the north,
759 central and east-central zones of Madagascar; explanatory note to the Republic of Madagascar,
760 Ministry of Energy and Mines (MEM/SG/ DG/ UCP/ PGRM); Geol. Comm. Rep. - British
761 Geological Survey Report: CR/08/078, 385-435, 1 Appendix
762 Tucker, R.D., Roig, Y.G., Moine, B., Delor, C., Peters, S.G., 2014. A geological synthesis of the
763 Precambrian shield in Madagascar. Journal of African Earth Sciences 94, 9-30.

764 Ulrych, J., Novak, J.K., Lang, M., Hegner, E., Randa Z., 2006. Petrology and geochemistry and K-
765 Ar ages for Cenozoic tinguaites from the Ohre/Eger Rift (NW Bohemia). Neues Jahrbuch für
766 Mineralogie Abhandlungen 183, 41-61.
767 Vatin-Perignon, N., 1968. Le formations eruptives et la structure de l'edifice volcanique au centre du
768 Cantal (Massif Central Français). Bulletin Volcanologique 32, 207-251.
769 Webster, J.D., Goldoff, B., Sintoni, M.F., Shimizu, N., De Vivo, B., 2014. C-O-H-Cl-S-F volatile
770 solubilities, partitioning, and mixing in phonolitic-trachytic melts and aqueous-carbonic
771 vapor±saline liquid at 200 MPa. Journal of Petrology 55, 2217-2248.
772 Weis, D., Kieffer, B., Maerschalk, C., Barling, J., de Jong, J., Williams, G.A., Hanano, D., Pretorius,
773 W., Mattielli, N., Scoates, J.S., Goolaerts, A., Friedman, R.M., Mahoney, J.B., 2006. High-precision
774 isotopic characterization of USGS BHVO-1 and BHVO-2 reference materials by TIMS and MC-
775 ICP-MS. Geochemistry Geophysics Geosystems 7, Q08006. doi: 10.1029/ 2006GC001283
776 White, J.C., Espejel-Garcia, V.V., Antony, E.Y., Omenda, P., 2012. Open system evolution of
777 peralkaline trachyte and phonolite from the Suswa volcano, Kenya Rift. Lithos 152, 84-104.
778 Woolley, A.R., 2001. Alkaline rocks and carbonatites of the world. Part 3: Africa: Geological
779 Society/Natural History Publishing House, Bath, UK, p. 372
780 Wörner, G., Schmincke, H.-U., 1984. Mineralogical and chemical zonation of the Laacher See
781 Tephra sequence (East Eifel, W. Germany). Journal of Petrology 25, 805-835.
782

783 **Appendix: analytical techniques**
784

785 Powders of the 69 samples of this study were obtained after carefully grinding washed chips in an
786 ultrapure agate mill. For each sample, four grams of micronized powder were used to prepare pressed
787 powder pellets. The powder (mixed with 1 ml of Polyvinyl alcohol solution) was pressed to twenty
788 tons for twenty seconds. The bulk-rock X-Ray Fluorescence compositional data (Table S1) were
789 obtained on pressed powder pellets with an Axios Panalytical spectrometer equipped with six analyzer
790 crystals, three primary collimators and two detectors (flow counter and scintillator), operating at
791 different kV and mA for each analyte. Analytical uncertainties are in the order of 1-2% for major
792 elements and 5-10% for trace elements. The weight loss on ignition has been obtained with
793 gravimetric techniques, firing at 1000°C small aliquots of powders previously dried at 110°C
794 overnight.
795 Data on a subset of samples were obtained through ICP-MS methods at Actlabs (Canada) (Table 1).
796 Samples were mixed with a flux of lithium metaborate and lithium tetraborate and fused in an
797 induction furnace. The molten material is immediately poured into a solution of 5% nitric acid
798 containing an internal standard, and mixed continuously until completely dissolved (~30 minutes). The

799 samples were run for major oxides and selected trace elements (Ba, Be, Sc, Sr, V, Y and Zr) on a
800 combination simultaneous/sequential Thermo Jarrell-Ash ENVIRO II ICP or a Varian Vista 735 ICP.
801 Calibration is performed using seven prepared USGS and CANMET certified reference materials. One
802 of the seven standards is used during the analysis for every group of ten samples. Sample fused are
803 diluted and analyzed by Perkin Elmer Sciex ELAN 6000, 6100 or 9000 ICP/MS for other trace
804 elements (Cr, Co, Ni, Cu, Zn, Ga, Ge, As, Rb, Nb, Mo, Ag, In, Sn, Sb, Cs, La, Ce, Pr, Nd, Sm, Eu,
805 Gd, Tb, Dy, Ho, Er, Tm, Yb, Lu, Hf, Ta, W, Tl, Pb, Bi, Th and U). Three blanks and five controls
806 (three before the sample group and two after) are analyzed per group of samples. Duplicates are fused
807 and analyzed every 15 samples. Analyses of international standards are reported in Cucciniello et al.
808 (2017).
809 Microprobe analyses were carried out on polished thin sections using Energy Dispersive Spectrometry
810 (EDS) at University of Napoli Federico II, utilizing a JEOL JSM-5310 microscope operating at 15 kV
811 primary beam voltage, 50-100 mA filament current, 50 s net acquisition time and a Oxford
812 Instruments Microanalysis Unit, equipped with an INCA X-act detector. For further details see
813 Melluso et al. (2014, 2017).
814 The Laser Ablation - Inductively Coupled Plasma - Mass Spectrometry analysis of the minerals in the
815 trachyphonolite RT-06I-355 was performed at IGG-CNR (Pavia, Italy), utilizing techniques described
816 in Rocco et al. (2017). Concentrations of Rare Earth Elements (REE) and other selected trace elements
817 (Li, B, Ba, Rb, Th, U, Nb, Ta, Sr, Zr, Hf, Ti, Y, Sc, V, Co and Ni) were determined in situ on polished
818 sections (100 μm) using a PerkinElmerSCIEX ELAN DRC-e quadrupole mass spectrometer coupled
819 with an UP213 deep-UV YAG Laser Ablation System (New Wave Research, Inc.). The laser was
820 operated at a repetition rate of 10 Hz, with 213 nm wavelength and a fluence of ~9.5 J/cm^2. Helium
821 was used as carrier gas and was mixed with Ar downstream of the ablation cell. Spot diameter was 55
822 μm. Data reduction was performed offline using the GLITTER software. For this study, the NIST
823 SRM 610 synthetic glass standards was used as external standard, CaO was used as internal standard
824 for clinopyroxene and amphibole, while SiO_2 was used for titanite and feldspar. Precision and
825 accuracy of the REE concentration values were assessed through repeated analysis of the BCR2-g
826 standard to be better than ±7% and ±10%, respectively, at the ppm concentration level (for further
827 details see Miller et al., 2012 and references therein).
828 The Sr-Nd-Pb-isotope data were obtained at the University of Cape Town, with techniques described
829 in le Roex et al. (2012). Sr, Nd and Pb were separated using conventional ion exchange techniques and
830 all radiogenic isotope analyses were performed on a NuPlasma multicollector inductively coupled
831 plasma-mass spectrometer (ICP-MS). To correct for mass fractionation effects, measured $^{87}Sr/^{86}Sr$ and
832 $^{143}Nd/^{144}Nd$ values were normalized to $^{86}Sr/^{88}Sr=0.1194$ and $^{146}Nd/^{144}Nd=0.7219$, respectively. Pb

isotopes were corrected for fractionation by normalizing ratios measured in international standards. Average standard values obtained during the course of this study are reported in the Table 3.

Table captions

Table 1: ICP-MS major and trace element composition of Itasy rocks. A few element ratios are also reported.

Table 2: LAM-ICP-MS and microprobe composition of titanite, amphibole, clinopyroxene and feldspar of the trachyphonolite RT-06I-355. The location of the laser pits is shown in the Supplementary Fig. S1c.

Table 3: Isotopic composition of the Itasy rocks. The composition of the standards which were run with the unknowns is also reported.

Supplementary Tables

Supplementary Table S1: XRF major trace element data and CIPW norms of the Itasy samples. The composition of international standards is also reported.

Supplementary Table S2: synopsis of the mineral assemblages of the main lithotypes of the Itasy complex.

Supplementary Table S3: composition of olivine of the Itasy rocks.

Supplementary Table S4: composition of oxides of the Itasy rocks.

Supplementary Table S5: composition of pyroxene of the Itasy rocks.

Supplementary Table S6: composition of amphibole, biotite and rhönite of the Itasy rocks.

Supplementary Table S7: composition of feldspar and glass of the Itasy rocks.

Supplementary Table S8: composition of feldspathoids of the Itasy rocks.

Supplementary Table S9: composition of titanite, apatite, other accessories of the Itasy rocks.

Supplementary Table S10: Recapitulation of mass balance calculations between rocks of different degree of magmatic evolution, and detailed results. The composition of the phases is reported in the supplementary tables.

Supplementary Table S11: average REE mineral/bulk rock ratios for titanite, amphibole and clinopyroxene. The partition coefficients of titanite, clinopyroxene, apatite and amphibole are taken from Olin and Wolff (2012), Fedele et al. (2009, 2015) and Tiepolo et al. (2007). Note that amphibole of RT-06I-355 could not be considered in equilibrium with the host rock (cf. Supplementary Fig. S1).

868 **Figure captions**

869

870 Figure 1: a) Simplified geological map of Madagascar, with the location of the main volcanic areas
871 of Cretaceous and Cenozoic; b) Geological sketch map with sample localities (Laborde
872 coordinates) and the main tectonic features of the Itasy area. c) Schematic section of the Itasy
873 region (redrawn after Pratt et al., 2017) with location of a possible mantle source region of the
874 Itasy mafic volcanic rocks.

875 Figure 2: Classification of the Itasy rocks according to the TAS and R_1R_2 diagrams. Symbols: Itasy
876 mafic rocks: red triangles; Itasy evolved rocks: blue circles. The data from other Cenozoic
877 districts of Madagascar are taken from: Melluso et al. (2007, 2011b); Cucciniello et al. (2011,
878 2016, 2017); Melluso and Morra (2000).

879 Figure 3: Classification of pyroxene and amphibole of the Itasy rocks. Symbols as in Fig. 2. The
880 pyroxene and amphibole composition of the Ankaratra alkaline rocks (black squares) are taken
881 from Cucciniello et al. (2017).

882 Figure 4: a) The composition of feldspars and bulk-rocks of the Itasy in the An-Ab-Or diagram
883 (mol.%). b) Composition of the Itasy volatile-rich feldspathoids in the CaO-Na_2O-K_2O diagram
884 (mol.%; after Lessing and Grout, 1971). c) The volatile concentration of the Itasy feldspathoids
885 (in wt.%). The feldspar composition of the Ankaratra alkaline rocks (black squares) are taken
886 from Cucciniello et al. (2017). The data on Mt. Vulture feldspathoids are taken from Melluso et
887 al. (1996, 2011a), references therein and unpublished data. Symbols as in Fig. 2.

888 Figure 5: a, b) Mantle normalized diagrams for the Itasy basanites. The data on the other
889 Madagascan basanites (grey patterns in the background) are taken from the database of Melluso
890 et al. (2016). The analyses of the Mt. Vulture basanites (MgO=9-12 wt.%) are taken from
891 Beccaluva et al. (2002), L.M. and V.M., unpublished data. The data on the Karisimbi leucite
892 basanites (green patterns in the background) are taken from Rogers et al. (1992). At a similar
893 MgO, the mantle-normalized patterns of the Mt. Vulture and Itasy basanites (as well other
894 geochemical characteristics) imply contrasting enrichment processes in their respective sources,
895 and a different mantle baseline preceeding metasomatic events; c) Mantle normalized diagrams
896 for the Itasy evolved rocks. The normalization values are taken from Lyubetskaya and Korenaga
897 (2007).

898 Figure 6: a, b) Mantle normalized diagrams of the coexisting phases of the trachyphonolite RT-06I-
899 355, together with those of the Itasy evolved rocks. Normalization values are those of
900 Lyubetskaya and Korenaga (2007). Potassium and Phosphorus are not reported.

901 Figure 7: Isotopic diagrams for the Itasy and the other Cenozoic volcanic rocks emplaced within the
902 cratonic domains of the Madagascan basement (cf. Fig. 1a). Symbols as in Fig. 2. The Ankaratra

data are taken from Cucciniello et al. (2017), and the Alaotra and Takarindiona olivine melilitites (black triangles) are taken from Melluso et al. (2011a).

Figure 8: a) The tetrahedral phase diagram diopside-nepheline-kalsilite-silica at one atmosphere (after Cucciniello, 2016) with the Itasy bulk-rock compositions (symbols as in Fig. 2); b) The Petrogeny Residua's System at 1 kbar P_{H2O} with the Itasy trachyphonolites (blue circles). The boundary lines are taken from Gupta (2015). The evolved rocks of the Ankaratra (black squares) are taken from Cucciniello et al. (2017); the Bobaomby phonolites (black triangles) are taken from Melluso et al. (2007); the trachytes of Mauritius (grey rhombs) are taken from Ashwal et al. (2016). Other evolved rocks can be found in Cucciniello et al. (2017). The compositions of glass of the evolved rocks is reported as light blue circles.

Figure 9: AFC modelling after DePaolo (1981). The composition of the contaminants (granitic rocks and felsic gneisses of the basement around Itasy: data from Kröner et al., 2000; Melluso et al., 2001; Cucciniello et al., 2017) is the following: $^{87}Sr/^{86}Sr$=0.7113, $^{143}Nd/^{144}Nd$=0.5113, $^{206}Pb/^{204}Pb$=16.62, Pb=10 ppm; Sr=499 ppm; Nd=16 ppm; Th=12 ppm. The bulk partition coefficients are reported along the curves (cf. Supplementary Fig. S7), together with the values of the residual liquid fraction (f) and the assimilation/accumulus rate (r). The AFC models in the diagram $^{143}Nd/^{144}Nd$ *vs.* Nd were performed taking into account the geochemical behaviour of Nd shown in Supplementary Fig. S7, and two starting compositions (the basanite RT-06I-354B and the benmoreite RT-06I-387). Symbols as in Fig. 2.

Supplementary Figures

Supplementary Fig. S1a: Petrographic, BSE (backscattered electron images), and field images of the Itasy rocks: a) basanite RT-06I-354B: phenocrysts of olivine, with Cr-spinels, set in a scoriaceous mesostasis; b) basanite RT-06I-354B: large phenocrysts of kaersutite enclosing diopsidic clinopyroxene, parallel nicols; c) phonotephrite RT-06I-398: rare phenocrysts of clinopyroxene and apatite set in a very fine-grained microlitic mesostasis, parallel nicols; d) basanite RT-06I-354B: large phenocryst of diopside-to-titanaugite clinopyroxene, parallel nicols; e) trachyphonolite RT-06I-355; phenocrysts of a zoned anorthoclase and titanite in a fine-grained feldspar-rich mesostasis, parallel nicols; f) trachyphonolite RT-06I-375: phenocrysts of (pleochroic) titanite and alkali feldspar in a fine-grained groundmass, parallel nicols. The horizontal scale of the thin section photomicrographs is 2.5 mm.

Supplementary Fig. S1b: g) groundmass of basanite RT-06I-354B: microlites of feldspar, feldspathoids, unmixed Fe-Ti oxides and clinopyroxene, BSE; h) trachyphonolite RT-06I-361: phenocrysts of amphibole, and microphenocrysts of titanite and apatite in a fine-grained

mesostasis; i) trachyphonolite RT-06I-363: microphenocrysts of Fe-Ti oxides, titanite, and clinopyroxene in a fine-grained mesostasis rich in alkali feldspar and light grey glass, BSE; j) phonotephrite RT-06I-398: a microlite of haüyne (darker grey) in the center of the groundmass made up of feldspar, clinopyroxene, magnetite and glass, BSE; k) l) m) n) o) feldspathoids in the groundmass of trachyphonolites RT-06I-361 and RT-06I-379; p), q), r) pyroclastic rocks, lava domes, and spatter cones in the northeastern part of Itasy.

Supplementary Fig. S1c: Petrographic characteristics of the trachyphonolite RT-06I-355. a) zoned green cpx phenocryst b), c) phenocrysts of alkali feldspar and titanite; d) microlites of alkali feldspar and altered amphibole. The laser pits after LAM-ICP-MS work (Table 2) can be easily seen. The horizontal scale of the thin section photomicrographs is 2.5 mm.

Supplementary Fig. S2: Composition of the titaniferous magnetite of the Itasy rocks in the MgO-MnO and TiO_2-Al_2O_3 diagrams (in wt.%). Symbols as in Fig. 2.

Supplementary Fig. S3: Clinopyroxene composition. Symbols: mafic rocks: red triangles; benmoreites and trachyphonolites: blue circles. The composition of olivine is plotted in the Ca-Mg-Fe diagram.

Supplementary Fig. S4: Amphibole composition (cations in apfu) indicating the *absence* of *evidence* for a high-pressure crystallization environment for this phase, as the calculated Al^{VI} is roughly 1:10 the calculated Al^{IV} in both mafic and evolved rocks. Symbols as in Fig. 2

Supplementary Fig. S5: composition of nepheline in the nepheline-kalsilite-silica diagram. The nephelines of the olivine melilitites and of the Ankaratra rocks are reported for comparison (data from Melluso et al., 2011a and Cucciniello et al., 2017).

Supplementary Fig. S6: XRF major oxides and trace elements vs. MgO wt.% (plotted on a logarithmic scale). The composition of olivine, amphibole and clinopyroxene of the basanites and tephrites is reported in a few diagrams for comparison. Symbols as in Fig. 2.

Supplementary Fig. S7: Fractional crystallization models using thorium (Th) as the most incompatible element (thus considered as a proxy of a quantitative differentiation index). The numbers along the curves indicate the fraction of residual liquid (f) starting from the basanite RT-06I-354B, and the bulk partition coefficients for the element (fitted also by visual guess) in the *ordinata* are reported in each part of the curves. Ticks on the curves are at f=0.9, 0.8, 0.7, 0.6, 0.5, 0.45, 0.4, 0.35, 0.3, 0.25 and 0.2, starting from basanite RT-06I-354B (unreported for clarity). Symbols as in Fig. 2.

Supplementary Fig. S8: a) REE patterns of the Itasy mafic rocks; b) the REE patterns of the mineral phases of RT-06I-355 and the host rock; c), d) REE patterns of the evolved rocks with c) model obtained by subtraction of 2% apatite and 1% titanite from sample RT-06I-387, by using the

partition coefficients of Fedele et al. (2015) and Olin and Wolff (2012); and d) model obtained after subtraction of 0.7 and 1% titanite from sample RT-06I-387; e) The REE concentration of the Itasy rocks normalized to that of the most primitive sample (RT-06I-354B). The effects of titanite and apatite removal (cf. figure c) are also shown; f) Ratios between the concentrations of the average composition of titanite, amphibole and clinopyroxene and that of the host rock. The experimental partition coefficients of titanite in phonolites (Olin and Wolff, 2012), clinopyroxene in trachyphonolites (Fedele et al., 2009), and amphibole in trachytes (Tiepolo et al., 2007) are reported for comparison (data in Supplementary Table 11). g) The REE patterns of the Itasy titanites and those of alkaline intrusive rocks of within-plate affinity (data from Marks et al., 2008 and Melluso et al., 2010). Prometium is always interpolated. The chondrite is the CI of Boynton (1984).

The magmatic evolution and genesis of the Quaternary basanite-trachyphonolite suite of Itasy (Madagascar) as inferred by geochemistry, Sr-Nd-Pb isotopes and trace element distribution in coexisting phases

L. Melluso*[1], R.D. Tucker**, C. Cucciniello*, A.P. le Roex***, V. Morra*, A. Zanetti****, R.L. Rakotoson*****

*DISTAR, Università di Napoli Federico II, Napoli, Italy
**BRGM, Orleans, France
***University of Cape Town, Rondebosch, Republic of South Africa
****IGG-CNR, Pavia, Italy
*****Analamaitsy, Antananarivo, Madagascar

[1]corresponding author: melluso@unina.it

Abstract

The Itasy is a Pleistocene-Holocene volcanic field in central Madagascar, located to the west of the Ankaratra volcanic complex. It comprises scoria cones and lava domes (>120), with associated pyroclastic fall and mafic lava flows, covering an area of ab. 400 km^2. The last volcanic episodes probably dated ca. 6000-7100 y BP; warm springs and geysers are active. The juvenile samples comprise a peculiar, almost bimodal, rock suite ranging from potassic leucite-kaersutite-bearing basanites, tephrites and phonotephrites, to benmoreites and titanite-haüyne-bearing trachyphonolites (MgO from 9-10 wt.% to 0.1 wt.%). These rocks show continuous and overlapping variations in the bulk-rock and phase composition (olivine, clinopyroxene, amphibole, feldspar, leucite, haüyne, nepheline, oxides, apatite, titanite, glass and other accessories). The basanites have homogeneous isotopic composition ($^{87}Sr/^{86}Sr$=0.70366-0.70378, $^{143}Nd/^{144}Nd$=0.51274-0.51277, $^{206}Pb/^{204}Pb$=18.7-18.9, $^{207}Pb/^{204}Pb$=15.53-15.56; $^{208}Pb/^{204}Pb$=38.89-39.01), and a marked enrichment in the most incompatible elements (LILE and HFSE reach 100-215 times primitive mantle). These features are consistent with low degrees of partial melting of a volatile-, LILE- and HFSE-rich, amphibole-bearing peridotitic mantle induced by uplift during an E-W-directed extensional regime, as is found in central Madagascar. The marked changes in the geochemical composition, and small variations of the Sr-Nd-Pb isotopes in the trachyphonolites ($^{87}Sr/^{86}Sr$=0.70425-0.70446, $^{143}Nd/^{144}Nd$=0.51266-0.51269, $^{206}Pb/^{204}Pb$=18.18-18.39, $^{207}Pb/^{204}Pb$=15.49-15.51; $^{208}Pb/^{204}Pb$=38.38-39.57) with respect to basanites and tephrites point to a limited amount of crustal contamination by the relatively low-

$^{206}Pb/^{204}Pb$, low-$^{143}Nd/^{144}Nd$, high-$^{87}Sr/^{86}Sr$ Precambrian basement rocks (of Middle Archean to Late Proterozoic age), and highlight the geochemical effects of titanite and anorthoclase removal on the trace element fractionation trends, a feature also shown in the trace element composition of the phenocrysts in the trachyphonolites.

Keywords: basanites, trachyphonolites, mineral trace elements, titanite removal, crustal contamination, Itasy, Madagascar

1. Introduction and Geological setting

Madagascar is the site of abundant Cenozoic-to-Recent volcanism (Woolley, 2001; Tucker et al., 2008; Cucciniello et al., 2011, 2016, 2017), which crops out from the northernmost regions of the island (Cap d'Ambre/Bobaomby, Massif d'Ambre) to the southwest (Ankililoaka, Tulear region; Fig. 1a). This volcanism is the response to extensional processes and uplift active since the Cenozoic of the Madagascan lithosphere, with changing orientation of the stress pattern in different sectors of the island (Nicollet, 1984; Piqué et al., 1999; Cucciniello et al., 2016, 2018). The changing ages and lithological characteristics of the exposed crustal domains are reflected in the different isotopic composition of the mantle-derived Cenozoic rocks, suggesting a strong lithospheric control in the genesis of the latter (Tucker et al., 2014; Melluso et al., 2016; Cucciniello et al., 2018).

The central field of alkaline igneous rocks consist of four different volcanic-dominated massifs, from east to west: Takarindiona, Alaotra, Ankaratra and Itasy (Fig. 1a). The eastern massifs of Takarindiona and Alaotra are relatively small, structurally controlled Miocene-Pliocene fissural eruptions and spatter cones (Melluso et al., 2011a), emplaced along or near the western margin of the oldest rocks in Madagascar (~3.2 Ga gneisses of the Antongil/Masora domain). The Ankaratra and Itasy are significantly larger in size and more diverse in morphology, as they include lava domes, massive flow eruptions, spatter cones, and various phreatomagmatic rings and cones (cf. Brenon and Bussiere, 1959; Woolley, 2001; Cuciniello et al., 2017). The Ankaratra covers an area of ~3600 km^2 and reaches 2395 mt. elevation. Like the eastern fields, the age of activity in the Ankaratra spans from Miocene to Recent (Tucker et al., 2008; Rufer et al., 2014; Cucciniello et al., 2017).

The Itasy volcanic field is a much smaller (roughly 400 km^2) and younger version of the Ankaratra; it crops out at roughly 1200 mt. a.s.l., in a north-south-trending graben located in the Precambrian basement (e.g., Andrianaivo and Ramasianoro, 2010, 2011), whose western limits are best indicated by a long NNE-SSW normal fault (Fig. 1b). The volcanic field is the coalescence of more than 120 scoria cones (e.g., Kassigie, also known for a presumed eruption in 2001, likely a landslide in its SW

sector), with lava flows (e.g., along the western master fault), lava domes (e.g., Ngilofotsy, west of Analavory; Fig. 1b; Supplementary Fig. 1), and pyroclastic rocks in the facies of pyroclastic fall deposits, small-scale pyroclastic flows and maar craters (cf. Supplementary Fig. 1; Razafiniparany et al., 1974). According to Bussiere (1957, and references therein), the sequence of volcanic events is established by cross-cutting relationships. It includes: *(a)* oldest eruptions of trachyte and trachyphonolite, *(b)* deposition of lacustrine sediments bearing fossils of Pleistocene or younger age (i.e. plant fragments, and bones of hippos, lemurs, and *Aepyornis*), (*c*) lava flows and pyroclastic eruptions of basanite and tephrite, and *(d)* recent strombolian and phreatomagmatic eruptions of basanitoids. Given the small volume, the scattered nature of magmatism and the structural complexity of this part of Madagascar, the eruptive history of the Itasy area is only generally known. What is clear, however, is that the age of the volcanism must be young, certainly less than 1 Ma. This is consistent with the geologic youthfulness of the volcanic landforms, their relationship to Pleistocene or younger fossils, the historical record of seismic and geothermal activity (Brown et al., 2015), and an $^{40}Ar/^{39}Ar$ plateau age of 97±6 ka for a trachyphonolite sampled near Analavory (R.D. Tucker, unpub. data). During and after formation of the lacustrine basins, the region is believed to have experienced regional E-W extension and differential uplift that fractured the natural dams, drained the tectonic lakes, and produced its rugged topography. The bounding faults of the Itasy graben (Fig. 1b) are but one manifestation of this near-surface extensional stress field. These features, including the volcanism of Itasy and Ankaratra, are a response to still unresolved forces, recently imaged in a regional seismological survey (Pratt et al., 2017; Fig. 1c) that acted throughout the Malagasy lithosphere in Miocene and younger time.

The Itasy and the Ankaratra are built upon a Precambrian basement complex of Neoarchean granitic gneiss (2.7-2.5 Ga, Betsiboka Suite) and Neoproterozoic quartzite and schist (<1.0 Ga, Ambatolampy Group), and both are bounded by faults near the apex of the Taná virgation, where the gneissic fabrics turn sharply from N-S to E-W strike directions (Roig et al., 2012; Tucker et al., 2014).

Petrogenetic studies on the Ankaratra volcanic rocks were recently published (Melluso et al., 2016; Cucciniello et al., 2017). This paper is focused on the petrogenesis of the Itasy, probably the least known Late Cenozoic *volcanic* field in Madagascar. Lacroix (1923) and Bussiere (1957) first identified the featuring petrographic characteristics of the main lithologies, including the presence of haüyne in the felsic samples, allowing them to make comparison to rocks of the Massif Central in France. The range of chemical and isotopic composition of bulk rocks and mineral phases, the magmatic processes which acted in the upper crust, and the petrogenetic relationships with the other Cenozoic volcanic districts of Madagascar, particularly those of the central Madagascar, will be highlighted here.

2. Classification and petrography

Sixty-nine samples were collected throughout the volcanic field (Fig. 1b). They are representative of scoria and lava flows cropping out in the graben, and of the several volcanic domes of evolved composition (trachytic *s.l.*), which occur in the same areas as scoria cones and lavas. The analytical techniques are fully described in the appendix. According to petrography, T.A.S., R_1R_2 classification diagrams (Fig. 2), and CIPW norms (Supplementary Table S1), the fresh samples are basanites, tephrites, rare phonotephrites and benmoreites (*trachyandesites*), and trachyphonolites, with a bimodal character (Fig. 2, Table 1 and Supplementary Table S1). The *mafic* rocks have potassic affinity, given that their Na_2O/K_2O ratios are close to the unity; however, CIPW norms have no normative leucite. The trachyphonolites do not reach fully peralkaline conditions [P.I., peralkaline index, molar (Na+K)/Al <0.98], with the exception of the groundmass of evolved samples (see below). The samples with L.O.I. values > 2 wt.% (mostly scoria) have signs of chemical alteration, and thus were excluded from the discussion and from the classification diagrams. A synopsis of the observed mineral assemblages for various lithotypes is reported in the Supplementary Table S2.

Basanites, **tephrites** and **phonotephrites** are variably porphyritic (in both lava and scoria facies), with zoned, Ti-rich purple-green clinopyroxene, olivine (with small Cr-spinel inclusions), amphibole and oxide phenocrysts and megacrysts in a fine grained, feldspar-rich mesostasis, to almost aphyric facies, with purple-green clinopyroxene, oxide and olivine microlites in fine-grained or glassy groundmass, often without amphibole. The latter phase is found in both scorias and lavas (Supplementary Fig. S1). Amphibole is almost always poikilitic over clinopyroxene (Supplementary Fig. S1), and may show reaction relationships with the latter; it is often replaced by secondary rhönite. There is complete lack of feldspar phenocrysts. Apatite microphenocrysts and microlites are ubiquitous, particularly in the phonotephrite RT-06I-398, and leucite is often present in the groundmass, together with haüyne, phonolitic glass and alkali feldspar (Supplementary Fig. S1; Supplementary Table S2).

Benmoreites; sample RT06I-387 (the "*ordanchite*" of Lacroix and Bussiere) has rare phenocrysts of plagioclase, clinopyroxene, amphibole and opaque oxides, set in a trachytic/aphanitic mesostasis (Supplementary Fig. S1).

Trachyphonolites range from porphyritic to nearly aphyric, and are characterized by phenocrysts of anorthoclase and/or sanidine, plus rarer titanite, green clinopyroxene, amphibole and opaque oxides, set in a trachytic mesostasis that also has apatite, nepheline, haüyne, sodalite, clinopyroxene, other accessories and interstitial glass (Supplementary Fig. S1; Supplementary Table S2).

3. Mineral compositions

Olivine in basanites and tephrites is usually zoned, with composition ranging from Fo_{81} to Fo_{55} [Fo is 100 Mg/(Mg+Fe) in atoms], with MnO up to 0.52 wt.% and CaO up to 0.73 wt.% in the most Fe-rich compositions (Supplementary Table S3). Some crystals appear too Mg-rich to be in equilibrium with the host rock composition [e.g., the rounded Fo_{81} (xeno)crystal in the RT-06I-398 phonotephrite; Supplementary Table S3].

Oxides. **Cr-spinel** is rare and chemically zoned in the Mg-rich olivine cores of basanite RT-06I-354B [Cr_2O_3 =8.7-28.7 wt.%; Cr#=47-57; Cr# is 100Cr/(Cr+Al) in atoms]. **Ilmenite** is also very rare; it was found in the basanite RT-06I-354b as an exsolved phase (Supplementary Fig. S1) and is rich in geikielite component (MgO=7.8-13.3 wt.%), consistent with its crystallization from a mafic melt. **Titaniferous magnetite** is the main oxide; it shows increase in MnO and magnetite component (*s.s.*) and decrease in TiO_2, Al_2O_3 and MgO from mafic to evolved rocks (Supplementary Table S4 and Supplementary Fig. S2).

Clinopyroxene ranges from diopside [Mg#=82, TiO_2=1.3 wt.%; Mg# is 100Mg/(Mg+Fe)] to titanaugite (Mg#=68; TiO_2=5.75 wt.%, ca. 19 mol.% $CaTiAl_2O_6$) in basanites and tephrites, and from titanaugite (Mg#=67; TiO_2=5.1 wt.%) to aegirinaugite (Mg#=22; Na_2O=5 wt.%, ca. 38 mol.% aegirine) in the trachyphonolites (Fig. 3). The composition of clinopyroxene is therefore indicative of the degree of evolution of the host lithotypes, as shown in the Ti-Al and Mg-Ti diagrams (Supplementary Fig. S3). The evolved rocks have the lowest Mg#, Ti and Al and the highest Mn (and Na) concentrations; the calculated Al^{VI} is absent or strongly subordinated with respect to Al^{IV} (Supplementary Fig. S3; Supplementary Table S5). The compositional ranges are well within those already observed in the Ankaratra and in the other Cenozoic volcanic areas of Madagascar (e.g., Melluso et al., 2011a; Cucciniello et al., 2017 and references therein).

Amphibole is potassian kaersutite in basanites and tephrites (TiO_2=4.1-5.1 wt.%; Mg#=58-72), and potassian kaersutite/Fe-kaersutite to pargasite (TiO_2=1.2-4.6 wt.%; Mg#=23-56) in benmoreite and trachyphonolites (Fig. 3). Amphibole has the highest Mg# in the most Mg-rich lava sample (RT-06I-354B), and has *systematically* lower Mg# than the coexisting clinopyroxene, confirming its later appearance in the crystallization order (Supplementary Table S6; Supplementary Fig. S1), and thus bearing no chemical evidence for its crystallization at mantle depths. As with clinopyroxene, there is no correlation between proxies of the crystallization pressure (e.g., the calculated Al^{VI}) and the composition of amphibole in its host lithology (Supplementary Fig. S4). **Biotite** (Mg#=70-76; TiO_2=6.5-6.8 wt.%) is very rare. **Rhönite** [$Ca_2(Mg,Fe^{2+},Fe^{3+},Ti)_6(Si,Al)_6O_{20}$] is often found as a (subsolidus) rim of amphibole.

Feldspar. Tiny microlites of labradorite (An_{56-59}) to oligoclase (An_{27}) are found in the groundmass of basanites and tephrites, with additional interstitial anorthoclase (Fig. 4a), whereas a continuous trend from andesine (An_{42}) to anorthoclase and sanidine (up to Or_{57}) is found in the trachyphonolites (Fig. 4a). Sr is higher than Ba in plagioclase; they reach 1.9 and 4 wt.%, as oxides, respectively, in alkali feldspar grains of trachyphonolites (Supplementary Table S7). The overall chemistry is more restricted than that observed for the feldspars at the Ankaratra volcanic complex (Fig. 4a).

The interstitial **glass** is trachyphonolitic to phonolitic in composition (Supplementary Table S7).

Feldspathoids. **Leucite** has been found in the groundmass of the basanites; **haüyne** is found in phonotephrites, benmoreites and, particularly, in the groundmass of the trachyphonolites. Haüyne has a significant compositional range, with an almost continuous increase of Na and Cl and decrease of Ca, K and S towards the late crystallized **sodalite** microlites, also found as rims of zoned crystals (Fig. 4b, 4c; Supplementary Fig. S1; Supplementary Table S8). The composition of the volatile-bearing feldspathoids broadly matches the chemical variation of the Mt. Vulture analogues (which are likely the most complete series of sodalite-group *magmatic* feldspathoids), with the exclusion of the most potassic varieties (cf. Fig. 4b, and Melluso et al., 2011b and references therein). A Si-rich **nepheline** ($Q_{8-24}Ks_{5-13}Ne_{68-78}$ in wt.%), with low K_2O (up to 4 wt.%) and variable CaO (up to 2.8 wt.%) completes the groundmass assemblage of holocrystalline samples, including basanites and tephrites (Supplementary Fig. S5; Supplementary Table S8). The Itasy nepheline differs most markedly from that of the Madagascan olivine melilitites, the latter having low silica and very high K (10-12.6 wt.% K_2O; Melluso et al., 2011a; Supplementary Fig. 5), though it still occurs as a groundmass phase.

Titanite occurs as rare phenocrysts in benmoreite and trachyphonolites (Supplementary Fig. 1) and modally decreases in the most evolved rocks; it usually co-crystallizes with clinopyroxene. The FeO_t varies from 1.6 and 7.4 wt.%, the $\sum REE_2O_3$ range from 1.4 to 5.7 wt.%, and ZrO_2 reaches concentrations as high as 7.8 wt.%, but it is usually far lower (0-4 wt.%). **Apatite** is ubiquitous as a groundmass phase, and can be found also as microphenocrysts in the phonotephrites. The concentration of F varies from 1.4 to 4.9 wt.% Cl can be high (up to 1.8 wt.%; average 1.19 wt.%), and SO_3 is locally significant (up to 1 wt.% in crystals of a tephrite and 2.3 wt.% in crystals of phonotephrite RT-06I-398; Supplementary Table S9). Rare crystals of **britholite** $[(Ca,LREE,Th)_5(SiO_4,PO_4)_3(OH,F)]$ (SiO_2=21.7 wt.%; $\sum REE_2O_3$=52 wt.%, F=1.9 wt.%, no Cl and SO_3) are found in the groundmass of trachyphonolites. **Zircon** has been found in the interstices of a trachyphonolite. **Fluorite** is also noted, as well as **hiortdahlite** [ideally $(Ca,Na)_3(Zr,Ti)Si_2O_7(F,O,OH)_2$] in the groundmass of the trachyphonolite RT-061-379 (Supplementary Table 9). Hiortdahlite has been noted in the Ampasindava phonolites (northern Madagascar; Cucciniello et al., 2016) and, together with the Na-rich clinopyroxene, indicates the

transition of the groundmass liquids to peralkaline compositions. Other accessories and secondary zeolites (mostly analcime around nepheline) are present in the interstices.

4. Bulk-rock geochemistry

The concentration of MgO, Cr and Ni in the most primitive basanites (9-9.2 wt.%, 277-288 ppm and 154-164 ppm, respectively), the Mg# (56-59) and the relatively low forsterite content of the olivine phenocrysts indicate that the most primitive Itasy rocks can be considered as evolved liquid compositions which suffered previous removal of Mg-rich olivine, Cr-spinel and Mg-rich clinopyroxene from more primitive basanites. At the same time, basanites and tephrites have high concentration of TiO_2 (3-4.7 wt.%) and P_2O_5 (0.6-1.9 wt.%) (Table 1; Supplementary Table S1). The variations of CaO, TiO_2, Al_2O_3, Fe_2O_{3t} and alkalies of the mafic rocks, and the mineral composition in basanites and tephrites depict trends at least qualitatively compatible with removal of pyroxene, amphibole, olivine and oxides, and minor or negligible removal of feldspar and apatite (Supplementary Fig. S5). The transition from phonotephrite to benmoreite and trachyphonolites is characterized by no significant variation of Al_2O_3, a change of slope of many minor and trace element trends, a drop in the concentration of P_2O_5, and a decrease of Y with MgO. The concentration of Ba and Sr also drops in the most evolved trachyphonolites (Supplementary Fig. S6). The variations of Rb and Ba of the basanites and other features suggest some heterogeneity in the composition of the mafic parental magmas. The Zr/Hf ratios increase from 45 in the basanites to 60 in the evolved trachyphonolites, whereas the Nb/Ta ratio is 14-15 in the basanites and 21-28 in the most evolved trachyphonolites (Table 1; Supplementary Fig. S7). The La/Nb, Ba/Nb, Ce/Pb and Nb/U ratios of the least evolved basanites (La/Nb=0.83-0.88, Ba/Nb=8-12, Ce/Pb=30-41 and Nb/U=42-52) match the values expected from mantle-derived magmas free of effects related to crustal contamination in the source or *en route* to the surface, and the low Zr/Nb of the basanites (4.2-4.8) indicate a highly enriched source region (Melluso et al., 2016 and references therein). The REE patterns of the mafic rocks (Supplementary Fig. S8a) are smooth and highly fractionated (La/Yb_n=24-27), have no peaks or troughs at Eu, and increase in the total REE concentration (279-800 ppm) from basanites to the phonotephrites. Starting from the phonotephrites RT-06I-398 and RT-06I-397, the REE patterns of benmoreites and trachyphonolites become increasingly concave, with a marked decrease of intermediate-REE to values even lower than those of the basanites (sample RT-061-357B; Supplementary Fig. S8a, c, d, e), largely constant La_n and Lu_n, and small troughs at Eu (Eu/Eu*=0.79). These characteristics are highlighted when REE are compared to the concentration of the least evolved basanite RT-061-354B (Supplementary Fig. S8e). The mantle normalized patterns of the Itasy basanites (Fig. 5a, 5b) are almost flat from Rb to Th, have a peak at

Nb and Ta, a trough at K and Pb, and a smooth decreasing slope towards the HREE, with no trough at Zr and Hf, confirming the similarity of the trace element enrichment in the mantle sources throughout the Cenozoic province (cf. Melluso et al., 2016). The very marked geochemical differences with the primitive (MgO=9-12 wt.%) *haüyne-leucite*-basanites of Mt.Vulture (Italy), which were generated in a subduction-modified upper mantle source (e.g., Beccaluva et al., 2002), and the similarities with the potassic basanites of the Virunga area (Congo-Rwanda, western branch of the East African Rift), another within-plate volcanic area as is Itasy (e.g., Rogers et al., 1992), are highlighted in Fig. 5.

5. The concentration of trace elements in titanite, clinopyroxene, kaersutite and anorthoclase of Itasy trachyphonolites

The mantle normalized patterns of the evolved rocks (Fig. 5c) show relative decrease of P, Ti, Ba, Sr, Ta, Y and middle-REE, and relative increase of Rb, Th, U, Nb, Zr and Hf from the least to the most evolved trachyphonolites. In order to understand the changes of the chemical composition of the trachyphonolites, we also investigated the geochemistry of titanite, kaersutite, clinopyroxene and anorthoclase phenocrysts of the trachyphonolite RT-06I-355 (Table 2; Fig. 6; Supplementary Fig. S8). The **titanites** have very high concentration of REE (ΣREE=28,000-31,500 ppm), Y (1730-2250 ppm), Ta (650-1130 ppm), Th (134-187 ppm), V (216-328 ppm) and Hf (140-202 ppm), high Zr (4500-5800 ppm), Nb (6200-15230 ppm), U (15-27 ppm) and La/Yb_n ratios (19-28), no troughs at Eu in the chondrite-normalized REE diagrams (Supplementary Fig. S8b), and low Ba (42-49 ppm), Pb (<1.1 ppm) and Sr (54-382 ppm). The Nb/Ta ratio of the titanites is low (8-13) and the Th/U is high (8.5-10.3), with respect to typical chondritic ratios (15 and 3.6-4, respectively). The titanites also have slight chemical zoning, with an increasingly concave REE pattern (Table 2; Supplementary Fig. S8b). The patterns of the Itasy titanites are generally similar, but displaced to higher REE concentrations, to those reported by Marks et al. (2008) and Melluso et al. (2010) on titanites of alkaline intrusive rocks of variable degree of evolution (clinopyroxenites, ijolites, monzosyenites, to agpaitic nepheline syenites; Supplementary Fig. 8g), which also have widely variable Nb/Ta ratios (8-66). The Itasy titanite/bulk-rock elemental ratios are of the same magnitude of the partition coefficients of Olin and Wolff (2012) only for La, Ce and Lu (Supplementary Fig. 8f). **Kaersutite** is a corroded phase, and has a different trace element pattern, with a concentration of ΣREE which is one or two orders of magnitude lower than the concentration of REE of the coexisting titanites (911 ppm; La_n= 419 times chondrite; Table 2). It still has relatively high Li (144 ppm), Y (81 ppm), Zr (732 ppm), Nb (200 ppm), moderate Ba (1100 ppm) and very low Rb, Pb, Th

and U, when compared to the host-rock bulk composition (Table 1; Fig. 6b). The **clinopyroxene** has low concentration of REE (ΣREE=350-690 ppm; La/Yb_n=8-15), and very low concentration of other elements (Table 2), excluding Zn (600-662 ppm). **Anorthoclase** has high and variable Ba (1500-28220 ppm), Sr (534-4300 ppm), Rb (7-98 ppm), Pb (4.6-9 ppm) and Eu (0.5-1.6 ppm). These elements peak in the mantle-normalized diagrams (Fig. 6b). Other chemical details can be found in the Table 2.

6. Isotopic composition of the Itasy rocks

The isotopic composition of Itasy rocks is reported in the Table 3. The basanites (MgO= 7-10 wt.%) have a restricted range of $^{87}Sr/^{86}Sr$ (0.70366-0.70378), $^{143}Nd/^{144}Nd$ (0.51274-0.51277) and Pb isotopes ($^{206}Pb/^{204}Pb$=18.7-18.9; $^{207}Pb/^{204}Pb$=15.53-15.56; $^{208}Pb/^{204}Pb$=38.89-39.01), which indicate a largely uniform mantle source, characterized by low time-integrated Rb/Sr and Sm/Nd ratios. This source is isotopically similar, but not identical, to that of the mafic alkaline rocks of the Ankaratra (nephelinites, basanites and alkali basalts; cf. Melluso et al., 2016; Cucciniello et al., 2017; Fig. 7) and to that of the olivine melilitites to the east and northeast of Ankaratra (Melluso et al., 2011a), which do not have evidence of crustal contamination. The phonotephrites have $^{87}Sr/^{86}Sr$=0.70394-0.70398, $^{143}Nd/^{144}Nd$= 0.51273-0.51274, $^{206}Pb/^{204}Pb$=18.74-18.84, $^{207}Pb/^{204}Pb$=15.53-15.54 and $^{208}Pb/^{204}Pb$=38.97-39.02, all values broadly similar (or indistinguishable in some isotope ratios) to those of the basanites, whereas the benmoreite and the trachyphonolites have higher $^{87}Sr/^{86}Sr$ (0.70430-0.70446) and lower $^{143}Nd/^{144}Nd$ (0.51266-0.512682), $^{206}Pb/^{204}Pb$ (18.18-18.39), $^{207}Pb/^{204}Pb$ (15.49-15.51) and $^{208}Pb/^{204}Pb$ (38.38-38.57) than the mafic rocks. Therefore, the isotopic composition of the Itasy rocks changes with MgO. A broadly similar isotopic variation between associated mafic and evolved rocks has been noted in both Cretaceous and Cenozoic volcanic rocks of Madagascar (cf. Cucciniello et al., 2010, 2013, 2017) and indicates that, if basanites and trachyphonolites (which crop out in the same area and have the same stratigraphic age) are part of a comagmatic suite, the evolved rocks suffered interaction with the old, low-Pb/Pb basement rocks during magmatic evolution in low-pressure magma reservoirs. This part is developed in the discussion.

7. Discussion

7.1. The unusual transition between basanites/tephrites and trachyphonolites

The Itasy volcanic rocks have some interesting petrogenetic features shared with those of other volcanic areas worldwide: 1) the leucite-bearing basanites recall analogues found in other areas (e.g., the Roman Province, the western branch of the East African Rift); 2) the presence of haüyne (±sodalite)-bearing alkaline volcanic rocks is found in alkaline rocks of various tectonic settings (e.g., Massif Central: Vatin-Perignon, 1968; Eifel: Wörner and Schmincke, 1984; Tenerife: Bryan, 2006; Mt. Etinde: Nkombou et al., 1995; Mt. Vulture: Beccaluva et al., 2002; Melluso et al., 1996, 2011b, among other places), and indicate abundant sulfur in the oxidized state (and chlorine as well); 3) trachyphonolites similar to those of Itasy are common evolved lithotype of other major volcanic areas (e.g., Suswa, Kenya; Phlegrean Fields-Ischia, Italy). These trachyphonolites are the product of low-pressure fractional crystallization processes, possibly in an open system. From a more general view, basanites and tephrites (and maybe also some nephelinite types) are associated with phonolites *s.s.*, rather than trachyphonolites, as is found in northernmost Madagascar and elsewhere (e.g., le Roex et al., 1990; Ablay et al., 1998; Melluso et al., 2007; Berger et al., 2014). In contrast, trachytes (trachyphonolites) are typically associated with (potassic or sodic) alkali and transitional basalts (e.g., Marion Island, le Roex et al., 2012; St. Helena, Kawabata et al., 2010 and references therein; Ischia-Phlegrean Fields, Fedele et al., 2008; Melluso et al., 2012, 2014; Libya, Lustrino et al., 2012; Mauritius: Sheth et al., 2003; Ashwal et al., 2016; Ethiopian Rift, Ronga et al., 2010; Kenya Rift: White et al., 2012).

The magmatic evolution of the Itasy basanites and tephrites (the most Mg-rich of them equilibrated with olivine at temperatures just lower than 1200°C, according to Roeder and Emslie, 1970), is without any evidence of removal of plagioclase or leucite, because these phases are found exclusively as tiny groundmass microlites (e.g., Supplementary Fig. 1). Sodic plagioclase appears as a phenocryst phase in benmoreites; anorthoclase and Na-sanidine (plus rare mafic phases) are the dominant phenocrysts and groundmass phases in the trachyphonolites. It is thus evident that removal of Na-feldspars was essential for the evolution of (sodic) trachyphonolitic liquids towards the phonolite minimum. This is also indicated by the position of the evolved samples in the Petrogeny Residua's System, which plot between the trachytic and the phonolitic minima (slightly less than 900°C, at 1 kbar P_{H2O}), hence within the silica undersaturated field (Fig. 8a, b). The tendency of the bulk-rock trachyphonolitic compositions to plot close to the composition of their (Na-rich) alkali feldspars (Fig. 4a) can be considered as the *normal* evolution towards the pertinent minimum melt compositions. The lack of *phenocrysts* of sodic feldspathoids is another indication that the bulk-rock compositions approach, but do not reach, the phonolitic minimum. For comparison, the phonolites (*s.s.*) of northernmost Madagascar (Melluso et al., 2007; Cucciniello et al., 2016) have nepheline phenocrysts, and plot on the alkali feldspar-nepheline cotectics (Fig. 8b).

The volatiles that left trace in the Itasy magmatic system are H_2O (hosted in amphibole, apatite, the rare biotite, and glass), SO_3 (hosted in the haüyne-sodalite solid solutions and in apatite), Cl (hosted in sodalite, apatite and glass) and F (hosted in apatite, amphibole, glass, fluorite and other accessories). No evidence for a significant role of CO_2 in the petrogenesis of the Itasy basanites and trachyphonolites has been found, as expected by the insignificant maximum quantity of this compound that can be theoretically dissolved in basanitic melts at low pressure, when compared to H_2O (e.g., Shishkina et al., 2014), a quantity even lower in trachytes and phonolites (Webster et al., 2014). The Itasy basanites and tephrites have significant amounts of kaersutite, indicating that the magmatic crystallization took place in a H_2O-rich environment at relatively early differentiation stages. Kaersutite is unknown in basanites and alkali basalts (and nephelinites too) of the nearby Ankaratra complex, that have mostly anydrous mineral assemblages, and occurs as a phenocryst phase only in a few benmoreites (Cucciniello et al., 2017). Kaersutite *s.s.* crystallizes in mafic, hydrous, feldspar-bearing (or -normative), high-Ti alkaline magmas, and has a range of crystallization depths from the uppermost mantle (e.g., Irving and Green, 2008; Pilet et al., 2010) to shallow conduits or shallow intrusions (e.g., Melluso et al., 2005, 2007); hence this phase is more a chemical than a barometric indicator (cf. Supplementary Fig. S4). Sulfur was at least partially partitioned in the S-bearing apatite before reaching saturation as haüyne, in the groundmass of the phonotephrites and in the evolved rocks; sulfur decreases in the latest crystallized groundmass, as testified by the presence of sodalite (cf. also Supplementary Fig. S1).

7.2. Petrogenetic modelling: the essential role of titanite and anorthoclase removal in the geochemical evolution of the trachyphonolites, and open-system processes

The petrogenetic study of the Itasy volcanic rocks is focused on the genetic relationships between this bimodal suite of mafic and evolved rocks, with their changing isotopic ratios and the marked decrease in the degree of silica undersaturation of the evolved rocks. Despite the compositional gap between mafic and evolved rocks shown in the diagrams, involving a marked change of density, temperatures and time of storage in shallow reservoirs, we observe the following: 1) the mineral phases have a continuous compositional change from mafic, through intermediate, to felsic rocks, as a typical consequence of fractional crystallization processes (see above); 2) the bulk-rock compositions have the expected changes considering the variety and amount of the phenocryst phases, thus excluding effects of magma mixing; 3) many basanites and tephrites are rich in phenocrysts/megacrysts of kaersutite (a phase significantly lower in silica than clinopyroxene but with similar density), whose significant removal could help increase the concentration of SiO_2 of residual melts.

The variation diagrams (Supplementary Fig. S6) and the petrography of the mafic rocks indicate that clinopyroxene, amphibole, olivine and magnetite (for Fe and Ti) are probably the best candidates to form the subtracted mineral assemblages in the transition from basanites to phonotephrites. Among several models using the major element compositions of bulk-rocks and their phenocryst phases, the transition from basanites (e.g. RT-06I-354B) to tephrites (RT-061-395) and benmoreite (RT-06I-387) can be accounted for by 37% and 56% removal of ultramafic assemblages, respectively. The transition from the benmoreite RT-06I-387 to the trachyphonolite RT-06I-375B needs 61% removal of monzonitic assemblages. The total transition from the basanite RT-06I-354B to a trachyphonolite (e.g., sample RT-06I-375B) was modelled with 71.4% removal of ultramafic assemblages (cf. Supplementary Table S10). The results we choose have low ΣR^2 (values of $\Sigma R^2 << $ or <0.5 can be considered for modelling, but they are not proof of geological reliability), but the high kaersutite/clinopyroxene ratio involved in some transitions between mafic rocks is always to be matched with the actual subtracted assemblages, which are, of course, largely unknown.

Thermodynamic models of magmatic evolution (e.g., MELTS) are not able to account for the presence of kaersutite, sodalite-group minerals, titanite and a number of other petrographic features of alkaline rock suites, including the crystallization sequence, the phase composition and their actual amount. LeMasurier et al. (2011) hypothesized a significant role for kaersutite removal in order to account for the petrogenesis of evolved silica oversaturated rocks starting from basanite parental magmas; in our case, we show that this effect is limited to the transition from tephrites to benmoreites, because the final transition to the most evolved Itasy trachyphonolites cannot involve significant removal of amphibole (kaersutite is already a minor phenocryst phase in the least evolved trachyphonolites).

A number of observations and models indicate that the Itasy benmoreites and trachyphonolites could be comagmatic with the basanites, through (also) the effects of kaersutite removal. The trace element variations using thorium as the most incompatible element were modelled using the Rayleigh equation (Supplementary Fig. S7). The following features are of interest: a) assuming that Th behaves in a closed system (an approximation that cannot be guaranteed during AFC processes, see below) and that is the most incompatible element, the total amount of crystallization needed to reach the phonotephritic liquids is roughly 60%, and is 75-80% to reach evolved trachyphonolites, starting from the least evolved basanites; b) the transition from basic to intermediate rocks is characterized by several major changes in the slope of the trace elements vs. the Th concentration and, therefore, in their bulk partition coefficients (D); this change in slope takes place at different evolution points (Supplementary Fig. S6 and S7); c) tantalum (Ta) behaves as a highly compatible element in the trachyphonolites, thus strongly decouples from the geochemically similar element Nb; roughly similar fractionation is noted between Hf and Zr, whereas U and Th behave sympathetically (the

Th/U ratio ranges between 3.6 and 4.4, both values in basanites); d) lead (Pb) increases more than that expected from a perfectly incompatible behaviour (modelling requires $D_{Pb}<0$; Supplementary Fig. S7), strongly suggesting the introduction of external Pb during crustal contamination processes; e) the chemical composition of the trachyphonolites is scattered, indicating that the magmatic evolution took place in independent magma feeder systems, hence with variable distribution, crystallization and removal of phases.

The petrography, the increasingly concave REE patterns of the trachyphonolites, the trace element concentration of the titanite phenocrysts, and numerical modelling using both published partition coefficients and the mineral composition determined by LA-ICP-MS (Supplementary Fig. S8) indicate a major effect of titanite on the fractionation of middle-REE, Y, Ta and other elements, even though full quantification of the extent of removal of an accessory phase cannot be obtained through major oxide mass balance calculations or trace element behaviour. The trend to the most evolved trachyphonolites can be obtained through 0.7-1% removal of titanite (cf. Supplementary Fig. S8c, d). Removal of small amounts of titanite is commonplace in evolved alkaline rocks (cf. the extremely similar patterns reported in Ulrych et al., 2006; Lustrino et al., 2012; Melluso et al., 2014, 2017 and references therein), and the effects observed in this work are broadly those expected utilizing the titanite/melt partitioning data of Olin and Wolff (2012) (Supplementary Fig. S8c, Supplementary Table S11). Apatite can have a roughly similar behaviour regarding middle-REE fractionation, although to a lower extent (the partition coefficients of apatite can be lower of a factor of 3-4; cf. Supplementary Table S11 and Supplementary Fig. S8c), but has minor or negligible effect on the concentration of Ta, Hf, Zr and Nb. Removal of other phases such as clinopyroxene or amphibole, in the amount observed in the least evolved trachyphonolites (Supplementary Fig. S1), cannot have appreciable role in preferentially removing middle- from heavy-REE in evolved melts (cf. partitioning data of Tiepolo et al. 2007; Fedele et al., 2009; Melluso et al., 2017; this work), and so is for other accessory phases *absent* at Itasy (e.g., melanite garnet, or significant zircon).

The evolved samples of Itasy show compelling evidence for open-system evolution, as seen from the isotopic variations and elemental evidence above. We performed an AFC model (DePaolo, 1981) utilizing all the isotopic systematics, pertinent trace elements and compositions of the Madagascan basement in the area. The results highlight the effects of prolonged fractional crystallization (roughly 70%) and limited, though widely variable, crustal contamination (the values of the assimilation/cumulus rate, -r-, are <0.3) of known felsic rocks of the Precambrian basement (details in Fig. 9). The model takes into account the marked changes in the bulk partition coefficients of many elements at varying levels of magmatic evolution (Supplementary Fig. S8). The phonotephrites (samples RT-06I-397 and RT-06I-398) still need limited amount of crustal contamination in order to account for their slightly differing isotopic ratios compared to those of

basanites and tephrites. The abrupt change of partition coefficients in the evolved rocks and a limited change of the parameter "r" (Fig. 9) led to the bimodal isotopic compositions. It is also evident that the effects of crustal contamination did not act uniformly throughout the Itasy suite, and that other processes could have been operative in the Itasy feeder system, including silica increase that may be expected from interaction with the felsic lithologies of the Madagascan basement, and the presence of alkali basaltic parental magmas (more SiO_2-rich than a basanite), of which there is no evidence, *to date*.

7.3. The mantle sources of Itasy in the context of the Cenozoic magmatism of Madagascar

The Itasy basanites have Sr-Nd-Pb-isotopic ratios indicating a source geochemically and isotopically different from that of convecting asthenosphere, which experienced a distinct evolution with time. This is fully consistent with what is known in the Cenozoic mafic rocks of the central Madagascar, which were emplaced above Archean crust (Melluso et al., 2011a, 2016; Cucciniello et al., 2017). Primitive basanitic magmas with the petrographic and geochemical characteristics similar to those of the Itasy imply low degrees of partial melting (ca. 3%) of a hydrous, amphibole-bearing lherzolite, and hence at depths and temperatures where *pargasitic* amphibole can be a stable phase of a peridotite (say, <90-100 km; e.g., Kovacs et al., 2017), as previously suggested by earlier work in central and northern Madagascar (Melluso and Morra, 2000; Melluso et al., 2016 and references therein; Rocco et al., 2017), and elsewhere (cf. le Roex et al., 2001; Green and Falloon, 2015). A relatively shallow depth of the (lithospheric) source region of the Itasy basanites is also indicated by a rootless low-velocity zone (supposedly melt-, volatile- or light phases-bearing) just beneath the Moho, extending at depths of 50-80 km (Fig. 1c; Pratt et al., 2017). The E-W-trending extensional processes active in central Madagascar seem to have favoured moderate uplift of this geochemically enriched, volatile-bearing lithospheric mantle, bringing it above the solidus and forming the Itasy low-volume basanitic lava field. The source of the Itasy basanites must be characterized by a significant enrichment of highly incompatible elements (cf. the low Ba/Nb and Zr/Nb ratios, and the shape of the mantle normalized patterns), with particular reference to the HFSE, in agreement with a fully within-plate origin, without subduction-related components or low-pressure crustal contamination. The source of the Itasy basanites cannot be depleted asthenospheric -or primitive-mantle, assuming any reasonable degrees of partial melting and considering the isotopic composition (cf. also Melluso et al., 2016 and Cucciniello et al., 2018, for a regional review). Finally, in terms of trace element and isotopic composition, the sources of the Cenozoic volcanic rocks of Madagascar share very little with those giving rise the Cretaceous *tholeiitic* magmatism (cf. Melluso et al., 2001, 2005, 2011a, 2016; Cucciniello et al., 2010, 2013, 2017).

8. Conclusions

The Itasy volcanic field, the most recently active in Madagascar, is characterized by an association of high-TiO_2, potassic basanites/tephrites/phonotephrites and benmoreites/ trachyphonolites, in the facies of pyroclastic rocks and lava flows, with the highly featuring presence of Ti-rich amphibole in mafic/intermediate rocks and haüyne-sodalite *s.s.* in evolved rocks. Recognizing the possibility of independent basanitic parental magmas and different liquid lines of descent, leucite basanite magmas evolved through removal of olivine, clinopyroxene, kaersutite and magnetite to reach the volumetrically minor benmoreitic and trachyphonolitic compositions. These latter rocks are likely the result of low-pressure fractional crystallization of anorthoclase/sanidine-bearing (*syenitic*) assemblages and minor crustal contamination of the high-$^{87}Sr/^{86}Sr$, low- $^{143}Nd/^{144}Nd$, -$^{206}Pb/^{204}Pb$, -$^{207}Pb/^{204}Pb$ and -$^{208}Pb/^{204}Pb$, old granitic-migmatitic basement of the area, with the evidence of minor titanite removal (perhaps <2%), as part of syenitic/monzosyenitic cumulates. Titanite is demonstrated to be a very efficient scavenge of intermediate-REE, Y, Ta and V, and slightly less so for Nb, Zr and Hf in the Itasy trachytic (*s.l.*) magmas (cf. Table 2); its removal, even in small amounts, significantly increases ratios between otherwise geochemically similar elements (e.g., Zr/Hf, Nb/Ta) when compared to those of the associated mafic rocks. Another minor but interesting result of this study is the evidence that the concentration of rare earths or other strategic elements in the most highly evolved alkaline magmas cannot be considered a rule working worldwide, due to the presence of accessory phases on the liquidus, which effectively scavenge these elements in less evolved melts. *Also* due to the removal of titanite and other accessory phases, the geochemical characteristics of trachytic (*s.l.*) rocks *worldwide* cannot give unambiguous indication about those of associated (or parental) mafic magmas, or even to indicate mantle signatures of any kind, including ratios of elements thought to be highly incompatible. The geochemical and isotopic characteristics of the leucite-basanites broadly match those of the nearby Ankaratra volcano and of the rest of the Cenozoic volcanic districts of Madagascar (Melluso et al., 2016), and testify to a mantle source having marked enrichment in LILE, HFSE and volatile elements (H_2O, Cl, F, SO_3), as noted in other within-plate strongly alkaline rocks worldwide and, intriguingly, also in some subduction-related alkaline rocks. The broadly E-W extensional processes common in central Madagascar triggered low-degree partial melting of enriched, volatile-rich, lithospheric mantle, and generated the low-volume Itasy basanites, without the need to invoke the action of mantle plumes. Enriched geochemical components of within-plate origin are commonplace in the Madagascan lithospheric mantle (Melluso et al., 2016; Rocco et al., 2017). Finally, the unusual petrogenetic association between basanites and trachyphonolites, and the likely significant removal of kaersutitic amphibole

in some basanites and tephrites, are of importance in identifying the volatile species of within-plate alkaline rocks in the mantle sources and during the magmatic evolution.

A high-resolution geochronological framework is now needed to establish an accurate age span for the Itasy, if a significant temporal lapse exists between mafic and evolved rocks, and the relationships between timing of volcanism and extensional tectonics of central Madagascar.

Acknowledgements

This paper is dedicated to the memory of Fabio Carmine Mazzeo.

Alessio Langella, Sergio Bravi, Petrus Le Roux, Roberto de' Gennaro, Vohangy Ratrimo, Dieudonné Razafimahatratra, Vincenza Guarino, Luigi Franciosi and Lorenzo Fedele are gratefully thanked for helping us in sampling, data acquisition and comments on an early draft of the manuscript. The constructive reviews of Jean-Paul Liégeois and Michael Marks and advice of the Editor-in-chief Xian-Hua Li were very helpful to improve contents and presentation of an early version of the manuscript. This paper was supported by grants provided by PRIN2015 (grant 20158A9CBM) and LR5 (Regione Campania) to L. Melluso, and Fondi Ricerca di Ateneo (DR_3450_2016) to C. Cucciniello.

References

Ablay, G.J., Carroll, M.R., Palmer, M.R., Martí, J., Sparks, R.S.J., 1998. Basanite–phonolite lineages of the Teide–Pico Viejo volcanic complex, Tenerife, Canary Islands. Journal of Petrology 39, 905-936.

Andrianaivo, L., Ramasianoro, V.J., 2010. Relation between regional lineament systems and geological structures: implications for understanding structural controls of geothermal system in the volcanic area of Itasy, Madagascar. Proceedings World Geothermal Congress, Bali, 1-9.

Andrianaivo, L., Ramasianoro, V.J., 2011. Relations between drainage pattern and fracture trend in the Itasy geothermal prospect, central Madagascar. Madamines 2, 22-39.

Ashwal, L.D., Torsvik, T.H., Horvath, P., Harris, C., Webb, S., Werner, S., Corfu, F., 2016. A mantle-derived origin for Mauritian trachytes. Journal of Petrology 57, 1645–1675.

Battistini, R., 1962. Le massif volcanique de l'Itasy (Madagascar). Annales Geographie 384, 167-178.

Beccaluva, L., Coltorti, M., Di Girolamo, P., Melluso, L., Milani, L., Morra, V., Siena, F., 2002. Petrogenesis and evolution of Mt. Vulture alkaline volcanism (Southern Italy). Mineralogy and Petrology 74, 277-297.

Berger, J., Ennih, N., Mercier, J.-C.C., Liegeois, J.-P., 2014. Extreme trace element fractionation in Cenozoic nephelinites and phonolites from the Moroccan Anti-Atlas (Eastern Saghro). Lithos 210-211, 69-88.

Boynton, W.B., 1984. Cosmochemistry of rare earth elements: meteorite studies. In Henderson P. (ed.) Rare Earth Element Geochemistry. Elsevier, Amsterdam, 63-114.

Brenon, P., Bussiere, P., 1959. Le volcanism à Madagascar. Bulletin Volcanologique 21, 77-93.

Brown, S.K., Sparks, R.S.J., Mee, K., Vye-Brown, C., Ilyinskaya, E., Jenkins, S.F., Loughlin, S.C., 2015. Country and regional profiles of volcanic hazard and risk. In: Loughlin S.C., Sparks, R.S.J., Brown, S.K., Jenkins, S.F., Vye-Brown, C. (eds.): Global Volcanic Hazards and Risk. Cambridge University Press.

Bryan, S.E., 2006. Petrology and geochemistry of the Quaternary caldera-forming, phonolitic Granadilla eruption, Tenerife (Canary Islands). Journal of Petrology 47, 1557-1589.

Bussiere, P., 1957. Part XII. Le massif volcanique de l'Itasy. In: Besairie, H., Boulanger, J., Brenon, P., Bussiere, P., Emberger, A., de St. Ours, J.: Le Volcanisme à Madagascar. Travaux du Bureau Géologique no. 83, Service Géologique de Madagascar, Tananarive, 240 pp.

Cucciniello, C., 2016. Tetra-Plot: A Microsoft Excel spreadsheet to perform tetrahedral diagrams. Periodico di Mineralogia 85, 115-119.

Cucciniello C., Langone A., Melluso L, Morra V., Mahoney J.J., Meisel T., Tiepolo M., 2010. U-Pb ages, Pb-Os isotopes and platinum group element (PGE) composition of the west-central Madagascar flood basalt province. The Journal of Geology 118, 523-541. http://dx.doi.org/10.1086/655012

Cucciniello C., le Roex A.P., Jourdan F., Morra V., Grifa C., Franciosi L., Melluso L., 2018. The mafic alkaline volcanism of SW Madagascar (Ankililoaka, Tulear region): $^{40}Ar/^{39}Ar$ ages, geochemistry and tectonic setting. Journal of the Geological Society, London, in press, http://dx.doi.org/10.1144/jgs2017-139

Cucciniello, C., Melluso, L., Jourdan, F., Mahoney, J.J., Meisel, T., Morra, V., 2013. ^{40}Ar-^{39}Ar ages and isotope geochemistry of Cretaceous basalts in northern Madagascar: refining eruption ages, extent of crustal contamination and parental magmas in a flood basalt province. Geological Magazine 150, 1-17. http://dx.doi.org/10.1017/S0016756812000088

Cucciniello, C., Melluso, L., le Roex, A.P., Jourdan, F., Morra, V., de' Gennaro, R., Grifa, C., 2017. From nephelinite, basanite and basalt to peralkaline trachyphonolite and comendite in the Ankaratra volcanic complex, Madagascar: $^{40}Ar/^{39}Ar$ ages, phase compositions and bulk-rock geochemical and isotopic evolution. Lithos 274-275, 263-271. http://dx.doi.org/10.1016/j.lithos.2016.12.026

591 Cucciniello, C., Melluso, L., Morra, V., Storey, M., Rocco, I., Franciosi, L., Grifa, C., Petrone,
592 C.M., Vincent, M., 2011. New ^{40}Ar-^{39}Ar ages and petrogenesis of the Massif d'Ambre volcano,
593 northern Madagascar. In: Beccaluva, L., Bianchini, G., Wilson, M. (eds.) Volcanism and
594 Evolution of the African Lithosphere. Geological Society of America Special Papers 478, 257-
595 282. http://dx.doi.org/10.1130/2011.2478(14)
596 Cucciniello, C., Tucker, R.D., Jourdan, F., Melluso, L., Morra, V., 2016. The age and petrogenesis
597 of the alkaline magmatism of Ampasindava Peninsula and Nosy Be archipelago, northern
598 Madagascar. Mineralogy and Petrology 110, 309-331. http://dx.doi.org/10.1007/s00710-015-
599 0387-1
600 DePaolo, D.J., 1981. Trace element and isotopic effects of coupled fractional crystallization and
601 crustal contamination processes. Earth and Planetary Science Letters 53, 189-202.
602 Fedele, L., Lustrino, M., Melluso, L., Morra, V., Zanetti, A., Vannucci, R., 2015. Trace element
603 distribution in plagioclase, alkali feldspar, Ti-magnetite, biotite and apatite in evolved potassic
604 liquids from Campi Flegrei (Southern Italy). American Mineralogist 100, 233-249. doi:
605 10.2138/am-2015-4995
606 Fedele, L., Scarpati, C., Lanphere, M.A., Melluso, L., Morra, V., Perrotta, A., Ricci, G., 2008. The
607 Breccia Museo formation, Campi Flegrei, southern Italy: geochronology, chemostratigraphy and
608 relationships with the Campanian Ignimbrite eruption. Bulletin of Volcanology 70, 1189-1219.
609 http://dx.doi.org/10.1007/s00445-008-0197-y
610 Fedele, L., Zanetti, A., Lustrino, M., Melluso, L., Morra, V., Vannucci, R., 2009. Insights on
611 clinopyroxene/liquid trace element partitioning in natural trachyte-phonolite systems: a EMP/LA-
612 ICP-MS case study from Campi Flegrei (Italy). Contributions to Mineralogy and Petrology 158,
613 337-356. http://dx.doi.org/10.1007/s00410-009-0386-5
614 Galer, S.J.G., Abouchami, W., 1998. Practical application of lead triple spiking for correction of
615 instrumental mass discrimination. Mineralogical Magazine 62A, 491-492.
616 Green, D.H., Falloon, T.J., 2015. Mantle-derived magmas: intraplate, hot-spots and mid-ocean
617 ridges. Scientific Bulletin 60, 1873-1900.
618 Gupta, A.K., 2015. Origin of potassium-rich silica-deficient igneous rocks. Springer, 536 pp. ISBN:
619 978-81-322-2082-1
620 Irving, A.J., Green, D.H., 2008. Phase relationships of hydrous alkalic magmas at high pressures:
621 production of nepheline hawaiitic to mugearitic liquids by amphibole-dominated fractional
622 crystallization within the lithospheric mantle. Journal of Petrology 49, 741-756.
623 Kawabata, H., Hanyu, T., Chang, Q., Kimura, J.-I., Nichols, A.R.L., Tatsumi, Y., 2011. The
624 petrology and geochemistry of St. Helena alkali basalts: evaluation of the oceanic crust-recycling
625 model for HIMU OIB. Journal of Petrology 52, 791-838.

626 http://dx.doi.org/10.1093/petrology/egr003
627 Kovacs, I., Lenkey, L., Green, D.H., Fancsik, T., Falus, G., Kiss, J., Orosz, L., Angyal, J., Vikor Z.,
628 2017. The role of pargasitic amphibole in the formation of major geophysical discontinuities in
629 the shallow upper mantle. Acta Geodynamica et Geophysica 52, 183–204.
630 Kröner, A., Hegner, E., Collins, A.S., Windley, B.F., Brewer, T.S., Razakamanana, T., Pidgeon,
631 R.T., 2000. Age and magmatic history of the Antananarivo Block, Central Madagascar, as
632 derived from zircon geochronology and Nd isotopic systematics. American Journal of Science
633 300, 251-288.
634 Lacroix, A., 1923. Mineralogie du Madagascar. vol. 3. Augustin Challamel, Paris.
635 LeMasurier, W.E., Choi, S.H., Kawachi, Y., Mukasa, S.B., Rogers, N.W., 2011. Evolution of
636 pantellerite-trachyte-phonolite volcanoes by fractional crystallization of basanite magma in a
637 continental rift setting, Marie Byrd Land, Antarctica. Contributions to Mineralogy and Petrology
638 162, 1175–1199.
639 le Roex, A.P., Chevallier, L., Verwoerd, W.J., Barends, R., 2012. Petrology and geochemistry of
640 Marion and Prince Edward islands, southern Ocean: magma chamber processes and source region
641 characteristics. Journal of Volcanology and Geothermal Research 223-224, 11-28.
642 le Roex, A.P., Cliff, R.A., Adair, B.J.I., 1990. Tristan da Cunha, South Atlantic: geochemistry and
643 petrogenesis of a basanite-phonolite lava series. Journal of Petrology 31, 779-812.
644 le Roex, A.P., Späth, A., Zartman, R.E., 2001. Lithospheric thickness beneath the southern Kenya Rift:
645 implications from basalt geochemistry. Contributions to Mineralogy and Petrology 142, 89-106.
646 Lessing, P., Grout, C.McD., 1971. Haüynite from Edwards, New York. American Mineralogist 56,
647 1096-1100.
648 Lustrino, M., Cucciniello, C., Melluso, L., Tassinari, C.C.G., de' Gennaro, R., Serracino, M., 2012.
649 Petrogenesis of Cenozoic volcanic rocks in the NW sector of the Gharyan volcanic field, Libya.
650 Lithos 155, 218-235. http://dx.doi.org/10.1016/j.lithos.2012.09.003
651 Lyubetskaya, T., Korenaga, J., 2007. Chemical composition of Earth's primitive mantle and its
652 variance: 1. methods and results. Journal of Geophysical Research 112, B03211.
653 http://dx.doi.org/10.1019/2005JB004223
654 Marks, M.A.W., Coulson, I.M., Schilling, J., Jacob, D.E., Schmitt, A.K., Markl, G., 2008. The
655 effect of titanite and other HFSE-rich mineral (Ti-bearing andradite, zircon, eudialyte)
656 fractionation on the geochemical evolution of silicate melts. Chemical Geology 257, 153–172.
657 Melluso, L., Cucciniello, C., le Roex, A.P., Morra, V., 2016. The geochemistry of primitive volcanic
658 rocks of the Ankaratra volcanic complex, and source enrichment processes in the genesis of the
659 Cenozoic magmatism in Madagascar. Geochimica et Cosmochimica Acta 185:435-452.
660 http://dx.doi.org/10.1016/j.gca.2016.04.005

661 Melluso, L., de' Gennaro, R., Fedele, L., Franciosi, L., Morra, V., 2012. Evidence of crystallization
662 in residual, Cl-F-rich, agpaitic, trachyphonolitic magmas and primitive Mg-rich basalt-
663 trachyphonolite interaction in the lava domes of the Phlegrean Fields (Italy). Geological
664 Magazine 149, 532-550.
665 Melluso, L., Guarino, V., Lustrino, M., Morra, V., de' Gennaro, R., 2017. The REE- and HFSE-
666 bearing phases in the Itatiaia alkaline complex (Brazil), and geochemical evolution of feldspar-
667 rich felsic melts. Mineralogical Magazine 81, 217-250. doi: 10.1180/minmag.2016.080.122
668 Melluso, L., le Roex, A.P., Morra, V., 2011a. Petrogenesis and Nd-Pb-Sr- isotope geochemistry of
669 the olivine melilitites and olivine nephelinites ("ankaratrites") in Madagascar. Lithos 127, 505-
670 521. http://dx.doi.org/10.1016/j.lithos.2011.08.003
671 Melluso, L., Morra, V., 2000. Petrogenesis of late Cenozoic mafic alkaline rocks of the Nosy Be
672 archipelago (northern Madagascar): relationships with the Comorean magmatism. Journal of
673 Volcanology and Geothermal Research 56, 129-142
674 Melluso, L., Morra, V., Brotzu, P., Mahoney, J.J., 2001. The Cretaceous igneous province of central-
675 western Madagascar: evidence for heterogeneous mantle sources, crystal fractionation and crustal
676 contamination. Journal of Petrology 42, 1249-1278.
677 Melluso, L., Morra, V., Brotzu, P., Tommasini, S., Renna, M.R., Duncan, R.A., Franciosi, L.,
678 d'Amelio, F., 2005. Geochronology and petrogenesis of the Cretaceous Antampombato-
679 Ambatovy complex and associated dyke swarm, Madagascar. Journal of Petrology 46, 1963-
680 1996.
681 Melluso, L., Morra, V., de' Gennaro, R., 2011b. Coexisting Ba-feldspar and melilite in a melafoidite
682 lava of Mt. Vulture, Italy: role of volatiles and alkaline earths in bridging a petrological
683 incompatibility. The Canadian Mineralogist 49, 983-1000.
684 http://dx.doi.org/10.3749/canmin.49.4.983
685 Melluso, L., Morra, V., Di Girolamo, P., 1996. The Mt. Vulture volcanic complex (Italy): evidence
686 for distinct parental magmas and for residual melts with melilite. Mineralogy and Petrology 56,
687 226-250.
688 Melluso, L., Morra, V., Guarino, V., de' Gennaro, R., Franciosi, L., Grifa, C., 2014. The
689 crystallization of shoshonitic to peralkaline trachyphonolitic magmas in a H_2O-Cl-F- rich
690 environment at Ischia (Italy), with implications for the feeder system of the Campania Plain
691 volcanoes. Lithos 210-211, 242-259. http://dx.doi.org/10.1016/j.lithos.2014.10.002
692 Melluso, L., Morra, V., Riziky, H., Veloson, J., Lustrino, M., Del Gatto, L., Modeste, V., 2007.
693 Petrogenesis of a basanite-tephrite-phonolite volcanic suite in the Bobaomby (Cap d'Ambre)
694 peninsula, northern Madagascar. Journal of African Earth Sciences 49, 29-42.

695 Melluso, L., Srivastava, R.K., Guarino, V., Zanetti, A., Sinha, A.K., 2010. Mineral compositions
696 and magmatic evolution of the Sung Valley ultramafic-alkaline-carbonatitic complex (NE India).
697 The Canadian Mineralogist 48, 205-229; http://dx.doi.org/10.3749/canmin.48.1.205
698 Miller, C., Zanetti, A., Thöni, M., Konzett, J., Klötzli, U., 2012. Mafic and silica-rich glasses in
699 mantle xenoliths from Wau-en-Namus, Libya: Textural and geochemical evidence for
700 peridotite–melt reactions. Lithos 128-131, 11-26.
701 Nkoumbou, C., Déruelle, B., Velde, D., 1995. Petrology of Mount Etinde nephelinite series. Journal
702 of Petrology 36, 373-395.
703 Nicollet, C., 1984. Le volcanism dans le Sud-Ouest de Madagascar. Journal of African Earth
704 Sciences 2, 383-388.
705 Olin, P.H., Wolff, J.A., 2012. Partitioning of rare earth and high field strength elements between
706 titanite and phonolitic liquid. Lithos 128, 46-54.
707 Pilet, S., Ulmer, P., Villiger, S., 2010. Liquid line of descent of a basanitic liquid at 1.5 GPa:
708 constraints on the formation of metasomatic veins. Contributions to Mineralogy and Petrology
709 159, 621–643.
710 Pratt, M.J., Wysession, M.E., Aleqabi, G., Wiens, D.A., Nyblade, A.A., Shore, P., Rambolamanana,
711 G., Andriampenomanana, F., Rakotondraibe, T., Tucker, R.D., Barruol, G., Rindraharisaona, E.,
712 2017. Shear velocity structure of the crust and upper mantle of Madagascar derived from surface
713 wave tomography. Earth and Planetary Science Letters 458, 405-417.
714 Razafiniparany, A., Joo, J., Rakotomavo, G., Rakotoarivony, X., 1974. Carte géologique
715 Soavinandriana (M47). Service Géologique, Antananarivo, Madagascar. 1/100,000.
716 Rocco, I., Zanetti, A., Melluso, L., Morra, V., 2017. Ancient depleted and enriched mantle
717 lithosphere domains in northern Madagascar: geochemical and isotopic evidence from spinel-to-
718 plagioclase-bearing ultramafic xenoliths. Chemical Geology 466, 70-85.
719 http://dx.doi.org/10.1016/j.chemgeo.2017.05.016
720 Roeder, P.L., Emslie, R.F., 1970. Olivine-liquid equilibrium. Contributions to Mineralogy and
721 Petrology 29, 275-289.
722 Rogers, N.W., De Mulder, M., Hawkesworth, C.J., 1992. An enriched mantle source for potassic
723 basanites: evidence from Karisimbi volcano, Virunga volcanic province, Rwanda. Contributions
724 to Mineralogy and Petrology 111, 543–556.
725 Ronga, F., Lustrino, M., Marzoli, A., Melluso, L., 2010. Petrogenesis of a basalt-comendite-
726 pantellerite rock suite: the Boseti volcanic complex, Main Ethiopian Rift. Mineralogy and
727 Petrology 98, 227-243. http://dx.doi.org/10.1007/s00710-009-0064-3.

728 Roig, J.Y., Tucker, R.D., Delor, C., Peters, S.G., Théveniaut, H., 2012. Carte géologique de la
729 République de Madagascar à 1/1,000,000. Ministère des Mines, PGRM, Antananarivo,
730 République de Madagascar, 1 color sheet.
731 Rufer, D., Preusser, F., Schreurs, G., Gnos, E., Berger, A., 2014. Late Quaternary history of the
732 Vakinankaratra volcanic field (central Madagascar): insights from luminescence dating of
733 phreatomagmatic eruption deposits. Bulletin of Volcanology 76, 817-837
734 Sheth, H.C., Mahoney, J.J., Baxter, A.N., 2003. Geochemistry of lavas from Mauritius, Indian
735 Ocean: mantle sources and petrogenesis. International Geology Review 45, 780-797.
736 Shishkina, T.A., Botcharnikov, R.E., Holtz, F., Almeev, R.R., Jazwa, A.M., Jakubiak, A.A., 2014.
737 Compositional and pressure effects on the solubility of H_2O and CO_2 in mafic melts. Chemical
738 Geology, 112-129.
739 Tanaka, T., Togashi, S., Kamioka, H., Amakawa, H., Kagami, H., Hamamoto, T., Yuhara, M.,
740 Orihashi, Y., Yoneda, S., Shimizu, H., Kunimaru, T., Takahashi, K., Yanagi, T., Nakano, T.,
741 Fujimaki, H., Shinjo, R., Asahara, Y., Tanimizu, M., Dragusanu C., 2000. JNdi-1: a neodymium
742 isotopic reference in consistency with LaJolla neodymium. Chemical Geology 167, 279-281.
743 Tiepolo, M., Bottazzi, P., Palenzona, M., 2003. A LASER probe coupled with ICP-double-focusing
744 sector-field mass spectrometer for in situ analysis of geological samples and U-Pb dating of
745 zircon. The Canadian Mineralogist 41, 259-272.
746 Tiepolo, M., Oberti, R., Zanetti, A., Vannucci, R., Foley, S.F., 2007. Trace-element partitioning
747 between amphibole and silicate melt. Reviews in Mineralogy and Geochemistry, 67, 417-452.
748 Tucker, R.D., Ashwal, L.D., Handke, M.J., Hamilton, M.A., LeGrange, M., and Rambeloson, R.A.
749 1999a. U–Pb geochronology and isotope geochemistry of the Archean and Proterozoic rocks of
750 north-central Madagascar. The Journal of Geology 107: 135–153. doi:10.1086/314337
751 Tucker, R.D., Conrad, J., Key, R.M., Pitfield, P.E.J., Randriamananjara, T., Taylor, C.D.,
752 Goodenough, K.M., Thomas, R.J., 2008. $^{40}Ar/^{39}Ar$ geochronology of Mesozoic and younger
753 igneous rocks, Madagascar, in: Revision of the geologic and mineral cartography of the north,
754 central and east-central zones of Madagascar; explanatory note to the Republic of Madagascar,
755 Ministry of Energy and Mines (MEM/SG/ DG/ UCP/ PGRM); Geol. Comm. Rep. - British
756 Geological Survey Report: CR/08/078, 385-435, 1 Appendix
757 Tucker, R.D., Roig, Y.G., Moine, B., Delor, C., Peters, S.G., 2014. A geological synthesis of the
758 Precambrian shield in Madagascar. Journal of African Earth Sciences 94, 9-30.
759 Ulrych, J., Novak, J.K., Lang, M., Hegner, E., Randa Z., 2006. Petrology and geochemistry and K-
760 Ar ages for Cenozoic tinguaites from the Ohre/Eger Rift (NW Bohemia). Neues Jahrbuch für
761 Mineralogie Abhandlungen 183, 41-61.

762 Vatin-Perignon, N., 1968. Le formations eruptives et la structure de l'edifice volcanique au centre du
763 Cantal (Massif Central Français). Bulletin Volcanologique 32, 207-251.
764 Webster, J.D., Goldoff, B., Sintoni, M.F., Shimizu, N., De Vivo, B., 2014. C-O-H-Cl-S-F volatile
765 solubilities, partitioning, and mixing in phonolitic-trachytic melts and aqueous-carbonic
766 vapor±saline liquid at 200 MPa. Journal of Petrology 55, 2217-2248.
767 Weis, D., Kieffer, B., Maerschalk, C., Barling, J., de Jong, J., Williams, G.A., Hanano, D., Pretorius,
768 W., Mattielli, N., Scoates, J.S., Goolaerts, A., Friedman, R.M., Mahoney, J.B., 2006. High-precision
769 isotopic characterization of USGS BHVO-1 and BHVO-2 reference materials by TIMS and MC-
770 ICP-MS. Geochemistry Geophysics Geosystems 7, Q08006. doi: 10.1029/ 2006GC001283
771 White, J.C., Espejel-Garcia, V.V., Antony, E.Y., Omenda, P., 2012. Open system evolution of
772 peralkaline trachyte and phonolite from the Suswa volcano, Kenya Rift. Lithos 152, 84-104.
773 Woolley, A.R., 2001. Alkaline rocks and carbonatites of the world. Part 3: Africa: Geological
774 Society/Natural History Publishing House, Bath, UK, p. 372
775 Wörner, G., Schmincke, H.-U., 1984. Mineralogical and chemical zonation of the Laacher See
776 Tephra sequence (East Eifel, W. Germany). Journal of Petrology 25, 805-835.
777

778 **Appendix: analytical techniques**
779

780 Powders of the 69 samples of this study were obtained after carefully grinding washed chips in an
781 ultrapure agate mill. For each sample, four grams of micronized powder were used to prepare pressed
782 powder pellets. The powder (mixed with 1 ml of Polyvinyl alcohol solution) was pressed to twenty
783 tons for twenty seconds. The bulk-rock X-Ray Fluorescence compositional data (Table S1) were
784 obtained on pressed powder pellets with an Axios Panalytical spectrometer equipped with six analyzer
785 crystals, three primary collimators and two detectors (flow counter and scintillator), operating at
786 different kV and mA for each analyte. Analytical uncertainties are in the order of 1-2% for major
787 elements and 5-10% for trace elements. The weight loss on ignition has been obtained with
788 gravimetric techniques, firing at 1000°C small aliquots of powders previously dried at 110°C
789 overnight.
790 Data on a subset of samples were obtained through ICP-MS methods at Actlabs (Canada) (Table 1).
791 Samples were mixed with a flux of lithium metaborate and lithium tetraborate and fused in an
792 induction furnace. The molten material is immediately poured into a solution of 5% nitric acid
793 containing an internal standard, and mixed continuously until completely dissolved (~30 minutes). The
794 samples were run for major oxides and selected trace elements (Ba, Be, Sc, Sr, V, Y and Zr) on a
795 combination simultaneous/sequential Thermo Jarrell-Ash ENVIRO II ICP or a Varian Vista 735 ICP.
796 Calibration is performed using seven prepared USGS and CANMET certified reference materials. One

of the seven standards is used during the analysis for every group of ten samples. Sample fused are diluted and analyzed by Perkin Elmer Sciex ELAN 6000, 6100 or 9000 ICP/MS for other trace elements (Cr, Co, Ni, Cu, Zn, Ga, Ge, As, Rb, Nb, Mo, Ag, In, Sn, Sb, Cs, La, Ce, Pr, Nd, Sm, Eu, Gd, Tb, Dy, Ho, Er, Tm, Yb, Lu, Hf, Ta, W, Tl, Pb, Bi, Th and U). Three blanks and five controls (three before the sample group and two after) are analyzed per group of samples. Duplicates are fused and analyzed every 15 samples. Analyses of international standards are reported in Cucciniello et al. (2017).

Microprobe analyses were carried out on polished thin sections using Energy Dispersive Spectrometry (EDS) at University of Napoli Federico II, utilizing a JEOL JSM-5310 microscope operating at 15 kV primary beam voltage, 50-100 mA filament current, 50 s net acquisition time and a Oxford Instruments Microanalysis Unit, equipped with an INCA X-act detector. For further details see Melluso et al. (2014, 2017).

The Laser Ablation - Inductively Coupled Plasma - Mass Spectrometry analysis of the minerals in the trachyphonolite RT-06I-355 was performed at IGG-CNR (Pavia, Italy), utilizing techniques described in Rocco et al. (2017). Concentrations of Rare Earth Elements (REE) and other selected trace elements (Li, B, Ba, Rb, Th, U, Nb, Ta, Sr, Zr, Hf, Ti, Y, Sc, V, Co and Ni) were determined in situ on polished sections (100 μm) using a PerkinElmerSCIEX ELAN DRC-e quadrupole mass spectrometer coupled with an UP213 deep-UV YAG Laser Ablation System (New Wave Research, Inc.). The laser was operated at a repetition rate of 10 Hz, with 213 nm wavelength and a fluence of ~9.5 J/cm^2. Helium was used as carrier gas and was mixed with Ar downstream of the ablation cell. Spot diameter was 55 μm. Data reduction was performed offline using the GLITTER software. For this study, the NIST SRM 610 synthetic glass standards was used as external standard, CaO was used as internal standard for clinopyroxene and amphibole, while SiO_2 was used for titanite and feldspar. Precision and accuracy of the REE concentration values were assessed through repeated analysis of the BCR2-g standard to be better than ±7% and ±10%, respectively, at the ppm concentration level (for further details see Miller et al., 2012 and references therein).

The Sr-Nd-Pb-isotope data were obtained at the University of Cape Town, with techniques described in le Roex et al. (2012). Sr, Nd and Pb were separated using conventional ion exchange techniques and all radiogenic isotope analyses were performed on a NuPlasma multicollector inductively coupled plasma-mass spectrometer (ICP-MS). To correct for mass fractionation effects, measured $^{87}Sr/^{86}Sr$ and $^{143}Nd/^{144}Nd$ values were normalized to $^{86}Sr/^{88}Sr=0.1194$ and $^{146}Nd/^{144}Nd=0.7219$, respectively. Pb isotopes were corrected for fractionation by normalizing ratios measured in international standards. Average standard values obtained during the course of this study are reported in the Table 3.

Table captions

832
833 Table 1: ICP-MS major and trace element composition of Itasy rocks. A few element ratios are also
834 reported.
835 Table 2: LAM-ICP-MS and microprobe composition of titanite, amphibole, clinopyroxene and
836 feldspar of the trachyphonolite RT-06I-355. The location of the laser pits is shown in the
837 Supplementary Fig. S1c.
838 Table 3: Isotopic composition of the Itasy rocks. The composition of the standards which were run
839 with the unknowns is also reported.
840
841 **Supplementary Tables**
842
843 Supplementary Table S1: XRF major trace element data and CIPW norms of the Itasy samples. The
844 composition of international standards is also reported.
845 Supplementary Table S2: synopsis of the mineral assemblages of the main lithotypes of the Itasy
846 complex.
847 Supplementary Table S3: composition of olivine of the Itasy rocks.
848 Supplementary Table S4: composition of oxides of the Itasy rocks.
849 Supplementary Table S5: composition of pyroxene of the Itasy rocks.
850 Supplementary Table S6: composition of amphibole, biotite and rhönite of the Itasy rocks.
851 Supplementary Table S7: composition of feldspar and glass of the Itasy rocks.
852 Supplementary Table S8: composition of feldspathoids of the Itasy rocks.
853 Supplementary Table S9: composition of titanite, apatite, other accessories of the Itasy rocks.
854 Supplementary Table S10: Recapitulation of mass balance calculations between rocks of different
855 degree of magmatic evolution, and detailed results. The composition of the phases is reported in
856 the supplementary tables.
857 Supplementary Table S11: average REE mineral/bulk rock ratios for titanite, amphibole and
858 clinopyroxene. The partition coefficients of titanite, clinopyroxene, apatite and amphibole are
859 taken from Olin and Wolff (2012), Fedele et al. (2009, 2015) and Tiepolo et al. (2007). Note that
860 amphibole of RT-06I-355 could not be considered in equilibrium with the host rock (cf.
861 Supplementary Fig. S1).
862
863 **Figure captions**
864
865 Figure 1: a) Simplified geological map of Madagascar, with the location of the main volcanic areas
866 of Cretaceous and Cenozoic; b) Geological sketch map with sample localities (Laborde

867 coordinates) and the main tectonic features of the Itasy area. c) Schematic section of the Itasy
868 region (redrawn after Pratt et al., 2017) with location of a possible mantle source region of the
869 Itasy mafic volcanic rocks.
870 Figure 2: Classification of the Itasy rocks according to the TAS and R_1R_2 diagrams. Symbols: Itasy
871 mafic rocks: red triangles; Itasy evolved rocks: blue circles. The data from other Cenozoic
872 districts of Madagascar are taken from: Melluso et al. (2007, 2011b); Cucciniello et al. (2011,
873 2016, 2017); Melluso and Morra (2000).
874 Figure 3: Classification of pyroxene and amphibole of the Itasy rocks. Symbols as in Fig. 2. The
875 pyroxene and amphibole composition of the Ankaratra alkaline rocks (black squares) are taken
876 from Cucciniello et al. (2017).
877 Figure 4: a) The composition of feldspars and bulk-rocks of the Itasy in the An-Ab-Or diagram
878 (mol.%). b) Composition of the Itasy volatile-rich feldspathoids in the CaO-Na_2O-K_2O diagram
879 (mol.%; after Lessing and Grout, 1971). c) The volatile concentration of the Itasy feldspathoids
880 (in wt.%). The feldspar composition of the Ankaratra alkaline rocks (black squares) are taken
881 from Cucciniello et al. (2017). The data on Mt. Vulture feldspathoids are taken from Melluso et
882 al. (1996, 2011a), references therein and unpublished data. Symbols as in Fig. 2.
883 Figure 5: a, b) Mantle normalized diagrams for the Itasy basanites. The data on the other
884 Madagascan basanites (grey patterns in the background) are taken from the database of Melluso
885 et al. (2016). The analyses of the Mt. Vulture basanites (MgO=9-12 wt.%) are taken from
886 Beccaluva et al. (2002), L.M. and V.M., unpublished data. The data on the Karisimbi leucite
887 basanites (green patterns in the background) are taken from Rogers et al. (1992). At a similar
888 MgO, the mantle-normalized patterns of the Mt. Vulture and Itasy basanites (as well other
889 geochemical characteristics) imply contrasting enrichment processes in their respective sources,
890 and a different mantle baseline preceeding metasomatic events; c) Mantle normalized diagrams
891 for the Itasy evolved rocks. The normalization values are taken from Lyubetskaya and Korenaga
892 (2007).
893 Figure 6: a, b) Mantle normalized diagrams of the coexisting phases of the trachyphonolite RT-06I-
894 355, together with those of the Itasy evolved rocks. Normalization values are those of
895 Lyubetskaya and Korenaga (2007). Potassium and Phosphorus are not reported.
896 Figure 7: Isotopic diagrams for the Itasy and the other Cenozoic volcanic rocks emplaced within the
897 cratonic domains of the Madagascan basement (cf. Fig. 1a). Symbols as in Fig. 2. The Ankaratra
898 data are taken from Cucciniello et al. (2017), and the Alaotra and Takarindiona olivine melilitites
899 (black triangles) are taken from Melluso et al. (2011a).
900 Figure 8: a) The tetrahedral phase diagram diopside-nepheline-kalsilite-silica at one atmosphere
901 (after Cucciniello, 2016) with the Itasy bulk-rock compositions (symbols as in Fig. 2); b) The

Petrogeny Residua's System at 1 kbar P_{H2O} with the Itasy trachyphonolites (blue circles). The boundary lines are taken from Gupta (2015). The evolved rocks of the Ankaratra (black squares) are taken from Cucciniello et al. (2017); the Bobaomby phonolites (black triangles) are taken from Melluso et al. (2007); the trachytes of Mauritius (grey rhombs) are taken from Ashwal et al. (2016). Other evolved rocks can be found in Cucciniello et al. (2017). The compositions of glass of the evolved rocks is reported as light blue circles.

Figure 9: AFC modelling after DePaolo (1981). The composition of the contaminants (granitic rocks and felsic gneisses of the basement around Itasy: data from Kröner et al., 2000; Melluso et al., 2001; Cucciniello et al., 2017) is the following: $^{87}Sr/^{86}Sr$=0.7113, $^{143}Nd/^{144}Nd$=0.5113, $^{206}Pb/^{204}Pb$=16.62, Pb=10 ppm; Sr=499 ppm; Nd=16 ppm; Th=12 ppm. The bulk partition coefficients are reported along the curves (cf. Supplementary Fig. S7), together with the values of the residual liquid fraction (f) and the assimilation/accumulus rate (r). The AFC models in the diagram $^{143}Nd/^{144}Nd$ *vs.* Nd were performed taking into account the geochemical behaviour of Nd shown in Supplementary Fig. S7, and two starting compositions (the basanite RT-06I-354B and the benmoreite RT-06I-387). Symbols as in Fig. 2.

Supplementary Figures

Supplementary Fig. S1a: Petrographic, BSE (backscattered electron images), and field images of the Itasy rocks: a) basanite RT-06I-354B: phenocrysts of olivine, with Cr-spinels, set in a scoriaceous mesostasis; b) basanite RT-06I-354B: large phenocrysts of kaersutite enclosing diopsidic clinopyroxene, parallel nicols; c) phonotephrite RT-06I-398: rare phenocrysts of clinopyroxene and apatite set in a very fine-grained microlitic mesostasis, parallel nicols; d) basanite RT-06I-354B: large phenocryst of diopside-to-titanaugite clinopyroxene, parallel nicols; e) trachyphonolite RT-06I-355; phenocrysts of a zoned anorthoclase and titanite in a fine-grained feldspar-rich mesostasis, parallel nicols; f) trachyphonolite RT-06I-375: phenocrysts of (pleochroic) titanite and alkali feldspar in a fine-grained groundmass, parallel nicols. The horizontal scale of the thin section photomicrographs is 2.5 mm.

Supplementary Fig. S1b: g) groundmass of basanite RT-06I-354B: microlites of feldspar, feldspathoids, unmixed Fe-Ti oxides and clinopyroxene, BSE; h) trachyphonolite RT-06I-361: phenocrysts of amphibole, and microphenocrysts of titanite and apatite in a fine-grained mesostasis; i) trachyphonolite RT-06I-363: microphenocrysts of Fe-Ti oxides, titanite, and clinopyroxene in a fine-grained mesostasis rich in alkali feldspar and light grey glass, BSE; j) phonotephrite RT-06I-398: a microlite of haüyne (darker grey) in the center of the groundmass made up of feldspar, clinopyroxene, magnetite and glass, BSE; k) l) m) n) o) feldspathoids in the

groundmass of trachyphonolites RT-06I-361 and RT-06I-379; p), q), r) pyroclastic rocks, lava domes, and spatter cones in the northeastern part of Itasy.

Supplementary Fig. S1c: Petrographic characteristics of the trachyphonolite RT-06I-355. a) zoned green cpx phenocryst b), c) phenocrysts of alkali feldspar and titanite; d) microlites of alkali feldspar and altered amphibole. The laser pits after LAM-ICP-MS work (Table 2) can be easily seen. The horizontal scale of the thin section photomicrographs is 2.5 mm.

Supplementary Fig. S2: Composition of the titaniferous magnetite of the Itasy rocks in the MgO-MnO and TiO_2-Al_2O_3 diagrams (in wt.%). Symbols as in Fig. 2.

Supplementary Fig. S3: Clinopyroxene composition. Symbols: mafic rocks: red triangles; benmoreites and trachyphonolites: blue circles. The composition of olivine is plotted in the Ca-Mg-Fe diagram.

Supplementary Fig. S4: Amphibole composition (cations in apfu) indicating the *absence* of *evidence* for a high-pressure crystallization environment for this phase, as the calculated Al^{VI} is roughly 1:10 the calculated Al^{IV} in both mafic and evolved rocks. Symbols as in Fig. 2

Supplementary Fig. S5: composition of nepheline in the nepheline-kalsilite-silica diagram. The nephelines of the olivine melilitites and of the Ankaratra rocks are reported for comparison (data from Melluso et al., 2011a and Cucciniello et al., 2017).

Supplementary Fig. S6: XRF major oxides and trace elements vs. MgO wt.% (plotted on a logarithmic scale). The composition of olivine, amphibole and clinopyroxene of the basanites and tephrites is reported in a few diagrams for comparison. Symbols as in Fig. 2.

Supplementary Fig. S7: Fractional crystallization models using thorium (Th) as the most incompatible element (thus as a proxy of a quantitative differentiation index). The numbers along the curves indicate the fraction of residual liquid (f) starting from the basanite RT-06I-354B, and the bulk partition coefficients for the element (fitted also by visual guess) in the *ordinata* are reported in each part of the curves. Ticks on the curves are at f=0.9, 0.8, 0.7, 0.6, 0.5, 0.45, 0.4, 0.35, 0.3, 0.25 and 0.2, starting from basanite RT-06I-354B (unreported for clarity). Symbols as in Fig. 2.

Supplementary Fig. S8: a) REE patterns of the Itasy mafic rocks ; b) the REE patterns of the mineral phases of RT-06I-355 and the host rock; c), d) REE patterns of the evolved rocks with c) model obtained by subtraction of 2% apatite and 1% titanite from sample RT-06I-387, by using the partition coefficients of Fedele et al. (2015) and Olin and Wolff (2012); and d) model obtained after subtraction of 0.7 and 1% titanite from sample RT-06I-387; e) The REE concentration of the Itasy rocks normalized to that of the most primitive sample (RT-06I-354B). The effects of titanite and apatite removal (cf. figure c) are also shown; f) Ratios between the

concentrations of the average composition of titanite, amphibole and clinopyroxene and that of the host rock. The experimental partition coefficients of titanite in phonolites (Olin and Wolff, 2012), clinopyroxene in trachyphonolites (Fedele et al., 2009), and amphibole in trachytes (Tiepolo et al., 2007) are reported for comparison (data in Supplementary Table 11). g) The REE patterns of the Itasy titanites and those of alkaline intrusive rocks of within-plate affinity (data from Marks et al., 2008 and Melluso et al., 2010). Prometium is always interpolated. The chondrite is the CI of Boynton (1984).

Figure 1

Click here to download high resolution image

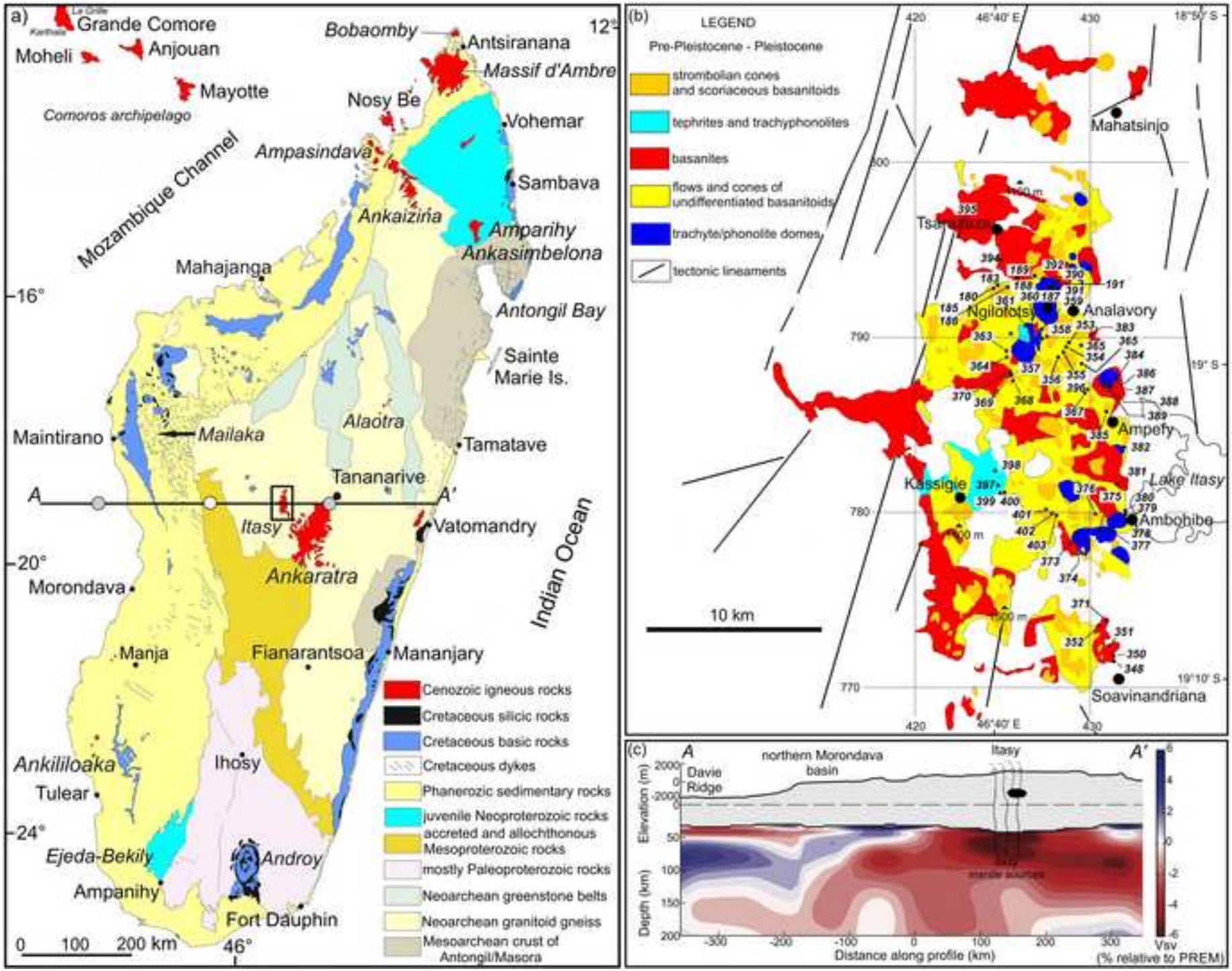

Figure 2

Click here to download high resolution image

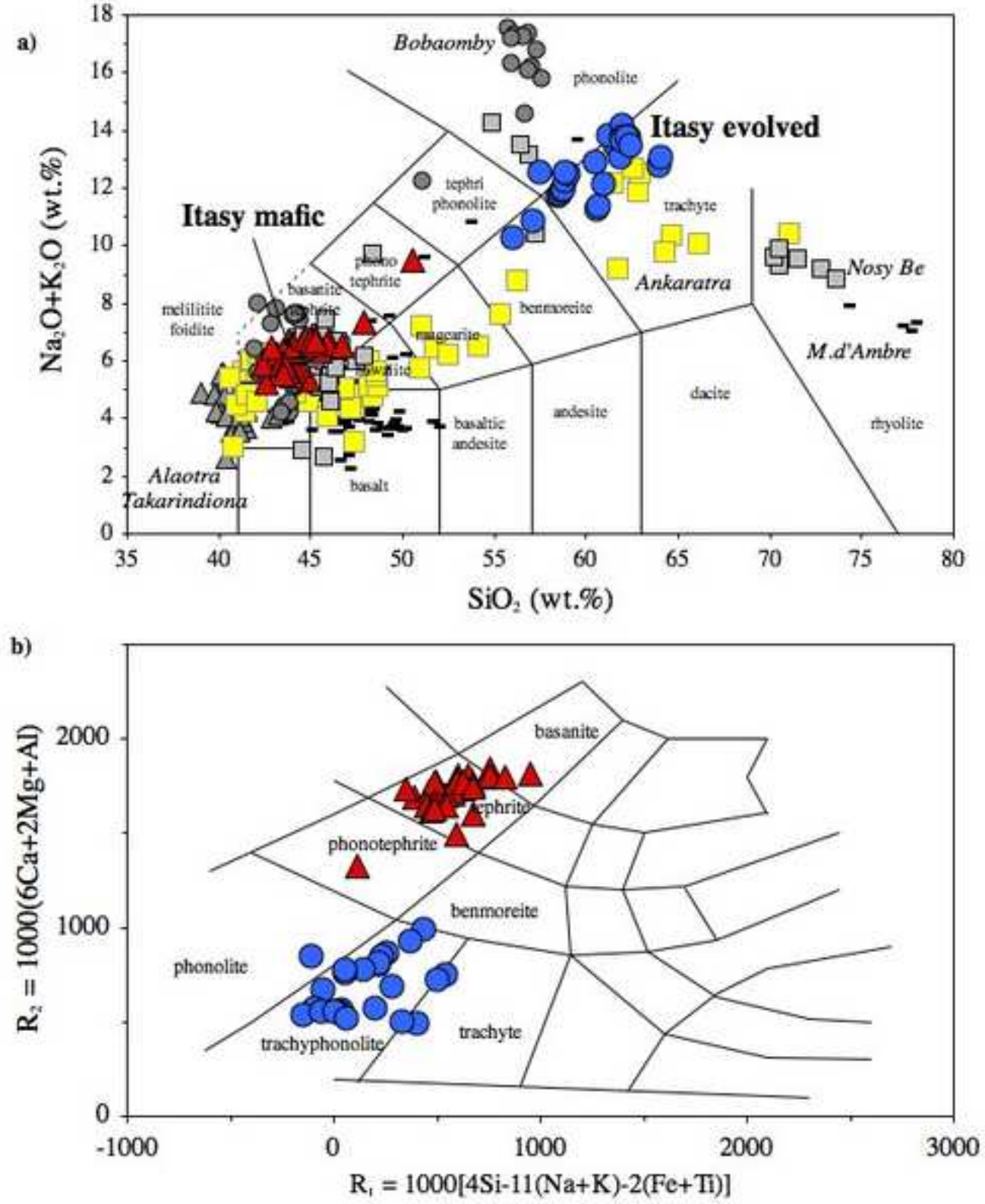

Figure 3

Click here to download high resolution image

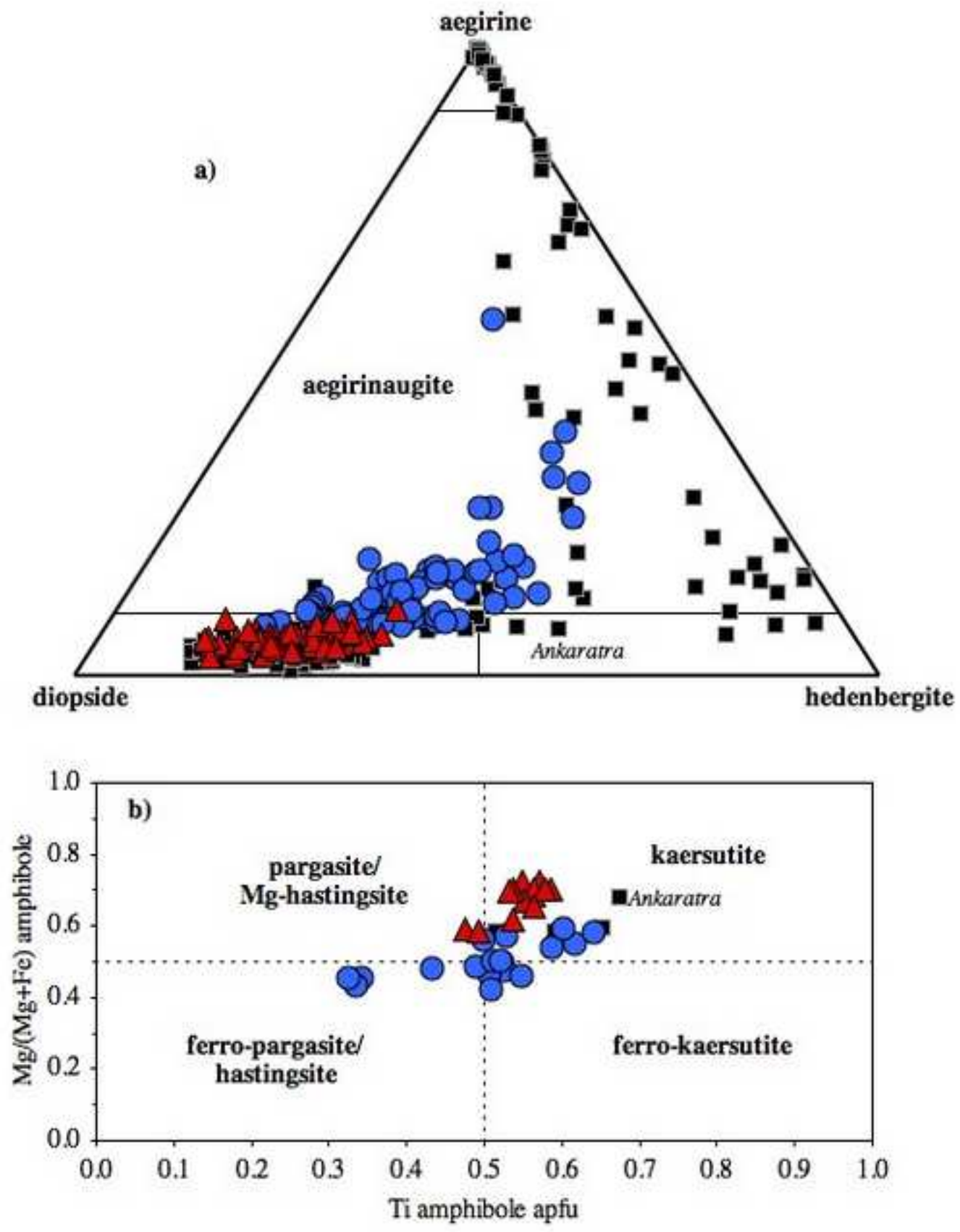

Figure 4

Click here to download high resolution image

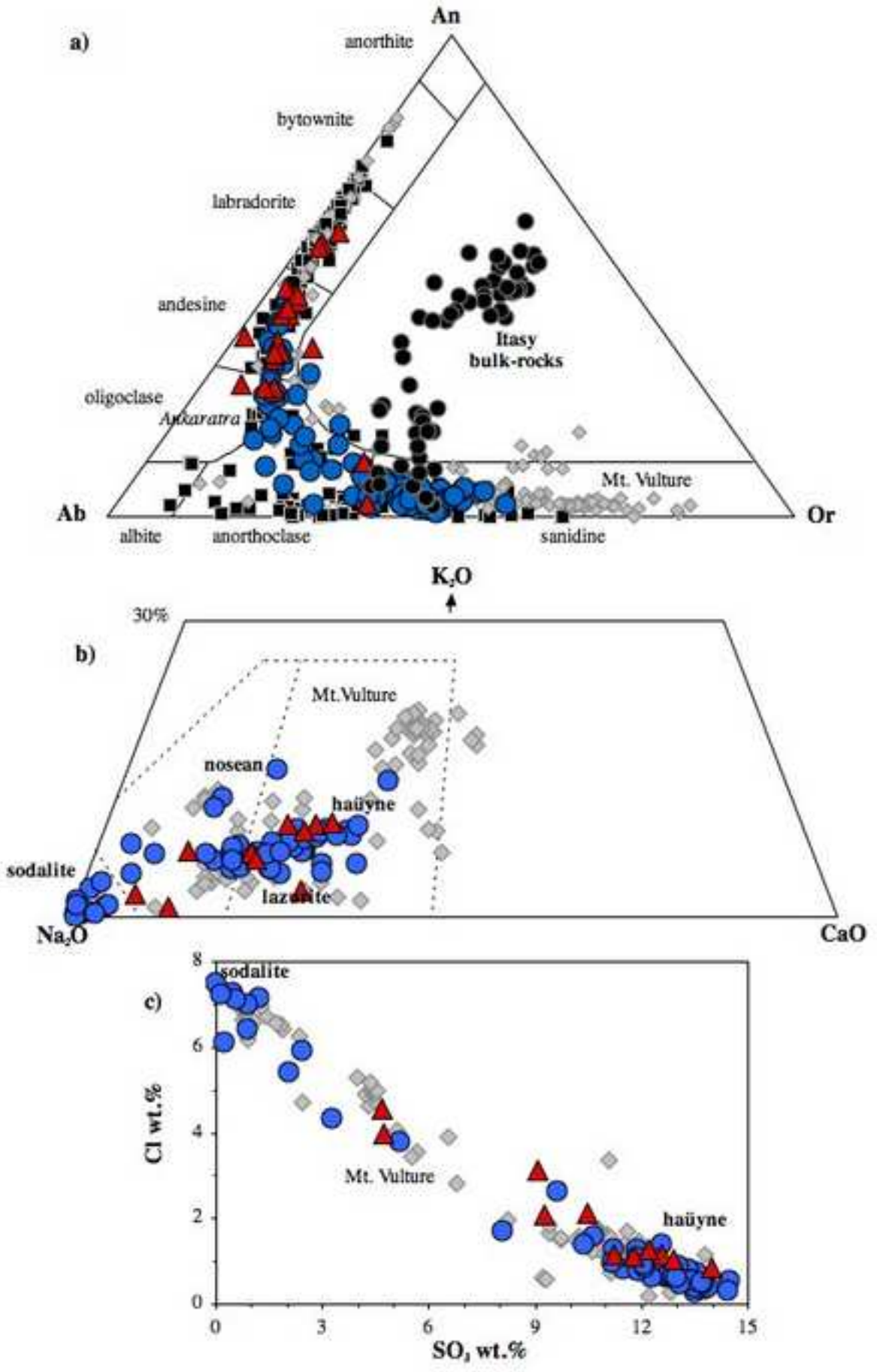

Figure 5

Click here to download high resolution image

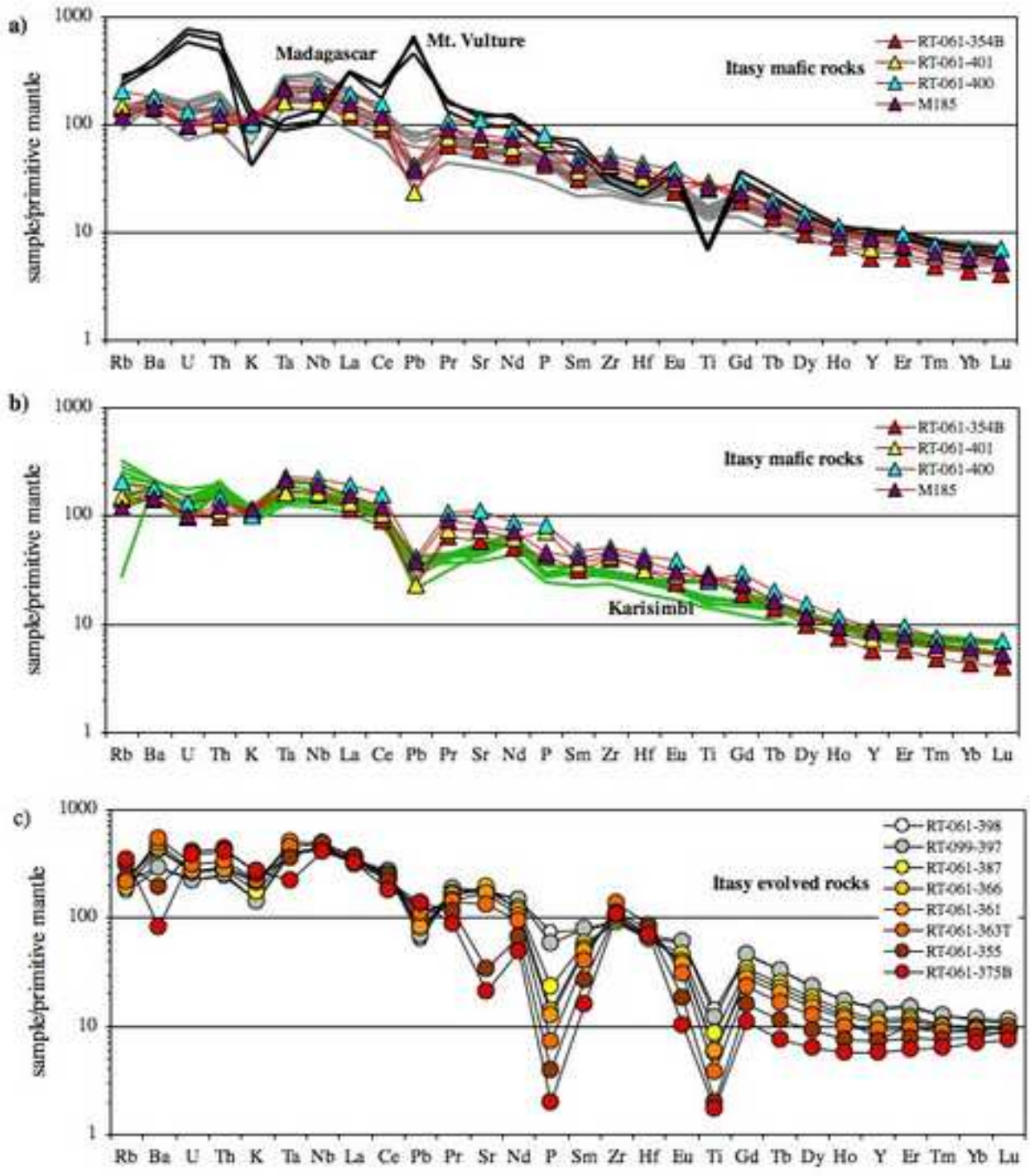

Figure 6

Click here to download high resolution image

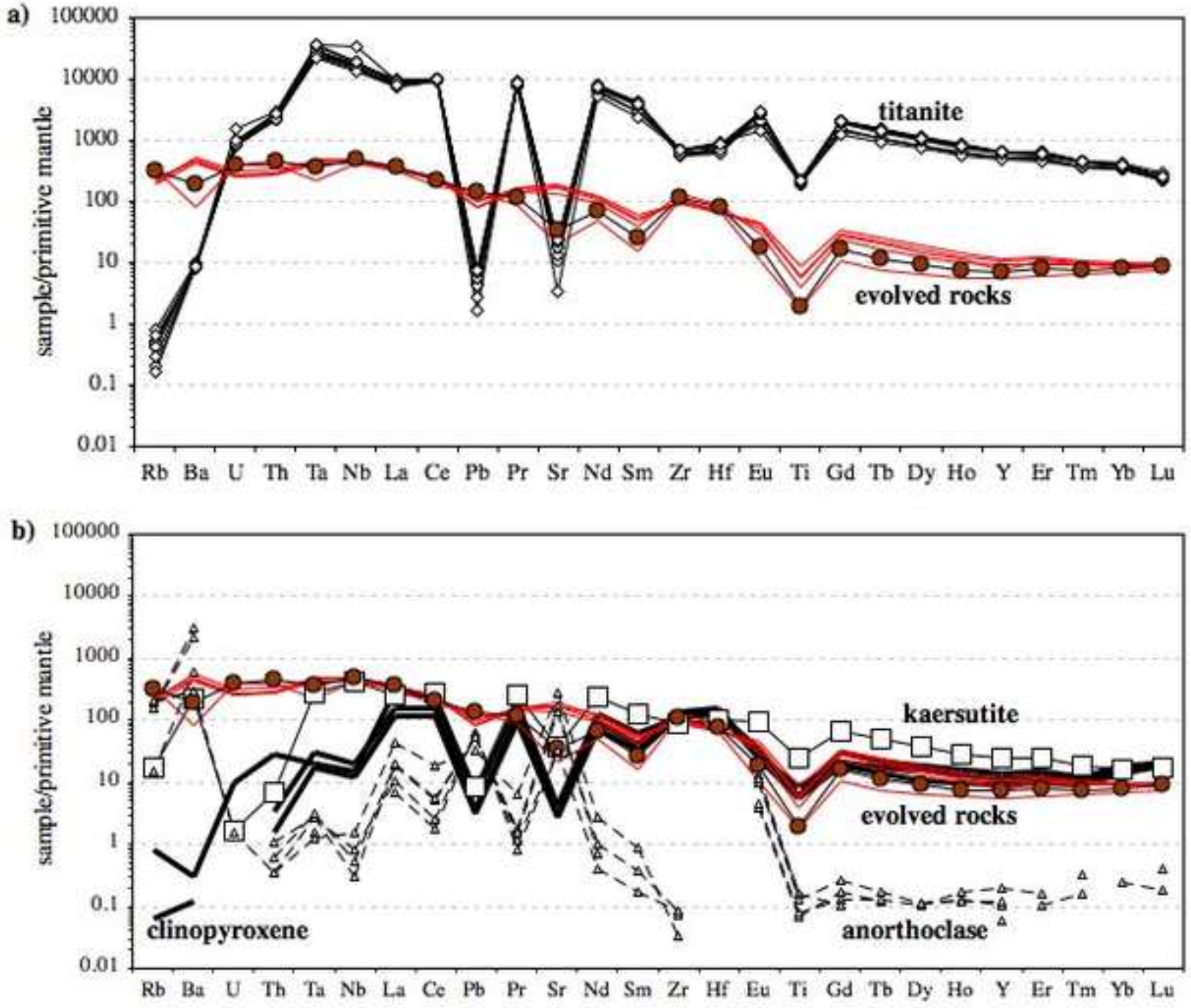

Figure 7

Click here to download high resolution image

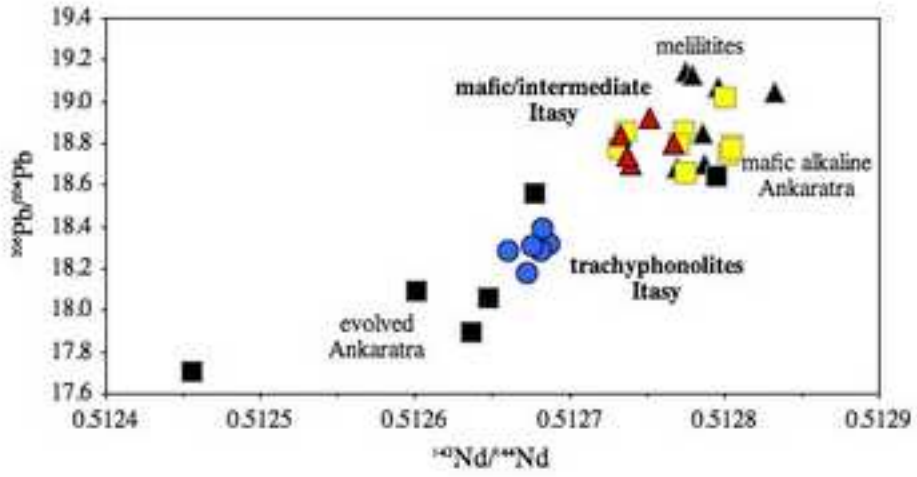

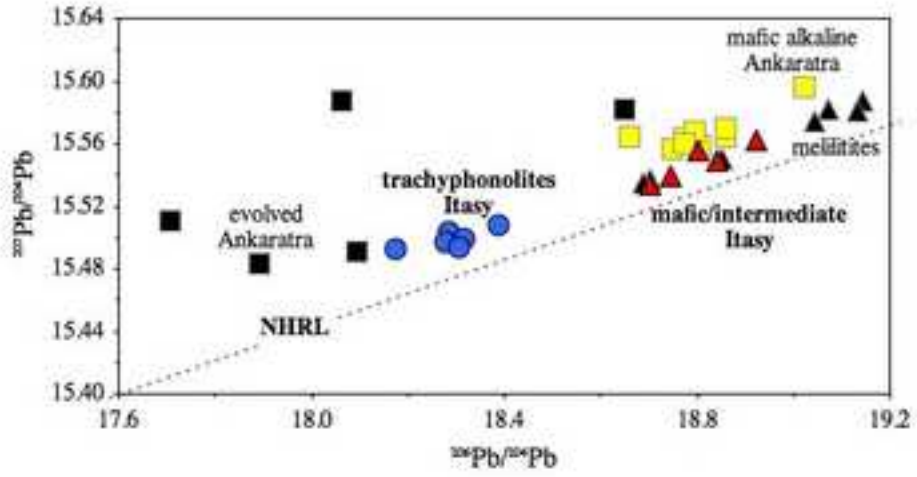

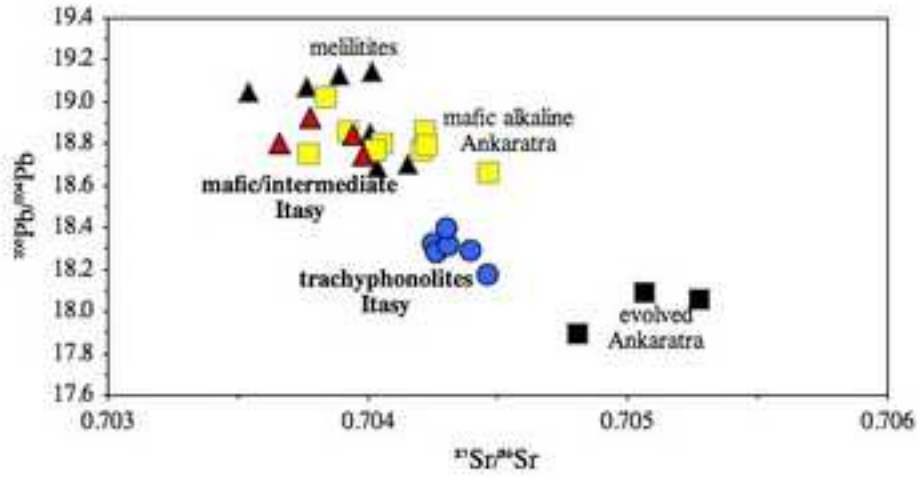

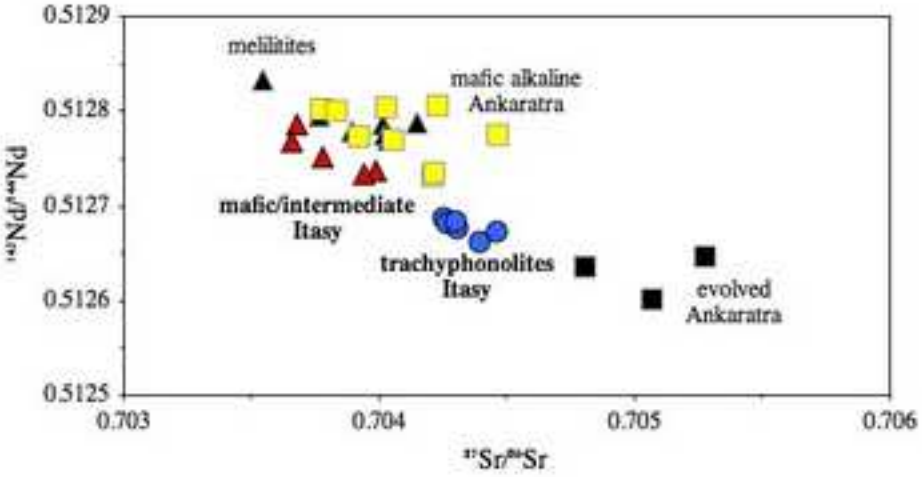

Figure 8

Click here to download high resolution image

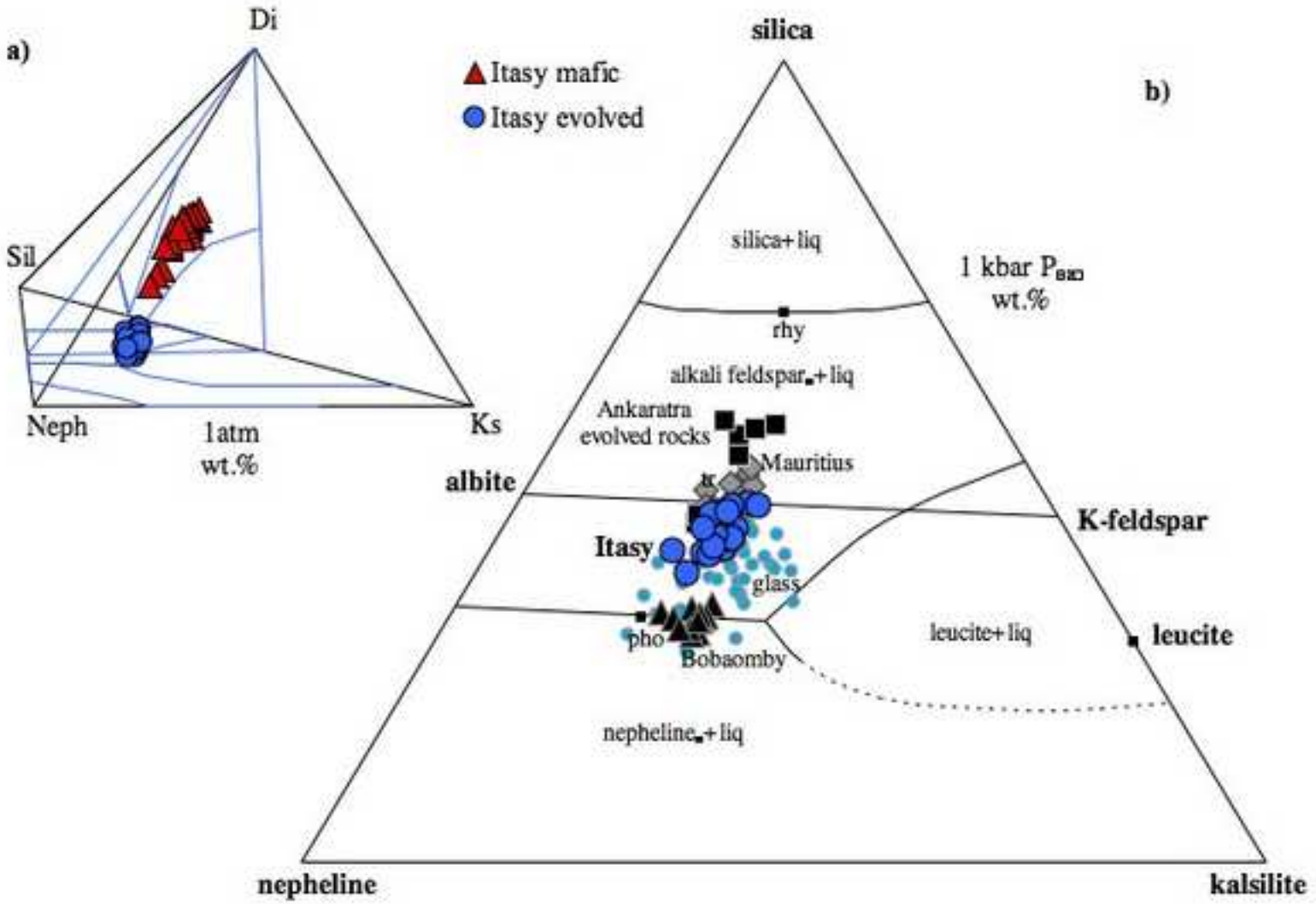

Figure 9

Click here to download high resolution image

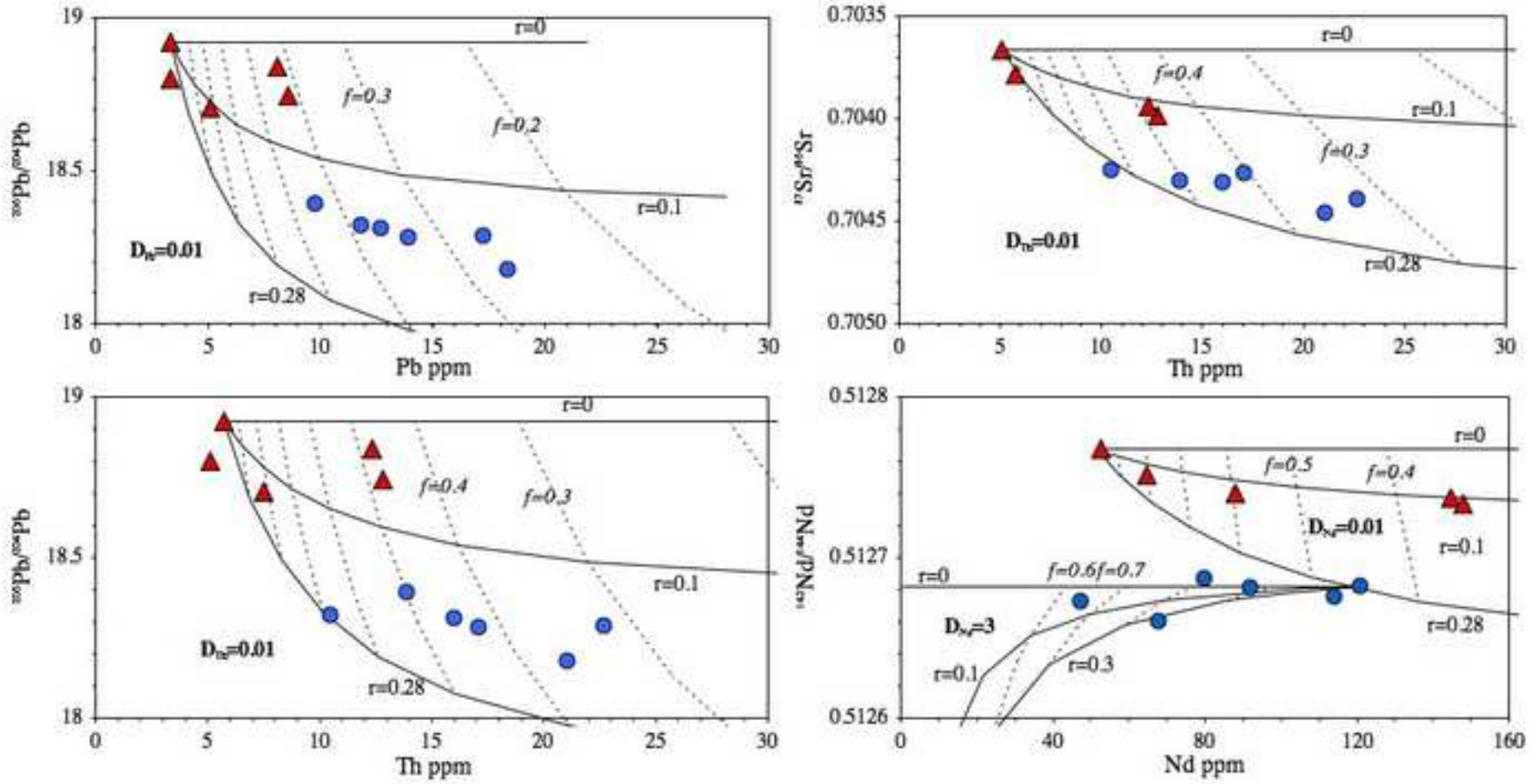

Table 1

Click here to download Table: Table1itasy.xls

Table 1: ICP-MS major and trace element composition of Itasy rocks. A few element ratios are also reported

	BSN	BSN	BSN	TPH	PHTPH	PHTPH	BEN	TRPHO	TRPHO	TRPHO	TRPHO	TRPHO
	RT-061-354B	M185	RT-061-401	RT-061-400	RT-061-398	RT-099-397	RT-061-387	RT-061-366	RT-061-361	RT-061-363T	RT-061-355	RT-061-375B
SiO_2	41.75	46.23	40.94	43.06	49.17	48.94	54.26	57.45	57.97	59.92	60.90	61.00
TiO_2	4.62	4.22	4.57	3.94	2.25	1.93	1.38	0.89	0.92	0.60	0.31	0.28
Al_2O_3	11.73	11.97	12.88	14.40	16.49	16.47	18.24	19.31	19.19	19.47	19.69	19.28
Fe_2O_{3t}	13.62	12.77	15.10	14.03	10.60	9.47	5.90	4.46	4.07	3.21	2.44	2.36
MnO	0.16	0.17	0.19	0.22	0.31	0.30	0.22	0.22	0.19	0.18	0.21	0.21
MgO	9.94	8.12	7.69	5.62	2.74	2.22	1.24	0.69	0.67	0.36	0.17	0.16
CaO	10.74	10.94	11.54	10.17	8.24	7.76	5.03	3.90	3.74	2.57	1.42	1.30
Na_2O	2.42	2.18	2.63	3.56	5.54	4.69	5.49	6.80	6.35	5.60	6.56	7.42
K_2O	2.64	2.69	2.44	2.34	3.37	3.23	3.99	4.83	4.83	5.08	5.90	6.17
P_2O_5	0.65	0.71	1.10	1.25	1.14	0.90	0.35	0.21	0.19	0.11	0.06	0.03
LOI	0.40	2.80	0.40	0.52	0.48	2.55	1.72	0.08	1.10	2.14	1.61	0.38
Total	98.66	102.80	99.48	99.11	100.3	98.46	97.83	98.84	99.23	99.25	99.27	98.59
Be	1	2	2	2	4	4	4	4	4	5	6	6
Sc	29		27	18	6	5	2	1	1			
V	407	353	395	301	126	104	76	50	47	29	17	16
Cr	330	184	200		80	50						80
Co	62	46	55	40	12	10	5	2	2	1		
Ni	170	98.7	80	30								
Cu	70	72.4	60	30								
Zn	110	155	120	160	220	220	160	160	140	150	180	160
Ga	23	25.6	24	27	32	31	31	31	30	30	35	32
Ge	2	1.18	2	2	2	2	2	2	2	1	2	2
Rb	65	55	69	94	81	102	89	107	104	96	142	157
Sr	918	1300	1170	1759	2776	2850	2727	3091	2666	2133	542	329
Y	19	29	24	31	49	48	38	36	25	31	24	19
Zr	341	387	362	434	781	804	768	816	870	1154	954	912
Nb	72	90	76	104	202	204	198	206	223	223	228	188
Mo		3.19	3	2	7	5	2	8	7	5	4	7
Ag	1.4	0.33	1.5	2.1	3.2	3.6	3.3	3.6	4.1		4.1	3.8
Sn	3	3.02	3	3	4	4	3	2	2	2	2	2
Cs		0.45	0.5	0.6	0.8	1.2	1	1	1	1.2	1.3	1.5
Ba	727	751	882	921	1482	1496	2135	2251	2468	2753	999	417
La	59.9	79.1	66.7	99.2	166.0	176.0	177.0	176.0	161.0	190.0	182.0	165.0
Ce	122.0	161.5	138.0	208.0	344.0	362.0	340.0	334.0	310.0	312.0	288.0	243.0
Pr	13.1	18.3	15.2	22.0	37.5	38.2	34.0	32.8	30.1	28.8	23.2	17.9
Nd	51.6	72.5	62.5	88.8	145.0	146.0	124.0	115.0	105.0	92.8	67.8	48.6
Sm	10.2	13.6	11.8	15.5	25.0	25.4	19.0	17.1	16.1	12.9	8.5	5.1
Eu	2.9	3.8	3.6	4.7	7.4	7.5	5.7	5.0	4.6	3.7	2.2	1.3
Gd	8.3	10.2	10.0	12.7	20.2	19.6	14.6	13.0	12.1	10.2	6.9	4.7
Tb	1.1	1.3	1.3	1.6	2.6	2.6	2.0	1.8	1.6	1.3	0.9	0.6
Dy	5.3	6.7	6.4	8.2	12.7	12.5	10.0	8.8	8.0	6.8	5.0	3.4
Ho	0.90	1.16	1.10	1.40	2.10	2.10	1.70	1.50	1.40	1.20	0.90	0.70
Er	2.00	2.65	2.50	3.30	5.30	5.10	4.20	3.90	3.60	3.30	2.70	2.10
Tm	0.26	0.34	0.32	0.41	0.67	0.67	0.56	0.54	0.49	0.49	0.41	0.34
Yb	1.50	2.03	1.90	2.40	3.90	4.00	3.40	3.30	3.10	3.20	2.80	2.40
Lu	0.22	0.29	0.28	0.38	0.57	0.61	0.50	0.52	0.47	0.54	0.48	0.40
Hf	7.4	8.7	7.2	9.8	14.3	15.6	14.7	14.7	16	19.2	18	15.5
Ta	5.1	6.51	4.9	7	11.8	12	12.6	12	15.1	13.6	11	6.8
Pb	3.35	5.44	3.35	6	9	10	12	14	12	16	20	20
Th	6.2	7.7	6.9	9.2	14.7	15.9	17.7	18.9	17.8	21.2	27.6	25.3
U	1.7	1.75	1.7	2.3	4	3.8	4.5	4.5	4.7	5.4	7	6.7
Zr/Hf	46	44	50	44	55	52	52	55	54	60	53	59
Nb/Ta	14	14	15	15	17	17	16	17	15	16	21	28
Th/U	3.6	4.4	4.1	4.0	3.7	4.2	3.9	4.2	3.8	3.9	3.9	3.8
La/Yb_n	26.9	26.3	23.7	27.9	28.7	29.7	35.1	36.0	35.0	40.0	43.8	46.4

BSN, basanite; TPH, tephrite; PHTPH, phonotephrite; BEN, benmoreite; TRPHO, trachyphonolite; La/Ybn is the chondrite normalized ratio

Table 2

Click here to download Table: Table2itasy.xls

Table 2: LAM-ICP-MS and microprobe composition of titanite, amphibole, clinopyroxene and feldspar in the trachyphonolite RT06I355

Table 2: LAM

	RT-06I-355 ttn	RT-06I-355 ttn	RT-06I-355 ttn	RT-06I-355 ttn	RT-06I-355 ttn	RT-06I-355 ttn	RT-06I-355 ttn	RT-06I-355 ttn	RT-06I-355 ttn	RT-06I-355 ttn	*RT-06I-355 av ttn*	
ppm			crystal n. 1					crystal n. 2				
Li	0.54	0.76	2.02	2.23	2.01	0.63					*1.4*	Li
B	47.78	49.26	43.04	69.42	73.42	68.24	72.75	74.78	69.97	52.65	*62.1*	B
Sc	7.70	7.92	8.31	8.05	8.12	7.58	5.27	5.36	6.42	5.79	*7.1*	Sc
Ti	178310	178699	181535	204264	206175	192850	212573	207348	207720	211055	*198053*	Ti
V	305.8	324.9	324.1	286.0	311.4	235.7	326.4	318.9	327.6	316.2	*307.7*	V
Cr	2.65										*2.7*	Cr
Co	0.13	0.12	0.11	0.34			0.31	0.19			*0.2*	Co
Ni	0.52	0.44	0.71		0.42		0.95	1.39	0.87	0.85	*0.8*	Ni
Zn	50.97	47.43	50.99	37.29	47.25	48.41	27.12	25.45	26.98	30.48	*39.2*	Zn
Rb	0.20	0.20	0.24	0.36	0.23	0.19	0.10	0.08	0.30	0.13	*0.2*	Rb
Sr	174.13	291.71	343.76	204.66	276.91	54.22	348.77	275.16	359.25	382.21	*271.1*	Sr
Y	1790.1	2249.9	2146.0	1734.8	2188.4	1616.5	2199.4	2223.5	2054.2	2198.4	*2040.1*	Y
Zr	5834.7	4930.9	5907.6	5933.6	5035.2	5702.6	4830.0	4574.9	5043.0	5836.6	*5362.9*	Zr
Nb	8629.9	7681.5	8876.7	8424.2	7207.8	15230.2	6469.2	6949.3	6168.9	8601.3	*8423.9*	Nb
Cs	0.02	0.01	0.01			0.04					*0.02*	Cs
Ba	46.10	47.03	48.57	49.06	46.57	48.21	43.47	45.29	42.16	45.08	*46.2*	Ba
La	4557.5	4600.0	4542.1	5055.2	4224.2	4890.9	3922.8	4056.2	3840.3	4142.6	*4383.2*	La
Ce	13139.3	13550.0	13500.0	13786.1	13157.6	13121.1	12700.0	13178.3	12082.8	12951.9	*13116.7*	Ce
Pr	1593.1	1816.5	1837.8	1653.2	1777.0	1483.3	1749.4	1769.1	1629.9	1754.4	*1706.4*	Pr
Nd	6030.2	7720.2	7733.4	6332.8	7680.5	5332.0	7605.9	7727.5	7047.1	7614.2	*7082.4*	Nd
Sm	922.3	1318.5	1306.6	949.3	1315.2	781.8	1351.1	1338.1	1218.3	1293.2	*1179.4*	Sm
Eu	236.1	344.3	339.9	252.5	345.5	179.6	362.6	349.0	332.1	351.7	*309.3*	Eu
Gd	618.4	888.5	873.2	644.6	883.3	520.9	897.9	874.7	806.5	868.6	*787.7*	Gd
Tb	85.0	121.5	116.9	88.2	118.6	75.1	123.4	120.8	110.0	118.5	*107.8*	Tb
Dy	424.6	596.9	583.6	441.0	598.4	392.0	614.1	600.1	553.1	587.2	*539.1*	Dy
Ho	73.4	99.4	97.4	77.3	100.5	68.7	101.8	104.0	92.0	98.2	*91.3*	Ho
Er	171.4	218.5	215.2	174.8	226.2	160.1	216.4	217.8	199.9	213.9	*201.4*	Er
Tm	19.9	24.8	24.4	19.9	25.3	19.5	24.5	25.0	23.1	25.0	*23.1*	Tm
Yb	116.1	135.9	134.4	119.8	141.3	117.6	136.6	141.1	127.6	133.0	*130.3*	Yb
Lu	12.1	13.8	13.7	12.7	15.4	11.9	13.7	13.2	13.6	14.0	*13.4*	Lu
Hf	183.1	155.1	189.4	201.9	171.4	211.4	151.2	140.5	156.6	191.8	*175.2*	Hf
Ta	718.8	838.6	1047.6	866.5	865.9	1133.7	708.5	763.4	655.2	1102.7	*870.1*	Ta
Pb	0.87	0.65	0.73	0.62	0.40	1.16	0.24	0.79	0.98	1.07	*0.8*	Pb
Th	151.6	137.8	154.8	168.0	140.6	187.3	133.6	141.4	139.6	173.8	*152.9*	Th
U	17.80	14.73	15.67	16.48	14.39	26.76	15.03	15.11	15.45	16.74	*16.8*	U
SREE	27999	31449	31319	29607	30609	27154	29820	30515	28076	30166		SREE
Zr/Hf	31.9	31.8	31.2	29.4	29.4	27.0	31.9	32.6	32.2	30.4		Zr/Hf
Nb/Ta	12.0	9.2	8.5	9.7	8.3	13.4	9.1	9.1	9.4	7.8		Nb/Ta
Zr/Y	3.3	2.2	2.8	3.4	2.3	3.5	2.2	2.1	2.5	2.7		Zr/Y
Th/U	8.5	9.4	9.9	10.2	9.8	7.0	8.9	9.4	9.0	10.4		Th/U
La/Ybn	26.5	22.8	22.8	28.4	20.2	28.0	19.4	19.4	20.3	21.0		La/Ybn

Table 3

Click here to download Table: Table3itasy.xls

Table 3: Isotopic composition of the Itasy rocks. The composition of the standards which were run with the unknowns is also reported

		$^{143}Nd/^{144}Nd$	±2s internal*10^6	$^{87}Sr/^{86}Sr$	±2s internal*10^6	$^{206}Pb/^{204}Pb$	±2s internal	$^{207}Pb/^{204}Pb$	±2s internal	$^{20}Pb/^{204}Pb$	±2s internal
BSN	RT-06I-354B	0.512768	10	0.703661	10	18.801	0.0010	15.556	0.0010	39.012	0.0027
BSN	RT-06I-400	0.512740	15			18.704	0.0009	15.534	0.0008	38.891	0.0027
BSN	IT185	0.512786	10	0.703678	10						
BSN	RT-06I-401	0.512752	12	0.703780	11	18.922	0.0008	15.562	0.0008	39.088	0.0027
phtph	RT-06I-397	0.512737	14	0.703984	12	18.744	0.0008	15.539	0.0007	38.965	0.0022
phtph	RT-06I-398	0.512733	11	0.703942	10	18.840	0.0008	15.549	0.0008	39.027	0.0021
ben	RT-06I-387	0.512682	9	0.704303	10	18.390	0.0009	15.507	0.0009	38.567	0.0025
trph	RT-06I-355	0.512660	7	0.704397	12	18.285	0.0009	15.503	0.0009	38.486	0.0029
trph	RT-06I-361	0.512687	13	0.704253	10	18.318	0.0010	15.499	0.0008	38.494	0.0026
trph	RT-06I-363T	0.512681	11	0.704266	11	18.279	0.0007	15.496	0.0008	38.464	0.0024
trph	RT-06I-366	0.512676	7	0.704312	11	18.308	0.0010	15.493	0.0010	38.493	0.0029
trph	RT-06I-375B	0.512673	13	0.704462	13	18.176	0.0008	15.492	0.0009	38.380	0.0000
Std	BHVO-2	0.512985	8	(0.512984 ±11, Weis et al., 2006)							
Std	BHVO-2	0.512974	11	(0.512987 ±19, long-term UCT average n=120/exclude 1)							
Std	BHVO-2	0.512976	9	(0.512980 ±12, GEOREM)							
Std	ref JNdi-1	0.512115	7	(Tanaka et al., 2000)							
Std	BHVO-2			0.703488	12	(0.703479 ±20, Weis et al., 2006)					
Std	BHVO-2			0.703452	13	(0.703489 ±44, long-term UCT average n=124/exclude 6)					
Std	BHVO-2			0.703466	10	(0.703469 ±17, GEOREM)					
Std	BHVO-2			0.703467	15						
Std	BHVO-2					18.6506	0.0007	15.5358	0.0006	38.2332	0.0019
Std	BHVO-2					18.6920	0.0008	15.5376	0.0010	38.2597	0.0028
Std	BHVO-2				Weis et al., 2006	18.6474	0.0242	15.5334	0.0094	38.2367	0.0182
Std	BHVO-2				GEOREM range	18.514-18.687		15.457-15.558		37.992-38.294	
Std	BHVO-2				(long-term UCT average n=58/exclude 3)	18.6306	0.0620	15.5337	0.0139	38.2237	0.0483
Std	ref NIST981				Galer & Abouchami 1998	16.9405	0.0015	15.4963	0.0016	36.7219	0.0044

BSN, basanite; phtph, phonotephrite; ben, benmoreite; trph, trachyphonolite

supplfig1

Click here to download Background dataset for online publication only: supplfig.1aitasy.jpg

supplfig1b

Click here to download Background dataset for online publication only: supplfig.1bitasy.jpg

supplfig1c

Click here to download Background dataset for online publication only: supplfig.1c.jpg

supplfig2

Click here to download Background dataset for online publication only: supplfig.2newmgtitasy.jpg

supplfig3

Click here to download Background dataset for online publication only: supplfig.3newpxitasy.jpg

supplfig4

Click here to download Background dataset for online publication only: supplfig.4newamphitasy.jpg

supplfig5

Click here to download Background dataset for online publication only: supplfig.5nephelineitasy.jpg

supplfig6a

Click here to download Background dataset for online publication only: supplfig.6anewitasy.jpg

supplfig6b

Click here to download Background dataset for online publication only: supplfig.6bnewitasy.jpg

supplfig7

Click here to download Background dataset for online publication only: supplfig.7newitasy.jpg

supplfig8

Click here to download Background dataset for online publication only: supplfig.8figreeitasy.jpg

suppltables

Click here to download Background dataset for online publication only: supptablesitasy.xls